NEW APPROACHES FOR CHANNEL ESTIMATION IN WIRELESS COMMUNICATIONS

HABİB ŞENOL

IŞIK UNIVERSITY
2006

NEW APPROACHES FOR CHANNEL ESTIMATION IN WIRELESS COMMUNICATIONS

HABİB ŞENOL

Submitted to the Graduate School of Science and Engineering
in partial fulfillment of the requirements for the degree of
Doctor of Philosophy
in
Electronics Engineering

IŞIK UNIVERSITY
2006

NEW APPROACHES FOR CHANNEL ESTIMATION
IN
WIRELESS COMMUNICATIONS

APPROVED BY:

Assoc. Prof. Uluğ BAYAZIT IŞIK UNIVERSITY
(Thesis Supervisor)

Assoc. Prof. Hakan A. ÇIRPAN İSTANBUL UNIVERSITY
(Thesis Co-supervisor)

Prof. Yorgo İSTEFANOPULOS IŞIK UNIVERSITY

Prof. Erdal PANAYIRCI BİLKENT UNIVERSITY

Prof. Ümit AYGÖLÜ İSTANBUL TECHNICAL UNIVERSITY

Asst. Prof. Hasan F. ATEŞ IŞIK UNIVERSITY

APPROVAL DATE: 10/March/2006

NEW APPROACHES FOR CHANNEL ESTIMATION IN WIRELESS COMMUNICATIONS

Abstract

This thesis first proposes a computationally efficient, pilot-aided linear minimum mean square error (MMSE) batch channel estimation algorithm for the orthogonal frequency division multiplexing OFDM systems in unknown wireless fading channels. The batch linear MMSE will be converted to the sequential linear MMSE estimator due to fast convergence property and the simple structure. In addition to OFDM systems, focusing on transmit diversity (OFDM) transmission through frequency selective channels, this thesis pursues a channel estimation approach in time-domain for both space-frequency OFDM (SF-OFDM) and space-time OFDM (ST-OFDM) systems. This thesis also proposes a computationally efficient, pilot-aided linear minimum mean square error (MMSE) time domain batch channel estimation algorithm for OFDM systems with transmit diversity in unknown wireless fading channels.

The proposed batch approaches (with or without transmit diversity) employ a convenient representation of the discrete multipath fading channel based on the Karhunen Loeve (KL) orthogonal expansion and finds MMSE estimates of the uncorrelated KL series expansion coefficients. Based on such an expansion, no matrix inversion is required in the proposed MMSE estimators. Moreover, optimal rank reduction is achieved by exploiting the optimal truncation property of the KL expansion resulting in a smaller computational load on the estimation algorithm. The performance of the proposed approaches is studied through analytical and experimental results.

Then, in order to explore the performances, the stochastic Cramer-Rao lower bounds are considered for the proposed approaches. The effect of a modeling mismatch on the performances of the estimator is also analyzed.

In order to explore the performance of the transmit diversity OFDM systems, the closed-form expression for the average symbol error rate (SER) probability is also derived for the maximum ratio receive combiner (MRRC) in these systems. Simulations results confirm our theoretical analysis, and illustrate that the proposed channel estimation algorithms for OFDM systems with and without transmit diversity are capable of tracking fast fading and frequency selective fading, respectively and improving overall performance.

TELSİZ HABERLEŞMEDE KANAL KESTİRİMİ İÇİN YENİ YAKLAŞIMLAR

Özet

Bu tez öncelikle, sönümlemeli, telsiz iletişim kanalı etkisi altındaki dik sıklık bölüşümlü çoğullama (OFDM) sistemleri için, işlem yükü az, pilot destekli doğrusal en küçük ortalama karesel hata (MMSE) toptan kanal kestirimcisi algoritması önerir. Toptan doğrusal MMSE kanal kestirimcisi, hızlı yakınsaması ve basit bir yapıya sahip olmasından dolayı dizisel doğrusal MMSE kestirimcisine dönüştürülecektir. Bunun yanısıra, bu tez; frekans seçici kanallar üzerinden iletim sağlayan verici çeşitlemeli OFDM sistemlerine odaklanarak, zaman düzleminde, hem uzay-zaman hem de uzay-frekans çeşitlemeli OFDM sistemleri için bir kanal kestirim yaklaşımı ortaya koyma amacını taşımaktadır. Ayrıca bu tez, sönümlemeli, telsiz iletişim kanalı etkisi altındaki verici çeşitlemeli OFDM sistemleri için de işlem yükü az, pilot destekli doğrusal en küçük ortalama karesel hata (MMSE) zaman düzlemi kanal kestirimcisi algoritması önerir.

Önerilen toptan yaklaşımlar (verici çeşitlemeli yada çeşitlemesiz), Karhunen Loeve (KL) dik açılımına dayanan, ayrık çokyollu sönümlemeli kanalı elverişli gösterilimine olanak tanır ve ilişkisiz KL açılım katsayılarının MMSE kestirim değerlerini bulur. Böyle bir açılıma göre, önerilen MMSE kestirimcilerinde matris evriğine gereksinim yoktur. Bunun ötesinde, uygun kerte indirgemesi, kestirim algoritması üzerinde daha küçük bir işlem yükü doğuran KL açılımının uygun kısaltılabilme özelliğinin kullanılması ile başarılır. Önerilen yaklaşımların başarımları analitik ve deneysel sonuçlarla incelenmektedir.

Daha sonra, başarımları araştırmak için önerilen yaklaşımlar için stokastik Cramer-Rao alt sınırları ele alınmaktadır. Modelleme hatasının kestirimcilerin başarımları üzerindeki etkileri analiz edilmektedir.

Verici çeşitlemeli OFDM sistemlerinin başarımını araştırmak için en yüksek oran alınan sinyal birleştiricisi (MRRC) için ortalama sembol hata olasılığının (SER) çıkartımı da yapılmaktadır. Benzetim sonuçları kuramsal sonuçlarımızı doğrulamakta, verici çeşitlemeli veya çeşitlemesiz OFDM sistemleri için önerilen kanal kestirim algoritmaları sırasıyla hızlı sönümlemeli ve frekans seçici sönümlemeli kanalları izlemekte ve bütün sistemin başarımını arttırmaktadır.

Acknowledgements

I wish to thank my supervisor Assoc. Prof. Uluğ BAYAZIT for his encouraging and comments on the technical content of my thesis.

I would like to express my most sincere appreciation to my co-supervisor Prof. Erdal PANAYIRCI for his constructive criticisms, suggestions, ideas and advises during the development of this thesis. I would also like to thank Assoc. Prof. Hakan A. ÇIRPAN for his patient guidance.

The deepest gratitude goes to my wife Canan and my two-year-old son Mert for their love and support.

Table of Contents

List of Figures

List of Symbols

$\mathbf{A}$: Diagonal pilot symbol matrix in linear model for OFDM system

$\mathbf{A}_n$: Diagonal symbol matrix for *n*th OFDM block

B_c : Coherence bandwidth

B_d : Doppler spread

$\mathbf{B}_{MSE}$: The Minimum Bayesian Mean Square Error

B_s : Bandwidth

C : Power normalization constant

$\mathbf{C}_{\boldsymbol{\varepsilon}}$: Covariance matrix of estimation error

$\mathbf{C}_{\hat{\boldsymbol{\varepsilon}}_{\mu}}$: Covariance matrix of $\hat{\boldsymbol{\varepsilon}}_{\mu}$

$\mathbf{C}_{\hat{\boldsymbol{\varepsilon}}_{\mu_r}}$: Covariance matrix of $\hat{\boldsymbol{\varepsilon}}_{\mu_r}$

$\mathbf{C}_{\mathbf{h}}$: Covariance matrix of the multipath channel $\mathbf{h}$

$\mathbf{C}_{\tilde{\mathbf{h}}}$: Covariance matrix of $\tilde{\mathbf{h}}$

$\mathbf{C}_{\mathbf{H}}$: Covariance matrix of the channel $\mathbf{H}$

$\mathbf{C}_{\tilde{\boldsymbol{\eta}}}$: Covariance matrix of the noise term $\tilde{\boldsymbol{\eta}}$

cos (.) : cosine function

$\mathbf{C}_{\Theta|Z}$: Posterior covariance matrix of the vector parameter Θ

$\mathbf{C}_{\mathbf{W}}$: Covariance matrix of the noise vector $\mathbf{w}$

E_S : signal energy

$\breve{E}_S$: faded signal energy at MRRC

$E[.]$: Expectation operator

$\mathbf{F}$: $K \times L$ Submatrix of the $K \times K$ FFT matrix

$\mathbf{F}^{-1}\{.\}$: Continuous frequency inverse Fourier transform operator

f_d : Doppler shift frequency

$f_d(\alpha)$: Instantaneous Doppler frequency

f_m : Maximum Doppler shift frequency

f_{m+1} : Prediction error of the sequential MMSE estimator at iteration (m+1)

$\mathbf{g}$: KL coefficient vector

$\hat{\mathbf{g}}$: estimate of $\mathbf{g}$

$\tilde{\mathbf{g}}$: KL coefficients vector for true multipath channel $\tilde{\mathbf{h}}$

$\mathbf{g}_\mu$: KL expansion coefficient vector for $\mathbf{h}_\mu$

$\tilde{\mathbf{g}}_\mu$: KL expansion coefficient vector for $\tilde{\mathbf{h}}_\mu$

$\hat{\mathbf{g}}_{\mu_r}$: Estimation value of $\mathbf{g}_\mu$ for the low rank approach

g_ℓ : *l*th element of KL coefficient vector $\mathbf{g}$

$\mathbf{g}_r$: Truncated KL coefficient vector

$\mathbf{h}$: multipath channel vector

$\hat{\mathbf{h}}$: Estimation value of the multipath channel $\mathbf{h}$

$\tilde{\mathbf{h}}$: True value of the multipath channel vector $\mathbf{h}$

$\mathbf{h}_i$: *i* th element of the multipath channel $\mathbf{h}$

$\mathbf{h}_\mu$: Multipath channel between the μ th transmitter and the receiver

$\tilde{\mathbf{h}}_\mu$: True value of $\mathbf{h}_\mu$

$\mathbf{h}_\mu(n)$: Multipath channel for μ th transmit antenna at time n

$\mathbf{h}_n$: channel impulse response during the *n*th OFDM block

$\hat{\mathbf{H}}$: Estimated frequency response of the channel

$\mathbf{H}_n$: Frequency domain channel vector for *n*th OFDM block

$\mathbf{H}_\mu(n)$: channel frequency response between the μ th transmitter and receiver

$\mathbf{H}_{\mu,e}(n)$: Even component vectors of the channel attenuations between μth transmitter and the receiver for *n*th block

$\mathbf{H}_{\mu,o}(n)$: Odd component vectors of the channel attenuations between μth transmitter and the receiver for *n*th block

$\mathbf{H}_{\mu,p}$: Frequency domain channel effect at pilot locations between μth transmitter and receiver

$\mathbf{I}_K$: $K \times K$ identity matrix

$\mathbf{I}_{Kp}$: $K_p \times K_p$ identity matrix

$\mathbf{I}_L$: $L \times L$ identity matrix

$\mathbf{J}(\mathbf{g})$: Conditional Fisher Information Matrix for $\mathbf{g}$

$\mathbf{J}_M(\mathbf{g})$: modified Fisher Information Matrix for $\mathbf{g}$

$J_0(.)$: *zero* th order Bessel function

$\mathbf{J}_P(\mathbf{g})$: Priori Fisher Information Matrix for $\mathbf{g}$

K : Number of the subcarriers in OFDM systems

$\boldsymbol{\kappa}_{m+1}$: Gain factor at iteration (m+1) in sequential MMSE estimator

K_p : Number of pilot symbols per OFDM block

ln : Natural logarithm

L : Multipath channel order

L_{CP} : cyclic prefix length

$\mathbf{M}_{m+1}$: Covariance matrix of estimation error at iteration (m+1)

n : block index

p (.) : probability density function

Pr (.) : probability of (.)

P_R : Total received power

$\mathcal{Q}(.)$: cost function

Q(.) : Q function

$\mathcal{R}$: Bayes risk

$S(f)$: Doppler power spectrum

sin (.) : sine function

T_c : Coherence time

T_S : Sampling period

T_{sym} : OFDM symbol duration

$\mathbf{u}^{\dagger}(m)$: mth element of the coefficient vector in sequential MMSE estimator

$\mathbf{X}(n)$: n^{th} OFDM symbol

$\mathcal{X}_e(n)$: Diagonal symbol matrix for even indexed subchannels

$\mathcal{X}_o(n)$: Diagonal symbol matrix for odd indexed subchannels

$\mathbf{X}(n,k)$: Transmitted symbol over k^{th} subchannel at time n

$\mathbf{X}_{\mu}(n)$: Transmitted symbol vector over μ^{th} antenna at time n

v : Velocity

$\mathbf{Y}$: Receive vector

$\tilde{\mathbf{Y}}$: Observation vector in OFDM model

$\mathbf{Y}_e(n)$: Even components of the receive vector for nth block

$\mathbf{Y}_o(n)$: Odd components of the receive vector for nth block

$\tilde{\mathbf{Y}}[m]$: mth component of the frequency domain receive vector $\tilde{\mathbf{Y}}$

$\mathbf{Y}_n$: Frequency domain receive vector for nth OFDM block

$\tilde{\mathbf{Y}}_p$: receive term in unified linear model for ST/SF-OFDM system

$\tilde{\mathbf{Y}}_{\mu,p}$: μth column vector of $\tilde{\mathbf{Y}}_p$

$\mathbf{Z}$: Observation vector in observation model

α : Spatial angle (angle of arrival)

α : transform variables in SER expression for ST/SF-OFDM

$\boldsymbol{\beta}$: Real part of the cross correlation matrix between $\tilde{\mathbf{g}}$ and $\mathbf{g}$

β_i : ith diagonal element of the real part of the cross correlation matrix between $\tilde{\mathbf{g}}$ and $\mathbf{g}$

$\gamma_1, \gamma_2, \gamma_3$: Terms in SER expression for ST/SF-OFDM

δ : Very small positive number

$\delta_{m+1|m}$: A small positive number used in calculation of MSE_{m+1} by using M_m

Δ : Pilot spacing interval

$\Delta\ell$: Difference between transmitter A and transmitter B paths

$\Delta\Phi$: Phase change

Δt : Time interval

ε : Estimation error in estimation theory (see Appendix A)

$\hat{\varepsilon}$: Estimation error

$\hat{\boldsymbol{\varepsilon}}_r$: Estimation error for truncated KL coefficient vector

$\hat{\boldsymbol{\varepsilon}}_\mu$: Estimation error for the parameter $\mathbf{g}_\mu$

$\hat{\boldsymbol{\varepsilon}}_{\mu_r}$: Estimation error of the parameter $\mathbf{g}_\mu$ for the low rank approach

ς : Transform variables in SER expression for ST/SF-OFDM

$\boldsymbol{\eta}$: Noise vector in linear model for OFDM system

$\tilde{\boldsymbol{\eta}}$: Noise term

$\boldsymbol{\eta}_n$: *n*th elements of noise vector in OFDM system model

$\boldsymbol{\eta}_e(n)$: Even components of the noise vector for *n*th block

$\tilde{\boldsymbol{\eta}}[m]$: *m*th element of the noise term in sequential MMSE estimator

$\boldsymbol{\eta}_o(n)$: Odd components of the noise vector for *n*th block

$\tilde{\boldsymbol{\eta}}_{\mu,p}$: μth column vector of $\tilde{\boldsymbol{\eta}}_p$

$\tilde{\boldsymbol{\eta}}_p$: Noise term in unified linear model for ST/SF-OFDM system

Θ : Parameter to be estimated

$\hat{\Theta}$: Estimated value of the parameter Θ

$\theta(\tau)$: Power delay profile

λ : Wave length

λ_i : *i*th singular value of the covariance matrix $\mathbf{C}_\mathbf{h}$

$\tilde{\lambda}_i$: *i*th diagonal element of $\boldsymbol{\Lambda}_{\tilde{\mathbf{g}}}$

ξ : Term in SER expression

σ^2 : Noise variance

τ : Excess delay

$\bar{\tau}$: Mean excess delay

τ_{rms} : Rms delay spread

$\boldsymbol{\Psi}$: Unitary matrix formed by orthonormal base vectors

$\boldsymbol{\psi}_{\ell}$: *l*th orthogonal column vector in KL expansion

Ω_{g} : Normalized variance of the channel gains

$\boldsymbol{\Lambda}_{\mathbf{g}}$: Covariance matrix of $\mathbf{g}$

$\boldsymbol{\Lambda}_{\mathbf{g}_r}$: Covariance matrix of $\mathbf{g}_r$

$\boldsymbol{\Gamma}$: Coefficient matrix appearing in the expression of the MMSE estimator for $\mathbf{g}$

$\boldsymbol{\Gamma}_{\mathsf{r}}$: Coefficient matrix appearing in the expression of the truncated MMSE estimator for $\mathbf{g}$

$\ddot{\boldsymbol{\Gamma}}_{\mathsf{r}}$: Coefficient matrix appearing in the expression of the truncated MMSE estimator for $\mathbf{g}_{\mu}$

$\|.\|^2$: Absolute square operator

$|.|$: Determinant operator

$(\cdot)^{\dagger}$: Hermitian transpose operator

$(\cdot)^{\mathsf{T}}$: Transpose operator

$(\cdot)^{-1}$: Inverse operator

List of Abbreviations

ADSL	: Asymetric Digital Subscriber Line
AWGN	: Additive White Gaussian Noise
CDMA	: Code Division Multiple Access
CRLB	: Cramer-Rao Lower Bound
CP	: Cyclic Prefix
DAB	: Digital Audio Broadcasting
DMT	: Discrete Multi Tone
DVB	: Digital Video Broadcasting
FDM	: Frequency Division Multiplexing
FIM	: Fisher Information Matrix
FFT	: Fast Fourier Transform
HF	: High Frequency
ICI	: Inter-carrier Interference
IFFT	: Inverse Fast Fourier Transform
ISI	: Intersymbol Interference
KL	: Karhunen-Loeve
LMS	: Least Mean Square
MAP	: Maximum a Posteriori
MC	: Multicarrier
ML	: Maximum Likelihood
MLE	: Maximum Likelihood Estimator
MMSE	: Minimum Mean Square Error
MRRC	: Maximal Ratio Receive Combiner
MSE	: Mean Square Error

MVU	: Minimum Variance Unbiased
OFDM	: Orthogonal Frequency Division Multiplexing
PDF	: Probability Density Function
PSK	: Phase Shift Keying
QPSK	: Quadrative Phase Shift Keying
RLS	: Recursive Least Squares
RF	: Radio Frequency
SER	: Symbol Error Rate
SF	: Space Frequency
SFBC	: Space Frequency Block Code
SF-OFDM	: Space Frequency Orthogonal Frequency Division Multiplexing
SNR	: Signal to Noise Ratio
ST	: Space Time
STBC	: Space Time Block Code
ST-OFDM	: Space Time Orthogonal Frequency Division Multiplexing
SVD	: Singular Value Decomposition
WGN	: White Gaussian Noise

Chapter 1

Introduction

With unprecedented demands on bandwidth due to the explosive growth of broadband wireless services usage, there is an acute need for a high rate and bandwidth efficient digital transmission. In response to this need, the research community has been extensively investigating efficient schemes that make efficient utilization of the limited bandwidth and cope with the adverse access environments, Van Nee and Prasad [1]. These access environments may create different channel impairments and dictate unique sets of advanced signal processing algorithms to combat specific impairments.

Multicarrier (MC) transmission scheme, especially, orthogonal frequency division multiplexing (OFDM), has recently attracted considerable attention since it has been shown to be an effective technique to combat delay spread or frequency selective fading of wireless or wireline channels thereby improving the capacity and enhancing the performance of transmission. This approach has been adopted as the standards in several outdoor and indoor high-speed wireless and wireline data applications, including terrestrial digital broadcasting (DAB and DVB) in Europe, and high speed modems over Digital Subscriber Lines in the US. It has also been implemented for broadband indoor wireless systems including IEEE802.11a, MMAC and HIPERLAN/2.

An OFDM system operating over a frequency selective wireless communication channel effectively forms a number of parallel frequency nonselective fading channels thereby reducing intersymbol interference (ISI) and obviating the need for

complex equalization thus greatly simplifying channel estimation/equalization task. Moreover, OFDM is bandwidth efficient since the spectra of the neighboring subchannels overlap, yet channels can still be separated through the use of orthogonality of the carriers. Furthermore, its structure also allows efficient hardware implementations using fast Fourier transform (FFT) and polyphase filtering, Sari *et al*. [2].

Transmit diversity can effectively combat multipath channel impairments due to the dispersive wireless channel that can cause deep fades in some subchannels. This is generally achieved by separating transmit antennas far enough so that to make zero or very low correlation between the transmission paths. The combination of the two techniques, OFDM and transmit diversity, can further enhance the data rates in a frequency selective fading environment. However, this enhancement requires accurate and computationally efficient channel estimation methods.

The motivation for the thesis is to develop a low complexity pilot aided channel estimation algorithms for OFDM systems with/without transmit diversity and to analyze its performance both theoretically and analytically.

1.1 Previous Works

Pilot aided channel estimation in OFDM systems with and without transmit diversity has been studied in [3–11] and [12–19] respectively. Pilot based algorithms assume known symbols (training or pilot symbols) are inserted in the transmitted signals. It is then possible to identify the channel at the receiver through exploiting knowledge of these known symbols.

Edfors *et al.* [3] applied the theory of optimal rank-reduction to linear MMSE estimator, and presented a low rank channel estimation algorithm, which exploits only the frequency domain channel correlation.

Although channel correlation and signal-to-noise ratio (SNR) are needed in the channel estimation algorithm, its performance is robust to changes in channel correlation and SNR. Two pilot-aided ML and MMSE estimator schemes are revisited and compared in terms of computational complexity by Morelli and Mengali [4]. The difference between these two estimators is in their assumptions of the channels. The ML algorithm regards the channel as a deterministic but unknown vector, whereas MMSE algorithm regards the channel as a random vector, whose particular realization is to be estimated. The ML algorithm achieves the Cramer-Rao Lower Bound (CRLB); therefore it is a Minimum Variance Unbiased (MVU) estimator. Minimum MSE is achieved on the condition that the channel is considered deterministic and the estimator is unbiased. With the aid of prior channel information, the MMSE algorithm outperforms the CRLB, because CRLB is a bound for deterministic channel. With more available information about the channel, MMSE algorithm obtains a better performance. Li *et al*. [5] proposed a MMSE channel estimator algorithm, which makes full use of the time and frequency correlation of the time-varying dispersive channel. The algorithm exploits both time domain and frequency domain channel correlation, and makes use of the fact that the OFDM channel correlation can be written as the product of time domain channel correlation and frequency domain channel correlation. Moreover, a low complexity MMSE doubly channel estimation approaches based on embedding Kronecker Delta pilot sequences were presented by Schniter [6]. Biglieri *et al*. [7] studied on multipath fading channels extensively, and developed several models to describe their variations. In many cases, the channel taps are modeled as general lowpass stochastic processes (e.g., Jakes [8]); the statistics depend on mobility parameters. Yip and Ng [9] proposed a different approach modeling the multipath channel taps by the Karhunen Loeve (KL) series representation. Senol *et al*. [10] and Siala and Dupontiel [11] have also been KL expansion models used in modeling multipath channel within OFDM and CDMA scenarios, respectively.

Transmit antenna diversity technique has been used for combating fading in mobile in multipath wireless channels by Li *et al*. [12], Alamouti [13], and Cirpan and Panayirci[14]. Among a number of antenna diversity methods, the Alamouti method

is very simple to implement. The simplicity of the receiver is attributed to the orthogonal nature of the code by Tarokh *et al*. [15, 16]. In Alamouti scheme, the orthogonal structure of these codes enables the maximum likelihood decoding to be implemented in a simple way through decoupling of the signal transmitted from different antennas rather than joint detection resulting in linear processing. The use of OFDM in transmits diversity systems motives exploitation of the diversity dimensions. Inspired by this, a number of coding schemes have been proposed recently to achieve maximum diversity gain by Lee and Williams [17], Liu *et al*. [18], and Bolcskei and Paulraj [19]. Among them, ST-OFDM has been proposed recently for delay-spread channels. On the other hand, transmit OFDM also offers the possibility of coding in the form SF-OFDM. Moreover, Lee and Williams [17] compared SF-OFDM and ST-OFDM transmit diversity systems, under the assumption that the channel responses are known or can be estimated accurately at the receiver. It was shown that the SF-OFDM system has the same performance as a previously reported ST-OFDM scheme in slow fading environments but shows better performance in the more difficult fast fading environments.

1.2 Contributions of the Thesis

This thesis is a deep and thorough study of channel estimation problems in OFDM systems with or without transmit diversity. Contributions of the thesis can be detailed as follows:

- To propose a computationally efficient, pilot aided MMSE channel estimation algorithms by exploiting Karhunen Loeve (KL) expansion. Based on such representation, no matrix inversion is required in the proposed batch approach. Moreover, optimal rank reduction can be achieved by exploiting the optimal truncation property of the KL expansion resulting in a smaller computational load on the estimation algorithm.
- To propose a simple sequential MMSE estimator implementation for the estimation of the KL expansion coefficients since it does not require performing matrix inversion as well without transmit diversity only.

- To propose a computationally efficient MMSE channel estimation algorithm for ST-OFDM and SF-OFDM systems focusing on transmit diversity OFDM transmissions through frequency selective fading channels. Again, the KL expansion scheme is employed in the development of the MMSE channel estimation algorithm for ST-OFDM and SF-OFDM systems in order to reduce the computational complexity. The complete analytical SER analysis for 2Tx-1Rx antennas SF/ST-OFDM scheme, which have not appeared in the literature yet, is derived.

In the thesis, the performances of the proposed approaches are explored based on the evaluation of the stochastic Cramer Rao bound for the random KL coefficients and the effect of the modeling mismatch on the performances of the estimators is also presented.

1.3 Organization

This thesis consists of five chapters, six appendices, and a bibliography. A brief summary of each chapter follows:

Chapter 1 is the introduction including the previous works and the contributions of the thesis.

Chapter 2 describes the fading channel types and includes their models needed for channel simulation. Basic principles of conventional OFDM systems are also included in this chapter.

Chapter 3 introduces the basic concepts of OFDM systems and presents a mathematical model of a conventional OFDM system. According to this mathematical model, a computational efficient pilot aided truncated MMSE channel estimation algorithm for OFDM systems is proposed and the performance analysis of the estimator is given. As an original contribution Chapter 3 includes also a simple sequential MMSE estimation for the estimation of the multipath channel KL

expansion coefficients and the performance analysis of the sequential estimator. Simulation results for both batch and sequential MMSE channel estimators are also discussed.

Chapter 4 introduces space-time and space-frequency transmits diversity coding scheme employed in an OFDM system. In this chapter, a computational efficient pilot-aided truncated MMSE channel estimation algorithm for space-time / space-frequency coded OFDM systems is proposed and the performance analysis is given. Simulation results for pilot aided truncated MMSE channel estimation algorithm for space-time / space-frequency coded OFDM systems are also given.

Finally, Chapter 5 presents the conclusion and the further works.

Chapter 2

Fading Channel Models and OFDM Principles

In this section, both frequency and time correlation of a channel and their parameters will be given. First, fading types will be presented since channel correlations depend on fading types effecting the wireless channel. Then, a conventional OFDM systems being a superior solution to overcome frequency selective fading will be introduced.

The rapid fluctuation of the amplitude of a radio signal over a short period of time is described by fading. Interference between attenuated, reflected, refracted, and diffracted versions of the transmitted signal causes multipath fading. These signals are combined at the receiver antenna, and amplitude and phase of the resulting signal can very in amplitude and phase depend on the distribution of the intensity and relative propagation time of the waves and the bandwidth of the transmitted signal.

The most important multipath fading effects can be given as:

- Multiple versions of the transmitted signals caused by multipath propagation delays.
- Randomness in frequency because of Doppler shifts on different multipath signals.
- Rapid changes in signal strength over a small time interval.

There are many physical factors influencing fading. These factors can be summarized as follows:

- Reflecting objects and scatters in the channel creates a constantly changing environment that dissipates the signal energy in amplitude, phase and time. These effects result in multiple versions of the transmitted signal that arrive at the

receiving antenna, displaced with respect to one another in time and spatial orientation. This causes intersymbol interference (ISI) at the receiver side.

- The relative motion between the base station and the mobile results in random frequency modulation due to different Doppler shifts on each of the multipath components. Doppler shift can be positive or negative depending on the direction of the mobile receiver.
- If surrounding objects in the radio channel are in motion, they causes a time varying Doppler shift on multipath components. If the surrounding objects move at a greater rate than the mobile, then this effect dominates fading. Otherwise, only the speed of the mobile need be considered.
- If the transmitted radio signal bandwidth is greater than the "bandwidth" of the multipath channel, the received signal will be distorted. If the transmitted signal has a narrow bandwidth as compared to the channel, the amplitude of the signal will change rapidly, but the signal will not be distorted in time. As will be shown, the bandwidth of the channel can be quantified by the *coherence bandwidth*, which is related to the specific multipath structure of the channel. The coherence bandwidth is a measure of the maximum frequency difference for which signals are still strongly correlated in amplitude.

2.1 Doppler Shift

Consider a mobile receiver moving at a velocity v from A to B and receiving signals from a source, as shown in Figure 2.1. Δt is the time required for the mobile to travel from A to B, and α is assumed to be the same at points A and B because the source is assumed to be very far away. The phase change in the received signal due

to the difference in path lengths is therefore

$$\Delta\Phi = \frac{2\pi(\Delta\ell)}{\lambda} = \frac{2\pi(v\,\Delta t)}{\lambda}\cos(\alpha) \tag{2.1}$$

where α is the spatial angle, and hence the apparent change in frequency, or Doppler

shift f_d is given as

$$f_d = \frac{1}{2\pi}\frac{\Delta\Phi}{\Delta t} = \frac{v}{\lambda}\cos(\alpha) \tag{2.2}$$

and the maximum Doppler shift is $f_m = v/\lambda$.

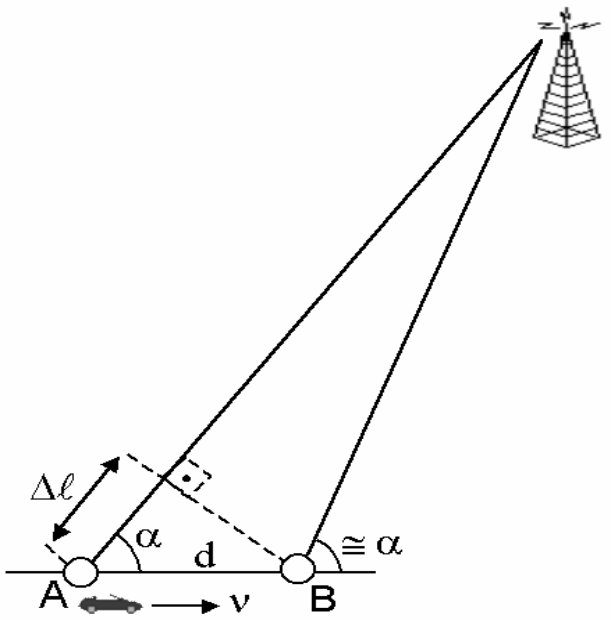

Figure 2.1 Illustration of Doppler Effect

From Equation (2.2), It can be deduced that if the mobile receiver is moving toward the direction of arrival of the wave, the Doppler shift is positive (in other words, received frequency is increased), and if the mobile is moving away from the direction of arrival of the wave, the Doppler shift is negative (received frequency is decreased).

2.2 Multipath Channel Parameters

The power delay profile plays an important role in the derivation of many multipath channel parameters. The power delay profile is the expected power per unit of time received with a certain excess delay.

2.2.1 Time Dispersion Parameters

The time dispersive properties of multipath channels are most commonly quantified by their mean excess delay $(\bar{\tau})$ and rms delay spread (τ_{rms}). The *mean excess delay and rms delay spread* are multipath channel parameters that can be determined from a power delay profile. The mean excess delay is the first moment of the power delay profile and is defined to be

$$\bar{\tau} = \frac{\int_0^\infty \theta(\tau)\tau\, d\tau}{\int_0^\infty \theta(\tau)\, d\tau} \tag{2.3}$$

The rms delay spread is the square root of the second central moment of the power delay profile and is defined to be

$$\tau_{rms} = \sigma_\tau = \sqrt{\overline{\tau^2} - \bar{\tau}^2} \tag{2.4}$$

where

$$\overline{\tau^2} = \frac{\int_0^\infty \theta(\tau)\tau^2\, d\tau}{\int_0^\infty \theta(\tau)\, d\tau} \tag{2.5}$$

In this thesis, the power delay profile for multipath channel will be characterized by an exponential function of excess delay τ as follows

$$\theta(\tau) = Ce^{-\tau/\tau_{rms}} \tag{2.6}$$

where C is the power normalization constant. It should be noted that the power delay

profile and the frequency domain correlation function of a mobile radio channel are related through the Fourier transform. We now assume that the excess delay is in the interval $0 \le \tau \le L$. Then the frequency domain correlation function of the channel is

$$c_f(f-f') = F\{\theta(\tau)\} = \int_0^L \theta(\tau) e^{-j2\pi(f-f')\tau} d\tau = C \frac{1 - e^{-L\left(\frac{1}{\tau_{rms}} + j2\pi(f-f')\right)}}{\frac{1}{\tau_{rms}} + j2\pi(f-f')} \tag{2.7}$$

where constant C is calculated as

$$C = \frac{1}{\int_0^L \theta(\tau)\, d\tau} = \frac{1}{\tau_{rms}\left(1 - e^{\frac{-L}{\tau_{rms}}}\right)} \tag{2.8}$$

for power normalization. Substituting (2.8) in (2.7), frequency domain correlation of the channel is obtained as follows,

$$c_f(f-f') = \frac{1 - e^{-L\left(\frac{1}{\tau_{rms}} + j2\pi(f-f')\right)}}{\tau_{rms}\left(1 - e^{\frac{-L}{\tau_{rms}}}\right)\left(\frac{1}{\tau_{rms}} + j2\pi(f-f')\right)} \tag{2.9}$$

Replacing $(f-f')$ by $(k-k')/K$ in (2.9), frequency domain discrete channel correlation can also be given as in Edfords *et al*. [3],

$$c_f(k-k') = \frac{1 - e^{-L\left(\frac{1}{\tau_{rms}} + j\frac{2\pi(k-k')}{K}\right)}}{\tau_{rms}\left(1 - e^{\frac{-L}{\tau_{rms}}}\right)\left(\frac{1}{\tau_{rms}} + j\frac{2\pi(k-k')}{K}\right)} \tag{2.10}$$

where K is the number of the discrete frequency points in the channel bandwidth (or the number of the subcarriers in OFDM systems).In this thesis, discrete channel correlation in (2.10) is used in order to generate a multipath channel.

Coherence bandwidth B_c is also used to characterize the channel in the frequency domain, like delay spread parameters in the time domain. The rms delay spread τ_{rms} and coherence bandwidths are inversely proportional to one another.

2.2.2 Coherence Bandwidth

Coherence bandwidth B_c, is a defined relation derived from the rms delay spread τ_{rms}. Coherence bandwidth is a statistical measure of the range of frequencies over which the channel can be considered "flat". In other words, the channel affects two sinusoids with frequency separation greater than B_c quite differently. If the coherence bandwidth is defined as the bandwidth over which the frequency correlation function is above 0.9, then the coherence bandwidth is approximately,

$$B_c \approx \frac{1}{50\,\tau_{rms}} \tag{2.11}$$

If the frequency correlation function is above 0.5, then the coherence bandwidth is approximately

$$B_c \approx \frac{1}{5\,\tau_{rms}} \tag{2.12}$$

and also called as 50% coherence bandwidth.

2.2.3 Coherence Time

Coherence bandwidth and delay spread are parameters describing the time dispersive nature of the channel in a local area. They don't offer information about the time varying nature of the channel caused by either relative motion between the mobile

and the base station, or by movement of objects in the channel. *Doppler spread* and *coherence time* are parameters describing the time varying nature of the channel.

Coherence time T_c is the time domain dual of Doppler spread and is used to characterize the time varying nature of the frequency dispersiveness of the channel in the time domain. The Doppler spread and coherence time are inversely proportional to one another. That is,

$$T_c \approx \frac{1}{f_m} \tag{2.13}$$

The definition of coherence time implies that two signals arriving with a time separation greater than T_c are affected differently by the channel. If the coherence time is defined as the time over which the time correlation function is above 0.5, then the coherence time is approximately,

$$T_c \cong \frac{9}{16\pi f_m} \tag{2.14}$$

where f_m is the maximum Doppler shift.

2.3 Fading Types

The time dispersion and frequency dispersion structures of a mobile radio channel lead to four possible distinct fading effects. While multipath delay spread leads to *time dispersion* and *frequency selective fading*, Doppler spread leads to *frequency dispersion* and *time selective fading*.

The two propagation mechanisms are independent of one another. According to the relation between the signal parameters (such as bandwidth, symbol period T_s, etc.) and the channel parameters (such as rms delay spread and Doppler spread), four types of fading can be defined. Figure 2.2 and Figure 2.3 show a tree of the four different types of fading.

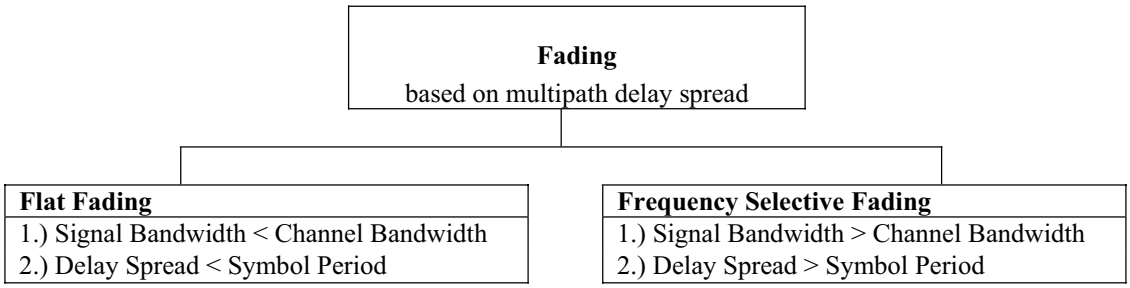

Figure 2.2 Types of fading based on multipath delay spread

2.3.1 Flat Fading

If the channel has a constant gain and linear phase response over a bandwidth, which is greater than the bandwidth of the transmitted signal, then the received signal undergoes *flat fading*. Therefore, flat fading channels can be considered as having no excess delay. The most common instantaneous amplitude distribution of the channel is the Rayleigh distribution. To summarize, a signal undergoes flat fading if

$$B_s << B_c \tag{2.15}$$

and

$$T_{sym} >> \tau_{rms} \tag{2.16}$$

where T_{sym} is the symbol period and B_s is the signal bandwidth, respectively, of the transmitted modulation, and τ_{rms} and B_c are the rms delay spread and coherence bandwidth, respectively, of the channel.

2.3.2 Frequency Selective Fading

If the channel impulse response has a multipath delay spread, which is greater than the symbol period, then the channel creates *frequency selective fading* on the received signal. When this occurs, the received signal includes multiple versions of the transmitted waveform, which are attenuated (faded) and delayed in time, and hence the received signal is distorted. Thus the frequencies selective fading channel

results in *intersymbol interference* (ISI). For frequency selective fading, the spectrum of the transmitted signal has a bandwidth, which is greater than the coherence bandwidth of the channel. In other words, in the frequency domain, the channel becomes frequency selective, where the gain is different for different frequency components. To summarize, a signal undergoes frequency selective fading if

$$B_s > B_c \tag{2.17}$$

and

$$T_{sym} < \tau_{rms} \tag{2.18}$$

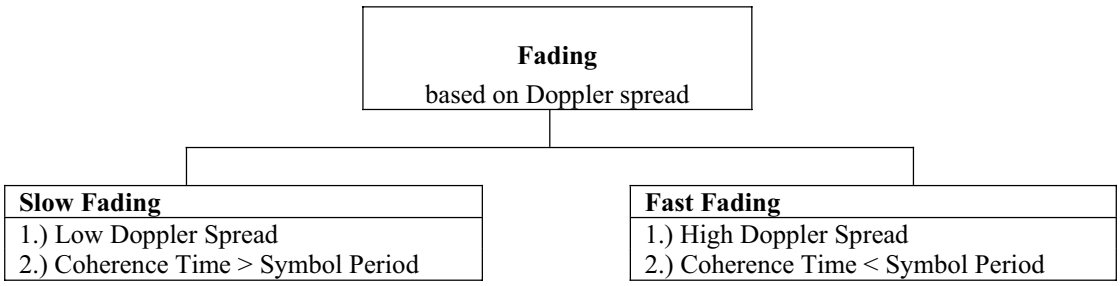

Figure 2.3 Types of fading based on Doppler spread

2.3.3 Slow Fading

The radio channel is called as slow fading channel, if the Doppler spread of the channel is much less than the bandwidths of the baseband signal. This implies that the channel impulse response changes at a rate much slower than the transmitted baseband signal. In this case, the channel may be assumed to be static over one or several symbol durations. Therefore, a signal undergoes slow fading if

$$T_{sym} << T_c \tag{2.19}$$

and

$$B_s >> B_d \tag{2.20}$$

where B_d is the Doppler spread.

Note that the velocity of the mobile and the baseband signalling determines whether a signal undergoes fast fading or slow fading.

2.3.4 Fast Fading

In a *fast fading* channel, the channel impulse response changes rapidly within the symbol duration. That is, the coherence time of the channel is smaller than the symbol period of the transmitted signal. Signal distortion due to fast fading increases with increasing Doppler spread relative to the bandwidth of the transmitted signal. Therefore, a signal undergoes fast fading if

$$T_{sym} > T_c \tag{2.21}$$

and

$$B_s < B_d \tag{2.22}$$

Fast fading only deals with the rate of change of the channel due to motion. In the case of the flat fading channel, we can approximate the impulse response to be simply a delta function (no time delay). Hence a *flat - fast fading* channel is a channel in which the amplitude of the delta function varies faster than the rate of the change of the transmitted baseband signal. In the case of a *frequency selective - fast fading* channel, the amplitudes, phases, and time delays of any one of the multipath components vary faster than the rate of change of the transmitted signal. Possible combinations of these fadings are illustrated in Figure 2.4 and Figure 2.5.

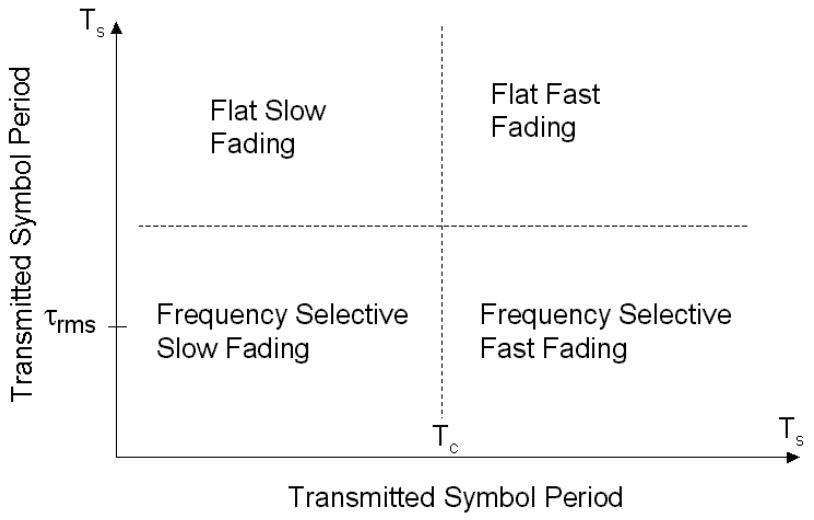

Figure 2.4 Matrix illustrating type of fading as a function of symbol period

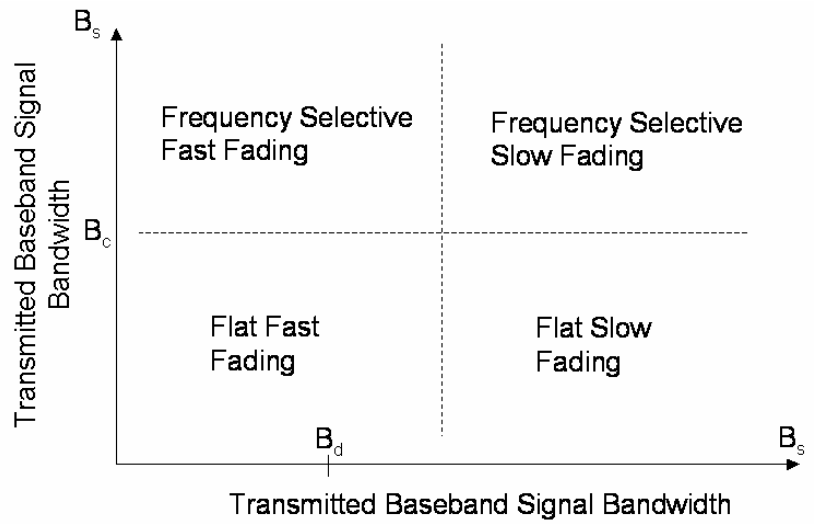

Figure 2.5 Matrix illustrating type of fading as a function of baseband signal bandwidth

2.4 Doppler Power Spectrum

Let $p_{f_d}(f_d)d(f_d)$ and $p_\alpha(\alpha)d(\alpha)$ denote percent of received power within $d\alpha$ and $d(f_d)$ respectively. Where α is the angle of arrival and $f_d(\alpha)$ is the instantaneous Doppler frequency $f_d(\alpha) = f_m\cos(\alpha)$ as in (2.2). Usually we have no information to specify that one angle of arrival is more likely than another, so we take α to be

uniformly distributed ($p_\alpha(\alpha)=\frac{1}{2\pi}$). Total received power (as percent) in the interval $-f_m < f_d \le f$ can be expressed as

$$\int_{-f_m}^{f} p_{f_d}(f_d)\,d(f_d) = \int_{-\pi}^{-\arccos(f/f_m)} p_\alpha(\alpha)\,d(\alpha) + \int_{\arccos(f/f_m)}^{\pi} p_\alpha(\alpha)\,d(\alpha)$$

$$= \frac{1}{2\pi}\left(\int_{-\pi}^{-\arccos(f/f_m)} d(\alpha) + \int_{\arccos(f/f_m)}^{\pi} d(\alpha) \right) \qquad (2.23)$$

Differentiating Equation (2.23) with respect to f

$$p_{f_d}(f) = \frac{1}{\pi}\frac{d(-\arccos(f/f_m))}{df}$$

$$= \frac{1}{\pi\sqrt{f_m^2 - f^2}} \quad , \quad |f| \le f_m \qquad (2.24)$$

Doppler power spectrum $S(f)$ can be obtained as follows

$$S(f) = P_R\, p_{f_d}(f) \qquad (2.25)$$

where P_R is total received power. Therefore, as a result Doppler power spectrum around the carrier frequency is

$$S(f) = \frac{P_R}{\pi\sqrt{f_m^2 - (f - f_c)^2}} \ , \ |f - f_c| \le f_m \qquad (2.26)$$

Doppler spectrum around carrier frequency f_c is shown in Figure 2.6.

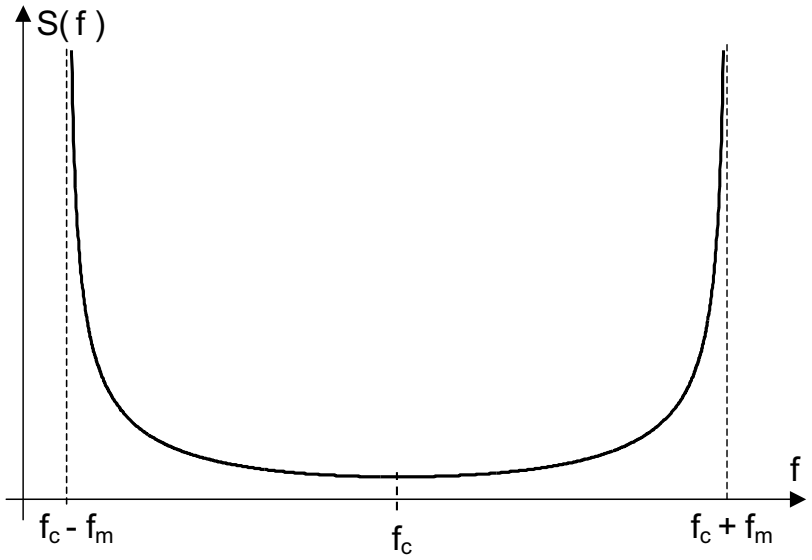

Figure 2.6 Doppler power spectrum around carrier frequency f_c

The autocorrelation function due to Doppler spread is the inverse Fourier transform of the Doppler power spectrum. Thus, the autocorrelation function is

$$c_t(t-t') = F^{-1}\{S(f)\} = F^{-1}\left\{\frac{P_R}{\pi\sqrt{f_m^2 - f^2}}\right\}$$
$$= P_R\, J_0\left(2\pi f_m (t-t')\right) \tag{2.27}$$

where $J_0(.)$ is the *zero* th order Bessel function. In thesis, total received power P_R will be normalized. Therefore, the autocorrelation function for normalized power is

$$c_t(t-t') = J_0\left(2\pi f_m (t-t')\right) \tag{2.28}$$

Replacing $(t-t')$ by $(n-n')T_s$, time domain discrete channel autocorrelation can also be given as

$$c_t(n-n') = J_0\left(2\pi f_m (n-n')T_s\right) \tag{2.29}$$

where T_s denotes the sampling period. In this thesis, discrete autocorrelation of the transmit diversity OFDM systems will be given by (2.29).

2.5 Basic Principles of OFDM

OFDM originated from the need of efficient communications through a frequency-selective fading channel. A channel is frequency-selective if the frequency response of the channel changes significantly within the band of the transmitted signal. While, a constant frequency response is called flat fading. Figure 2.7.a, b exemplifies the frequency-selective and flat fading channels. Digitally modulated signals going through a frequency-selective channel will be distorted, resulting in intersymbol interference (ISI). To mitigate the ISI, a complex equalizer is usually needed to make the frequency response of the channel flat within the bandwidth of interest; or the symbol duration must be long enough so that the ISI affected portion of a symbol can be negligible. From the frequency domain viewpoint, the latter approach means to transmit a narrow band signal within whose bandwidth the channel can be well considered to be flat fading, as shown in Figure 2.7.d.

This fact gives the idea that one can transmit several low rate data streams, each at a different carrier frequency through the channel in parallel and each data stream is ISI free and only a simple one tap equalizer is need to compensate the flat fading. This idea is illustrated in Figure 2.8. That is actually the idea of Frequency Division Multiplexing (FDM).

However, this multi-carrier transmission scheme may suffer inter carrier interference (ICI), i.e., the signals of neighboring carriers may interfere each other. To avoid the ICI, guarding bands are employed in FDM to separate different sub-carriers.

This results in a waste of the spectrum. OFDM follows the very similar multi-carrier modulation strategy. However, it employs the orthogonality among sub-carriers to eliminate the ICI without the need of the guarding bands.

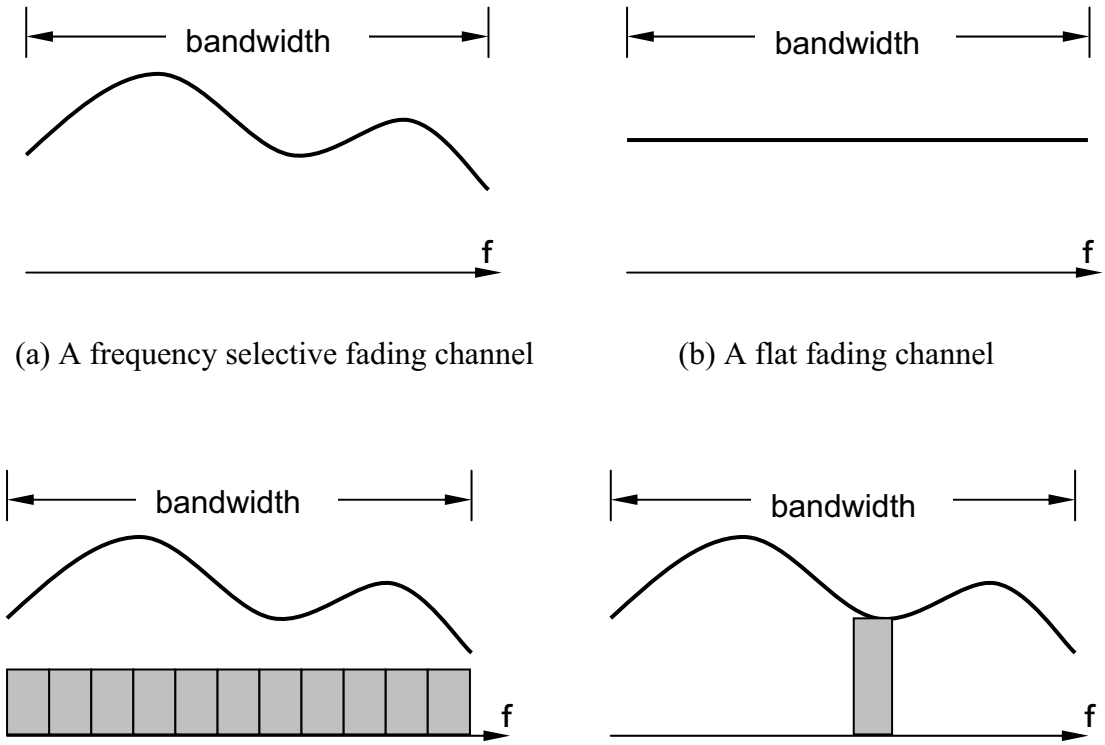

(a) A frequency selective fading channel

(b) A flat fading channel

(c) Modulated signal

(d) Narrow band signal

Figure 2.7 Signals transmitted through frequency-selective channels

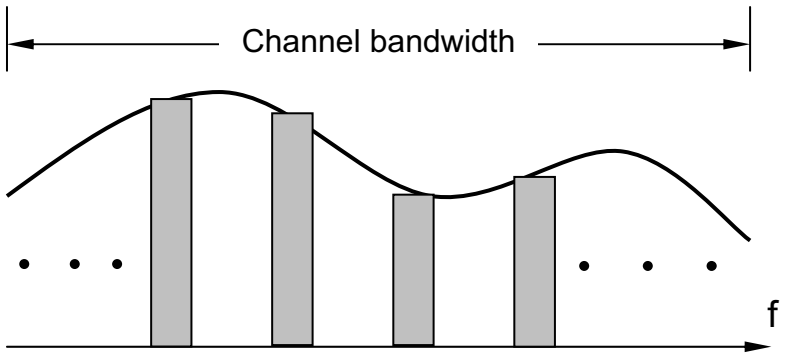

Figure 2.8 Multi carrier modulation scheme

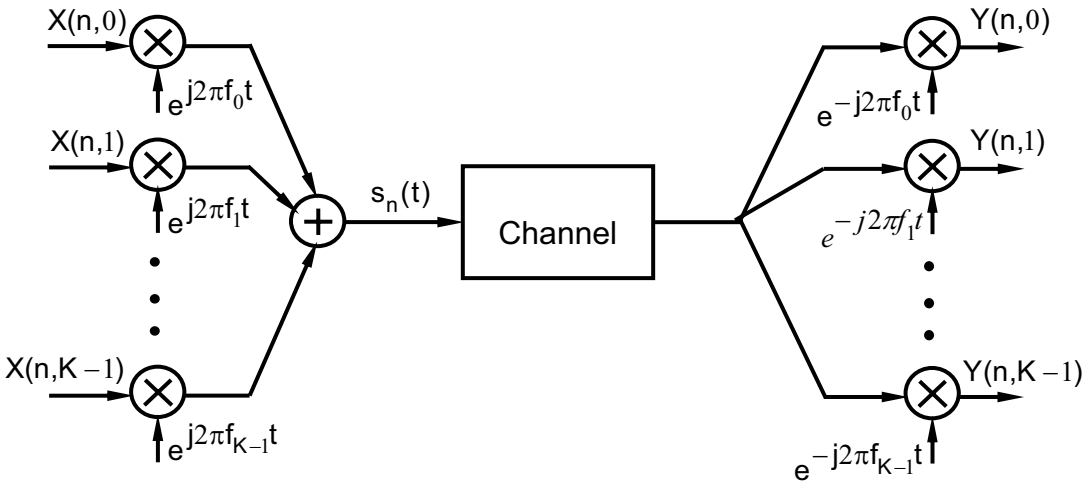

Figure 2.9 Frequency Division Multiplexing System

As illustrated in Figure 2.9, frequency-multiplexed digitally modulated signals in one symbol duration are of the form

$$s_n(t) = \sum_{k=0}^{K-1} X(n,k)\, e^{j2\pi f_k t} \quad , \quad nT_{sym} \le t \le (n+1)T_{sym} \tag{2.30}$$

where K information symbols $X(n,k)$, $k=0, \ldots, K-1$ are transmitted simultaneously and are considered a block, n indicates index block, f_k is the k th sub-carrier, and T_{sym} is the OFDM symbol duration.

In OFDM signaling, the following orthogonality condition is satisfied,

$$\int_0^{T_{sym}} e^{j2\pi f_i t} e^{-j2\pi f_j t} = \int_0^{T_{sym}} e^{j2\pi (f_i - f_j)t} = 0 \tag{2.31}$$

That means the space between the frequencies of the sub carriers should be

$$\Delta f = f_i - f_j = \frac{i-j}{T_{sym}} \tag{2.32}$$

Note that the smallest space for orthogonality is equal to the symbol rate $1/T_{sym}$.

With the orthogonality, each sub carrier can be demodulated independently without ICI. It should be noted that the passbands of the subcarriers may overlap in OFDM, as shown in Figure 2.10.

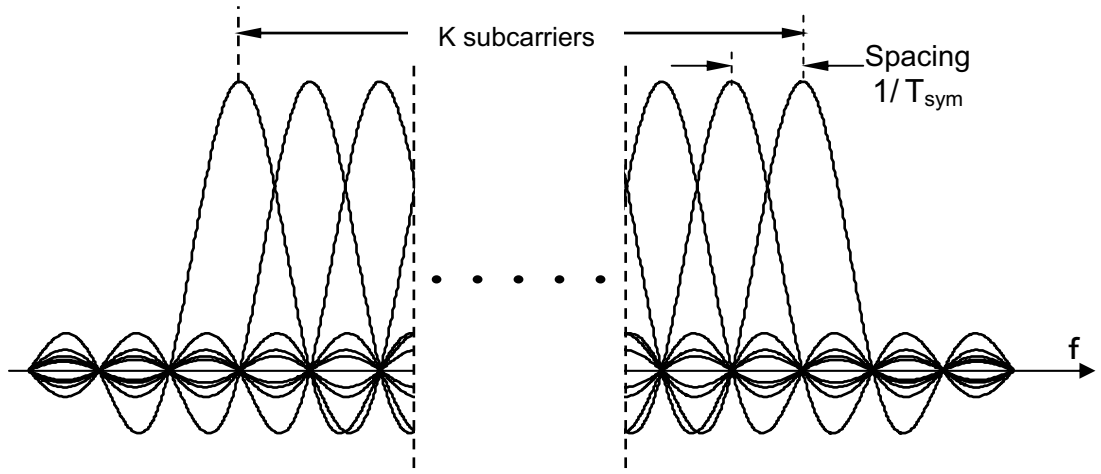

Figure 2.10 An OFDM system with K subcarriers

This allows one to pack the sub carriers into a given spectral band in a densest fashion, so a high spectral efficiency is achieved. Figure 2.11 illustrates the difference between the conventional non-overlapping multi carrier technique and the OFDM.

OFDM signal $s_n(t)$ in (2.30) can also be obtained using a digital method, as shown in Figure 2.12, if we note that the K/T_{sym} rate samples of $s_n(t)$ is the Inverse Fast Fourier Transform (IFFT) of the information symbols $X(n,k)$, $k=0, \ldots, K-1$,

$$s_n(t)\Big|_{t=i\frac{T_{sym}}{K}} = \sum_{k=0}^{K-1} X_n(k) e^{j2\pi \frac{k}{T_{sym}} i \frac{T_{sym}}{K}} = \sum_{k=0}^{K-1} X_n(k) e^{j2\pi \frac{ik}{K}}, \quad i=0, .., K-1 \qquad (2.33)$$

where i is the time sample index.

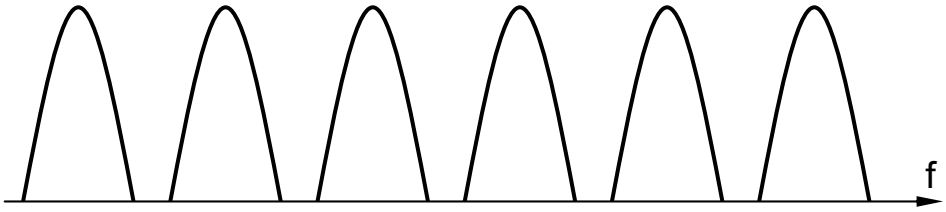

(a) conventional multicarrier

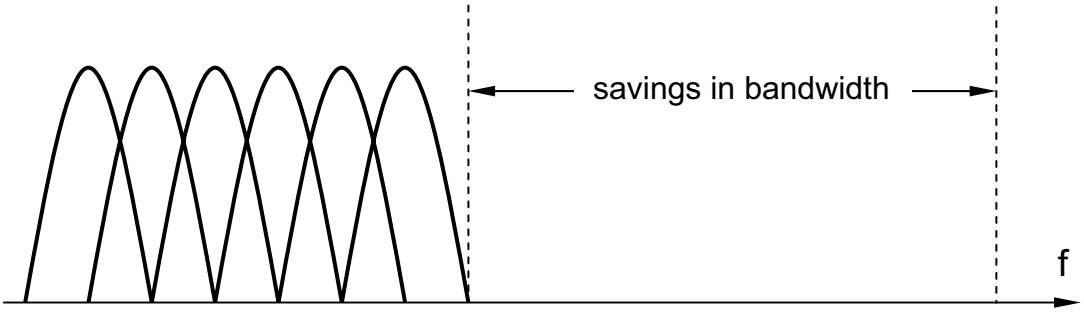

(b) OFDM

Figure 2.11 Comparison between conventional multi carrier technique and OFDM

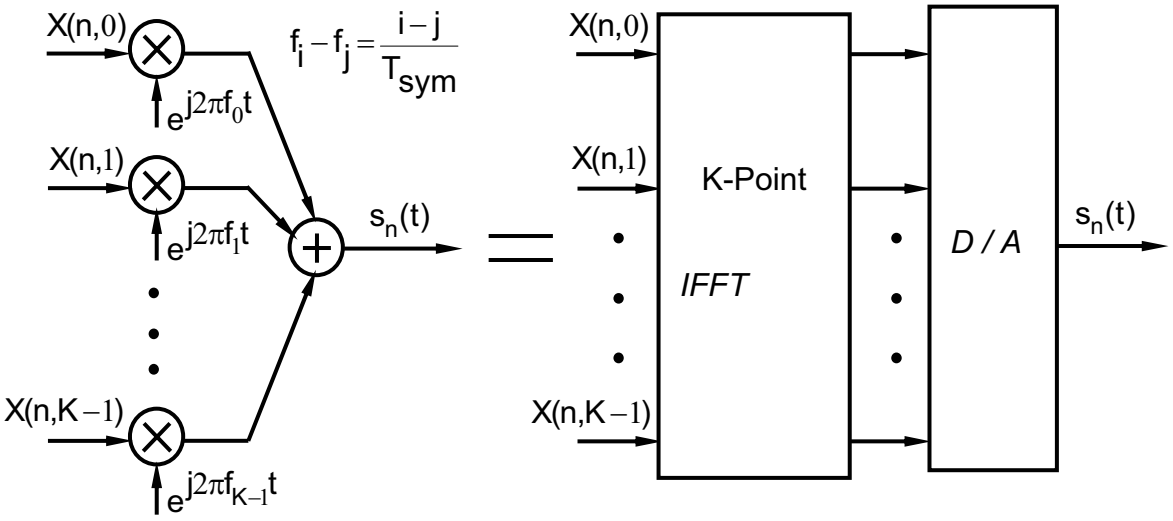

Figure 2.12 FFT implementation of transmitted waveform

Then, the FFT algorithm makes the implementation of the OFDM scheme very efficient. In addition to the high spectral efficiency and simple equalization, the advantages of OFDM include:

- OFDM can easily achieve optimal “bit-loading”, i.e., assign different power and constellation size to each sub-carrier to enhance system capacity.
- OFDM is robust against narrow band interference because such interference affects only sum of the sub carriers.
- OFDM allows efficient FFT implementation.

Chapter 3

Ofdm Channel Estimation by Karhunen Loeve Expansion

OFDM is a multicarrier modulation technique (or a multiplexing technique) where a single data stream is transmitted over a number of lower rate subcarriers. One of the main reasons to use OFDM is to increase the robustness against frequency selective fading. In a single carrier system, a single fade can cause the entire channel to fail, but in a multicarrier system, only a small percentage of the subcarriers will be affected.

In order to eliminate ISI arising due to multipath channel and preserve orthogonality of the subcarrier frequencies (tones), conventional OFDM systems first take the IFFT of data symbols and then insert redundancy in the form of a Cyclic Prefix (CP) of length L_{CP} larger than the channel order L. CP is discarded at the receiver and the remaining part of the OFDM symbol is FFT processed. Combination of IFFT and CP at the transmitter with the FFT at the receiver divides the frequency-selective channel into several separate flat-fading subchannels.

An OFDM system with K subcarriers is considered for the transmission of K parallel data symbols. Thus, the information stream is parsed into K long blocks: $\mathbf{X}_n = [X(n,0), X(n,1), ..., X(n,K-1)]^T$ where n = 1, 2, ... is the block index and the superscript $(.)^T$ indicates the vector transpose. The $K \times 1$ symbol block is then mapped to a $(K+L)\times 1$ vector by first taking the IFFT of $\mathbf{X}_n$ and then replicating the last L_{CP} elements as

$$\mathbf{s}_n = [s_n(0), s_n(1), ..., s_n(K+L_{CP}-1)]^T \tag{3.1}$$

$\mathbf{s}_n$ is serially transmitted over the channel. At the receiver, the CP of length L_{CP} is removed first and FFT is performed on the remaining $K \times 1$ vector. Therefore, the output of the FFT unit in matrix form can be written as

$$\mathbf{Y}_n = \mathbf{A}_n \mathbf{H}_n + \boldsymbol{\eta}_n \tag{3.2}$$

where $\mathbf{A}_n$ is the diagonal matrix $\mathbf{A}_n = \text{diag}\{\mathbf{X}_n\}$ and $\mathbf{H}_n$ is the channel vector. The elements of $\mathbf{H}_n$ are the values of the channel frequency response evaluated at the subcarriers.

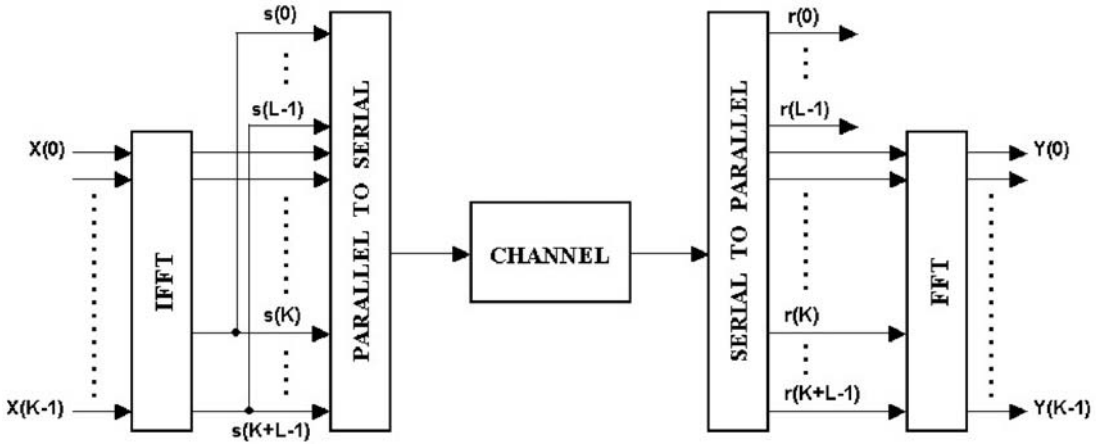

Figure 3.1 OFDM system block diagram

Therefore, $\mathbf{H}_n = \left[H(n,0),\ H(n,e^{j2\pi/K}),\ \ldots,\ H(n,e^{j2\pi(K-1)/K})\right]^T$ can be written as $\mathbf{H}_n = \mathcal{F}\mathbf{h}_n$ where $\mathcal{F}$ is the FFT matrix with (k,i) entry $e^{-j2\pi ki/K}$ and $\mathbf{h}_n = \left[h_n(0), h_n(1), \ldots, h_n(L-1)\right]^T$. $\mathbf{h}_n$ modeled as a complex Gaussian vector with $\mathbf{h}_n \sim \mathcal{N}(\mathbf{0}, \mathbf{C}_\mathbf{h})$ represents the overall channel impulse response during the *n*th OFDM block. Finally, $\boldsymbol{\eta}_n$ is a $K \times 1$ zero-mean, i.i.d complex Gaussian vector that models additive noise in the K subchannels (tones), and $E[\boldsymbol{\eta}_n \boldsymbol{\eta}_n^\dagger] = \sigma^2 \mathbf{I}_K$ where $\mathbf{I}_K$ represents an $K \times K$ identity matrix, σ^2 is the variance of the additive noise entering the system and the superscript $(.)^\dagger$ indicates the Hermitian transpose. Based on the model (3.2), main objective in this work is to develop both batch and sequential

pilot-aided channel estimation algorithm according to MMSE criterion and then explore the performance of the estimators. A batch approach adapted herein explicitly models the channel parameters by the KL series representation and estimates the uncorrelated expansion coefficients. Furthermore, the computational load of the proposed MMSE estimation technique is further reduced with the application of the KL expansion optimal truncation property, Yip and Ng [9].

3.1 Batch MMSE Channel Estimator

A low-rank approximation to the frequency-domain linear MMSE channel estimator is provided by Edfords *et al*. [3] to reduce the complexity of the estimator. Optimal rank reduction is achieved in this approach by using the singular value decomposition (SVD) of the channel attenuations covariance matrix $\mathbf{C_H}$ of dimension $K \times K$. In contrast, the MMSE estimator is adopted for the estimation of multipath channel parameters $\mathbf{h}$ that uses covariance matrix of dimension $L \times L$. The proposed approach employs KL expansion of multipath channel parameters and reduces the complexity of the Singular Value Decomposition (SVD) used in eigen decomposition since L is usually much less than K. MMSE batch estimator will be now developed for pilot assisted OFDM system in the sequel.

3.1.1 MMSE Multipath Channel Estimator

Pilot symbol assisted techniques can provide information about an under sampled version of the channel that may be easier to identify. In this thesis, the problem of estimating multipath channel parameters is addressed by exploiting the distributed training symbols. Considering (3.2), and in order that the pilot symbols are included in the output vector for the estimation purposes, let us focus on an under-sampled signal model. Assuming K_p pilot symbols are uniformly inserted at known locations of the *i*th OFDM block, the $K_p \times 1$ vector corresponding to the FFT output at the pilot locations becomes

$$\mathbf{Y} = \mathbf{AFh} + \boldsymbol{\eta} \tag{3.3}$$

where $\mathbf{A} = \left[A_i(0), A_i(\Delta), ..., A_i((K_p - 1)\Delta)\right]^T$ is a diagonal matrix with pilot symbol entries Δ is pilot spacing interval, $\mathbf{F}$ is an $K_p \times L$ FFT matrix generated based on pilot indices, and similarly $\boldsymbol{\eta}$ is the under-sampled noise vector.

For the estimation of $\mathbf{h}$, the new linear signal model can be formed by premultiplying both sides of (3.3) by $\mathbf{A}^\dagger$ and assuming pilot symbols are taken from a Phase Shift Keying (PSK) constellation $\mathbf{A}^\dagger\mathbf{A} = \mathbf{I}_{K_p}$, then the new form of (3.3) becomes

$$\mathbf{A}^\dagger\mathbf{Y} = \mathbf{F}\mathbf{h} + \mathbf{A}^\dagger\boldsymbol{\eta}$$

$$\tilde{\mathbf{Y}} = \mathbf{F}\mathbf{h} + \tilde{\boldsymbol{\eta}} \tag{3.4}$$

where $\tilde{\mathbf{Y}}$ and $\tilde{\boldsymbol{\eta}}$ are related to $\mathbf{Y}$ and $\boldsymbol{\eta}$ by the linear transformation respectively. Furthermore, $\tilde{\boldsymbol{\eta}}$ is statistically equivalent to $\boldsymbol{\eta}$.

Equation (3.4) offers a Bayesian linear model representation. Based on this representation, the minimum variance estimator for the time-domain channel vector $\mathbf{h}$ for the *i*th OFDM block, i.e., conditional mean of $\mathbf{h}$ given $\tilde{\mathbf{Y}}$, can be obtained using MMSE estimator. Let us clearly make the assumptions that $\mathbf{h} \sim \mathcal{N}(\mathbf{0}, \mathbf{C}_\mathbf{h})$, $\tilde{\boldsymbol{\eta}} \sim \mathcal{N}(\mathbf{0}, \mathbf{C}_{\tilde{\boldsymbol{\eta}}})$ and $\mathbf{h}$ is uncorrelated with $\tilde{\boldsymbol{\eta}}$. Therefore, MMSE estimate of $\mathbf{h}$ is given by Kay[11]:

$$\hat{\mathbf{h}} = (\mathbf{F}^\dagger\mathbf{C}_{\tilde{\boldsymbol{\eta}}}^{-1}\mathbf{F} + \mathbf{C}_\mathbf{h}^{-1})^{-1}\mathbf{F}^\dagger\mathbf{C}_{\tilde{\boldsymbol{\eta}}}^{-1}\tilde{\mathbf{Y}} \tag{3.5}$$

For details of the derivation of (3.5) the reader is referred to Appendix A, where summary results of Bayesian estimation are presented. Due to PSK pilot symbol assumption together with the result $\mathbf{C}_{\tilde{\boldsymbol{\eta}}} = E[\tilde{\boldsymbol{\eta}}\tilde{\boldsymbol{\eta}}^\dagger] = \sigma^2\mathbf{I}_{K_p}$, (3.5) is therefore expressed by

$$\hat{\mathbf{h}} = (\mathbf{F}^{\dagger}\mathbf{F} + \sigma^2 \mathbf{C}_{\mathbf{h}}^{-1})^{-1}\mathbf{F}^{\dagger}\tilde{\mathbf{Y}} \tag{3.6}$$

Under the assumption that uniformly spaced pilot symbols are inserted with pilot spacing interval Δ and $K = \Delta \times K_p$, correspondingly, $\mathbf{F}^{\dagger}\mathbf{F}$ reduces to $\mathbf{F}^{\dagger}\mathbf{F} = K_p \mathbf{I}_L$. Then according to (3.6) and $\mathbf{F}^{\dagger}\mathbf{F} = K_p \mathbf{I}_L$, following expression is obtained

$$\hat{\mathbf{h}} = (K_p \mathbf{I}_L + \sigma^2 \mathbf{C}_{\mathbf{h}}^{-1})^{-1}\mathbf{F}^{\dagger}\tilde{\mathbf{Y}} \tag{3.7}$$

Since MMSE estimation still requires the inversion of $\mathbf{C}_{\mathbf{h}}^{-1}$, it therefore suffers from a high computational complexity. However, it is possible to reduce complexity of the MMSE algorithm by diagonalizing channel covariance matrix with a KL expansion.

3.1.2 Karhunen Loeve Expansion of Multipath Channel

Channel impulse response $\mathbf{h}$ is a zero-mean Gaussian process with covariance matrix $\mathbf{C}_{\mathbf{h}}$. The KL transformation is therefore employed here to rotate the vector $\mathbf{h}$ so that all its components are uncorrelated. The vector $\mathbf{h}$, representing the channel impulse response during *i*th OFDM block, can be expressed as a linear combination of the orthonormal basis vectors as follows:

$$\mathbf{h} = \sum_{\ell=0}^{L-1} g_\ell \boldsymbol{\psi}_\ell = \boldsymbol{\Psi}\mathbf{g} \tag{3.8}$$

where $\boldsymbol{\Psi} = [\boldsymbol{\psi}_0, \boldsymbol{\psi}_1, \ldots, \boldsymbol{\psi}_{L-1}]$, $\boldsymbol{\psi}_\ell$'s are the orthonormal basis vectors, $\mathbf{g} = [g_0, g_1, \ldots g_{L-1}]^T$, and g_ℓ's are the weights of the expansion. If the covariance matrix $\mathbf{C}_{\mathbf{h}}$ is formed as

$$\mathbf{C}_{\mathbf{h}} = \boldsymbol{\Psi}\boldsymbol{\Lambda}_{\mathbf{g}}\boldsymbol{\Psi}^{\dagger} \tag{3.9}$$

where $\mathbf{\Lambda_g} = \mathsf{E}[\mathbf{g}\mathbf{g}^\dagger]$, the KL expansion is the one in which $\mathbf{\Lambda_g}$ of $\mathbf{C_h}$ is a diagonal matrix (i.e., the coefficients are uncorrelated). If $\mathbf{\Lambda_g}$ is diagonal, then the form $\mathbf{\Psi\Lambda_g\Psi}^\dagger$ is called an eigen decomposition of $\mathbf{C_h}$. The fact that only the eigenvectors diagonalize $\mathbf{C_h}$ leads to the desirable property that the KL coefficients are uncorrelated. Furthermore, in Gaussian case, the uncorrelateness of the coefficients renders them independent as well, providing additional simplicity.

Thus, the channel estimation problem in this application is equivalent to estimating the independent identical distributed complex Gaussian vector $\mathbf{g}$, KL expansion coefficients.

3.1.3 Estimation of Karhunen Loeve Coefficients

In contrast to (3.4) in which only $\mathbf{h}$ is to be estimated, let us now assume the KL coefficients $\mathbf{g}$ is unknown. Thus the data model (3.4) is rewritten for each OFDM block as

$$\tilde{\mathbf{Y}} = \mathbf{F\Psi g} + \tilde{\boldsymbol{\eta}} \tag{3.10}$$

which is also recognized as a Bayesian linear model, and recall that $\mathbf{g} \sim \mathcal{N}(\mathbf{0}, \mathbf{\Lambda_g})$. As a result, the MMSE estimator of $\mathbf{g}$ is

$$\hat{\mathbf{g}} = \mathbf{\Lambda_g}(K_p\mathbf{\Lambda_g} + \sigma^2\mathbf{I}_L)^{-1}\mathbf{\Psi}^\dagger\mathbf{F}^\dagger\tilde{\mathbf{Y}}$$

$$= \mathbf{\Gamma\Psi}^\dagger\mathbf{F}^\dagger\tilde{\mathbf{Y}} \tag{3.11}$$

where

$$\mathbf{\Gamma} = \mathbf{\Lambda_g}(K_p\mathbf{\Lambda_g} + \sigma^2\mathbf{I}_L)^{-1} \tag{3.12}$$

$$= \text{diag}\left\{ \frac{\lambda_0}{\lambda_0 K_p + \sigma^2}, \ldots, \frac{\lambda_{L-1}}{\lambda_{L-1} K_p + \sigma^2} \right\}$$

and $\lambda_0, \lambda_1, \ldots, \lambda_{L-1}$ are the singular values of $\mathbf{\Lambda_g}$.

It is clear that the complexity of the MMSE estimator in (3.7) is reduced by the application of KL expansion. However, the complexity of the $\hat{\mathbf{g}}$ can be further reduced by exploiting the optimal truncation property of the KL expansion, Yip and Ng [9]. MMSE estimator of $\mathbf{g}$ requires $4L^2 + 4LK_p + 2L$ real multiplications. From the results presented in Morelli and Mengali [4], ML estimator of $\mathbf{g}$ is obtained as follows:

$$\hat{\mathbf{g}} = \frac{1}{K_p} \mathbf{\Psi}^{\dagger} \mathbf{F}^{\dagger} \tilde{\mathbf{Y}} \tag{3.13}$$

Note that, according to (3.13), the ML estimator of $\mathbf{g}$ requires $4L^2 + 4LK_p$ real multiplications.

3.1.4 Truncated MMSE Channel Estimator

A truncated expansion $\mathbf{g}_r$ can be formed by selecting r orthonormal basis vectors among all basis vectors that satisfy $\mathbf{C_h \Psi} = \mathbf{\Psi \Lambda_g}$. The optimal one that yields the smallest average mean-squared truncation error $\frac{1}{L} E[\boldsymbol{\varepsilon}_r^{\dagger} \boldsymbol{\varepsilon}_r]$ is the one expanded with the orthonormal basis vectors associated with the first largest *r* eigen values as given by

$$\frac{1}{L} E[\boldsymbol{\varepsilon}_r^{\dagger} \boldsymbol{\varepsilon}_r] = \frac{1}{L} \sum_{i=r}^{L-1} \lambda_i \tag{3.14}$$

where $\boldsymbol{\varepsilon}_r = \mathbf{g} - \mathbf{g}_r$. For the problem at hand, truncation property of the KL expansion

results in a low-rank approximation as well. Thus, a rank-r approximation to $\mathbf{\Lambda}_{\mathbf{g}_r}$ is defined as

$$\mathbf{\Lambda}_{\mathbf{g}_r} = \text{diag}\{\lambda_0, \lambda_1, \ldots, \lambda_{r-1}, 0, \ldots, 0\} \tag{3.15}$$

Since the trailing L-r variances $\{\lambda_\ell\}_{\ell=r}^{L-1}$ are small compared to the leading *r* variances $\{\lambda_\ell\}_{\ell=0}^{r-1}$, then the trailing L-r variances are set to zero to produce the approximation. However, typically the pattern of eigen values for $\mathbf{\Lambda}_{\mathbf{g}}$ splits the eigenvectors into dominant and subdominant sets. Then the choice of r is more or less obvious. The optimal truncated KL (rank-r) estimator of (3.11) now becomes

$$\hat{\mathbf{g}}_r = \mathbf{\Gamma}_r \mathbf{\Psi}^\dagger \mathbf{F}^\dagger \tilde{\mathbf{Y}} \tag{3.16}$$

where

$$\begin{aligned} \mathbf{\Gamma}_r &= \mathbf{\Lambda}_{\mathbf{g}_r} (K_p \mathbf{\Lambda}_{\mathbf{g}_r} + \sigma^2 \mathbf{I}_L)^{-1} \\ &= \text{diag}\left\{ \frac{\lambda_0}{\lambda_0 K_p + \sigma^2}, \ldots, \frac{\lambda_{r-1}}{\lambda_{r-1} K_p + \sigma^2}, 0, \ldots, 0 \right\} \end{aligned} \tag{3.17}$$

Since the ultimate goal is to obtain MMSE estimator for the channel frequency response $\mathbf{H}$, from the invariance property of the MMSE estimator, it follows that if $\hat{\mathbf{g}}$ is the estimate of $\mathbf{g}$, then the corresponding estimate of $\mathbf{H}$ can be obtained for the *i* th OFDM block as

$$\hat{\mathbf{H}} = \mathcal{F} \mathbf{\Psi} \hat{\mathbf{g}} \tag{3.18}$$

Thus, from (3.16) and (3.17), the truncated MMSE estimator of $\mathbf{g}$ requires $4Lr + 4LK_p + 2r$ real multiplications.

3.1.5 Performance Analysis

Let us turn our attention to analytical performance results of the batch MMSE approach. First, the CRLB and derive the closed-form expression for the random KL coefficients will be considered, and then the performance of the MMSE channel estimator based on the evaluation of minimum Bayesian MSE will be exploited.

3.1.5.1 Cramer-Rao Bound for Karhunen Loeve Coefficients

The mean-squared estimation error for unbiased estimation of a nonrandom parameter has a lower bound, the *Cramer-Rao Lower Bound* (CRLB), which defines the ultimate accuracy of unbiased estimation procedure.

Suppose $\hat{\mathbf{g}}$ is an unbiased estimator of a vector of unknown parameters $\boldsymbol{g}$ (i.e. E[$\hat{\mathbf{g}}$] = $\mathbf{g}$) then the mean-squared error matrix is lower bounded by the inverse of the Fisher information matrix (FIM):

$$\mathrm{E}[(\mathbf{g}-\hat{\mathbf{g}})(\mathbf{g}-\hat{\mathbf{g}})^{\dagger}] \geq \mathbf{J}^{-1}(\hat{\mathbf{g}}) \tag{3.19}$$

Since the estimation of unknown random parameters $\mathbf{g}$ via MMSE approach is considered in this work, the modified FIM needs to be taken into account in the derivation of stochastic CRLB, Van Trees [12], and Senol *et al*. [17]. Fortunately, the modified FIM can be obtained by a straightforward modification of (3.19) as,

$$\mathbf{J}_{\mathrm{M}}(\mathbf{g}) = \mathbf{J}(\mathbf{g}) + \mathbf{J}_{\mathrm{P}}(\mathbf{g}) \tag{3.20}$$

where $\mathbf{J}_{\mathrm{P}}(\mathbf{g})$ represents the a priori information.

Under the assumption that $\boldsymbol{g}$ and $\tilde{\boldsymbol{\eta}}$ are independent of each other and $\tilde{\boldsymbol{\eta}}$ is a zero-mean, from Van Trees [12], Senol *et al*. [17] and (3.10) the conditional PDF is given by

$$p(\tilde{\mathbf{Y}} \mid \mathbf{g}) = \frac{1}{\pi^{K_p} \mid \mathbf{C}_{\tilde{\eta}} \mid} \exp\left\{-(\tilde{\mathbf{Y}}-\mathbf{F}\Psi\mathbf{g})\mathbf{C}_{\tilde{\eta}}^{-1}(\tilde{\mathbf{Y}}-\mathbf{F}\Psi\mathbf{g})^{\dagger}\right\} \tag{3.21}$$

from which the derivatives follow as

$$\frac{\partial \ln p(\tilde{\mathbf{Y}} \mid \mathbf{g})}{\partial \mathbf{g}^{T}} = (\tilde{\mathbf{Y}}-\mathbf{F}\Psi\mathbf{g})^{\dagger}\mathbf{C}_{\tilde{\eta}}^{-1}(\tilde{\mathbf{Y}}-\mathbf{F}\Psi\mathbf{g}) \tag{3.22}$$

$$\frac{\partial^2 \ln p(\tilde{\mathbf{Y}} \mid \mathbf{g})}{\partial \mathbf{g}^{*}\partial \mathbf{g}^{T}} = -\Psi^{\dagger}\mathbf{F}^{\dagger}\mathbf{C}_{\tilde{\eta}}^{-1}\mathbf{F}\Psi \tag{3.23}$$

where the superscript $(.)^{*}$ indicates the conjugation operation.

Using $\mathbf{C}_{\tilde{\eta}} = \sigma^2\mathbf{I}_{K_p}$, $\Psi^{\dagger}\Psi = \mathbf{I}_L$ and $\mathbf{F}^{\dagger}\mathbf{F} = K_p\mathbf{I}_L$ and taking the expected value yields the following simple form:

$$\begin{aligned}\mathbf{J}(\mathbf{g}) &= -\,E\left[\frac{\partial^2 \ln p(\tilde{\mathbf{Y}} \mid \mathbf{g})}{\partial \mathbf{g}^{*}\partial \mathbf{g}^{T}}\right] \\ &= -\,E\left[-\frac{K_p}{\sigma^2}\mathbf{I}_L\right] \\ &= \frac{K_p}{\sigma^2}\mathbf{I}_L\end{aligned} \tag{3.24}$$

Second term in (3.20) is easily obtained as follows. Consider the prior PDF of $\mathbf{g}$ as,

$$p(\mathbf{g}) = \frac{1}{\pi^{L} \mid \Lambda_{\mathbf{g}} \mid} \exp\{-\mathbf{g}^{\dagger}\Lambda_{\mathbf{g}}^{-1}\mathbf{g}\} \tag{3.25}$$

The respective derivatives are found as

$$\frac{\partial \ln p(\mathbf{g})}{\partial \mathbf{g}^{T}} = -\mathbf{g}^{\dagger}\Lambda_{\mathbf{g}}^{-1} \tag{3.26}$$

$$\frac{\partial^2 \ln p(\mathbf{g})}{\partial \mathbf{g}^* \partial \mathbf{g}^T} = -\boldsymbol{\Lambda}_{\mathbf{g}}^{-1} \tag{3.27}$$

Upon taking the negative expectations, second term in (3.20) becomes

$$\begin{aligned} \mathbf{J}_P(\mathbf{g}) &= -E\left[\frac{\partial^2 \ln p(\mathbf{g})}{\partial \mathbf{g}^* \partial \mathbf{g}^T}\right] \\ &= -E[-\boldsymbol{\Lambda}_{\mathbf{g}}^{-1}] \\ &= \boldsymbol{\Lambda}_{\mathbf{g}}^{-1} \end{aligned} \tag{3.28}$$

Substituting (3.24) and (3.28) in (3.20) produces for the modified FIM as follows

$$\begin{aligned} \mathbf{J}_M(\mathbf{g}) &= \mathbf{J}(\mathbf{g}) + \mathbf{J}_p(\mathbf{g}) \\ &= \frac{K_p}{\sigma^2}\mathbf{I}_L + \boldsymbol{\Lambda}_{\mathbf{g}}^{-1} \\ &= \frac{1}{\sigma^2}(K_p\mathbf{I}_L + \sigma^2\boldsymbol{\Lambda}_{\mathbf{g}}^{-1}) \\ &= \frac{1}{\sigma^2}\boldsymbol{\Gamma}^{-1} \end{aligned} \tag{3.29}$$

Inverting the matrix $\mathbf{J}_M(\mathbf{g})$ yields

$$\begin{aligned} \text{CRLB}(\hat{\mathbf{g}}) &= \mathbf{J}_M^{-1}(\mathbf{g}) \\ &= \sigma^2\boldsymbol{\Gamma} \end{aligned} \tag{3.30}$$

3.1.5.2 Bayesian MSE

For the MMSE estimator $\hat{\mathbf{g}}$, the error is

$$\hat{\boldsymbol{\varepsilon}} = \mathbf{g} - \hat{\mathbf{g}} \tag{3.31}$$

Since the diagonal entries of the covariance matrix of the error represent the minimum Bayesian MSE, let us now derive covariance matrix $\mathbf{C}_{\hat{\boldsymbol{\varepsilon}}}$ of the error vector. From the Performance of the MMSE estimator for the Bayesian Linear model Theorem, Kay[11], the error covariance matrix is obtained as

$$\begin{aligned}\mathbf{C}_{\hat{\boldsymbol{\varepsilon}}} &= (\boldsymbol{\Lambda}_{\mathbf{g}}^{-1} + (\mathbf{F}\boldsymbol{\Psi})^{\dagger}\mathbf{C}_{\tilde{\boldsymbol{\eta}}}^{-1}(\mathbf{F}\boldsymbol{\Psi})) \\ &= \sigma^2(K_p\mathbf{I}_L + \sigma^2\boldsymbol{\Lambda}_{\mathbf{g}}^{-1})^{-1} \\ &= \sigma^2\boldsymbol{\Gamma}\end{aligned} \tag{3.32}$$

and then the minimum Bayesian MSE of the full rank estimator becomes (see Appendix A)

$$B_{MSE}(\hat{\mathbf{g}}) = \frac{1}{L}\text{trace}(\mathbf{C}_{\hat{\boldsymbol{\varepsilon}}}) = \frac{1}{L}\text{trace}(\sigma^2\boldsymbol{\Gamma}) = \frac{1}{L}\sum_{i=0}^{L-1}\frac{\lambda_i}{1+K_p\lambda_i SNR} \tag{3.33}$$

where $SNR = 1/\sigma^2$.

Comparing (3.30) with (3.32), the error covariance matrix of the MMSE estimator coincides with the stochastic CRLB of the random vector estimator. Thus, $\hat{\mathbf{g}}$ achieves the stochastic CRLB.

As the details are given in Appendix A, $\mathbf{B}_{MSE}(\hat{\mathbf{g}})$ given in (3.33) can also be computed for the truncated (low-rank) case as follows:

$$\mathbf{B}_{MSE}(\hat{\mathbf{g}}_r) = \frac{1}{L}\sum_{i=0}^{r-1}\frac{\lambda_i}{1+K_p\lambda_i SNR} + \frac{1}{L}\sum_{i=r}^{L-1}\lambda_i \tag{3.34}$$

Notice that, the second term in (3.34) is the sum of the powers in the KL transform coefficients not used in the truncated estimator. Thus, truncated $\mathbf{B}_{MSE}(\hat{\mathbf{g}}_r)$ can be lower bounded by $\frac{1}{L}\sum_{i=r}^{L-1}\lambda_i$ which will cause an irreducible error floor in the SER results.

3.1.6 Mismatch Analysis

Once the true frequency-domain correlation, characterizing the channel statistics and the SNR, are known. However, in mobile wireless communications, the channel statistics depend on the particular environment, for example, indoor or outdoor, urban or suburban, and change with time. Hence, it is important to analyze the performance degradation due to a mismatch of the estimator to the channel statistics as well as the SNR, and to study the choice of the channel correlation, and SNR for this estimator so that it is robust to variations in the channel statistics. As a performance measure, uncoded Symbol Error Rate (SER) is used for QPSK signaling. The SER expression for this case is given in Proakis [13] as a function of the SNR and the average $\mathsf{B}_{\mathsf{MSE}}(\hat{\mathbf{g}})$ as follows:

$$\mathsf{SER}_{\mathsf{QPSK}} = \frac{3}{4} - \frac{\xi}{2} - \frac{\xi}{\pi}\arctan(\xi) \tag{3.35}$$

where

$$\xi = \frac{\Omega_{\mathsf{g}}}{\sqrt{(\Omega_{\mathsf{g}} + \mathbf{B}_{\mathsf{MSE}}(\hat{\mathbf{g}}))(1 + \frac{2}{\mathsf{SNR}})}}$$

and Ω_{g} represents the normalized variance of the channel gains $(\Omega_{\mathsf{g}} = \sum_{\mathsf{i}=0}^{\mathsf{L}-1} \lambda_{\mathsf{i}} = 1)$ and $\mathsf{SNR} = 1/\sigma^2$. In practice, the true channel correlations and SNR are not known. If the MMSE channel estimator is designed to match the correlation of a multipath channel impulse response $\mathbf{C}_{\tilde{\mathbf{h}}}$ and SNR, but the true channel parameters $\tilde{\mathbf{h}}$ has the correlation $\mathbf{C}_{\tilde{\mathbf{h}}}$ and the true $\tilde{\mathsf{SNR}}$, then average Bayesian MSE for the designed channel estimator is obtained as (see Appendix B and C)

- SNR mismatch:

$$B_{MSE}(\hat{\mathbf{g}}) = \frac{1}{L}\sum_{i=0}^{L-1}\frac{\lambda_i}{(1+K_p\lambda_i SNR)^2}\left[1+K_p\lambda_i\frac{SNR^2}{\widetilde{SNR}}\right] \tag{3.36}$$

- Correlation mismatch:

$$\mathbf{B}_{MSE}(\hat{\mathbf{g}}) = \frac{1}{L}\sum_{i=0}^{L-1}\frac{\tilde{\lambda}_i + K_p SNR\,\lambda_i(\tilde{\lambda}_i+\lambda_i-2\beta_i)}{1+K_p SNR\,\lambda_i} \tag{3.37}$$

where $\tilde{\lambda}_i$ is the i^{th} diagonal element of $\mathbf{\Lambda}_{\tilde{\mathbf{g}}} = \mathbf{\Psi}^{\dagger}\mathbf{C}_{\tilde{\mathbf{h}}}\mathbf{\Psi}$, and β_i is ith diagonal element of the real part of the cross correlation matrix between $\tilde{\mathbf{g}}$ and $\mathbf{g}$.

3.2 Sequential MMSE Channel Estimator

Let us now turn our attention to the derivation of the sequential MMSE algorithm with simple structure. The sequential MMSE approach is proposed in this work to follow the channel variations by exploiting only channel correlations in frequency. The block diagram for this is shown in Figure 3.2. To begin with the algebraic derivation, let us use (3.10) to write m th component of $\tilde{\mathbf{Y}}$ as

$$\tilde{\mathbf{Y}}[m] = \mathbf{u}^{\dagger}(m)\mathbf{g} + \tilde{\eta}[m] \tag{3.38}$$

where $\mathbf{u}^{\dagger}(m)$ is the *m*th row of $\mathbf{F\Psi}$ and $\tilde{\eta}[m]$ is the *m*th element of the noise vector $\tilde{\eta}$.

If a MMSE estimator of $\tilde{\mathbf{Y}}[m+1]$ can be found based on $\tilde{\mathbf{Y}}[m]$, denoted for $\hat{\tilde{\mathbf{Y}}}_{m+1|m}$, the prediction error $f_{m+1} = \tilde{\mathbf{Y}}[m+1] - \hat{\tilde{\mathbf{Y}}}_{m+1|m}$ will be orthogonal to $\tilde{\mathbf{Y}}[m]$. Therefore $\mathbf{g}$ can be projected onto each vector separately and add the results, so that

$$\hat{\mathbf{g}}_{m+1} = \hat{\mathbf{g}}_m + \boldsymbol{\kappa}_{m+1} f_{m+1}$$

$$= \hat{\mathbf{g}}_m + \boldsymbol{\kappa}_{m+1}(\tilde{\mathbf{Y}}[m+1] - \mathbf{u}^{\dagger}(m+1)\hat{\mathbf{g}}_m) \tag{3.39}$$

where $\hat{\mathbf{g}}_{m+1}$ is the $(m+1)^{th}$ estimate of $\mathbf{g}$, and $\boldsymbol{\kappa}_{m+1}$ is the gain factor given as

$$\boldsymbol{\kappa}_{m+1} = \frac{\mathbf{M}_m \, \mathbf{u}(m+1)}{\mathbf{u}^{\dagger}(m+1)\,\mathbf{M}_m \, \mathbf{u}(m+1) + \sigma^2} \tag{3.40}$$

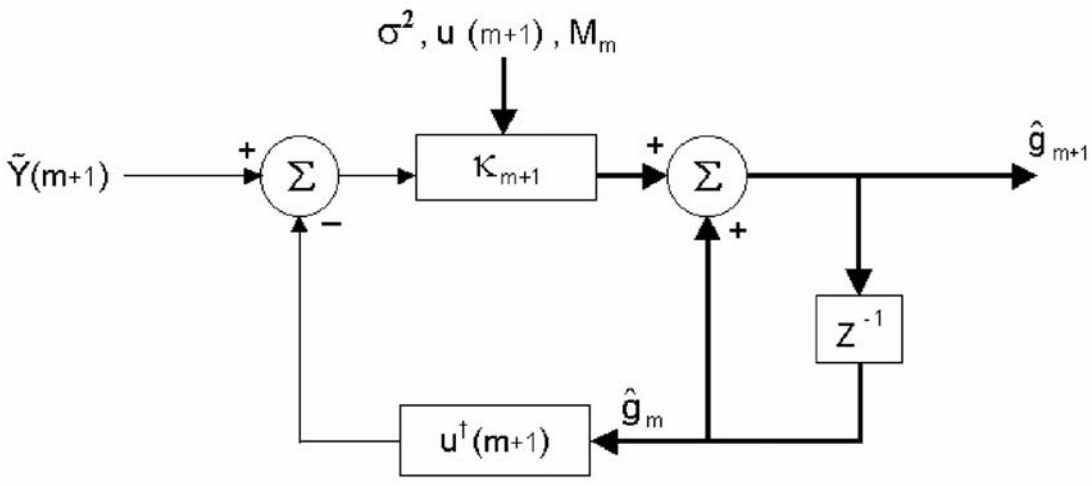

Figure 3.2 Block diagram of sequential MMSE estimator

It can be seen that $\mathbf{M}_m = \mathrm{E}[(\mathbf{g} - \hat{\mathbf{g}}_m)(\mathbf{g} - \hat{\mathbf{g}}_m)^{\dagger}]$ is needed in (3.40), hence update equation for the minimum MSE matrix should also be given. If (3.39) is substituted in $\mathbf{M}_{m+1} = \mathrm{E}[(\mathbf{g} - \hat{\mathbf{g}}_{m+1})(\mathbf{g} - \hat{\mathbf{g}}_{m+1})^{\dagger}]$, an update equation for $\mathbf{M}_{m+1}$ is obtained as

$$\mathbf{M}_{m+1} = (\mathbf{I}_L - \boldsymbol{\kappa}_{m+1}\mathbf{u}^{\dagger}(m+1))\mathbf{M}_m \tag{3.41}$$

Based on these results, the steps of the sequential MMSE estimator for $\mathbf{g}$ can be summarized as follows:

Initialization: Set the parameters to some initial value $\hat{\mathbf{g}}_0 = 0$, $\mathbf{M}_0 = \boldsymbol{\Lambda}_{\mathbf{g}}$

1. Compute the gain $\boldsymbol{\kappa}_{m+1}$ from (3.40)

2. Update the estimate of $\mathbf{g}$ from (3.39)

3. Update the minimum MSE matrix from (3.41).

4. Repeat step 1 - step 3 until $m = K_p - 1$.

Some remarks and observations are now in order:

i.No matrix inversions are required.

ii. Since the MMSE estimator (3.11) requires $\mathbf{F}^{\dagger}\mathbf{F}$ being equal to $K_p\mathbf{I}_L$ which is satisfied only when $\Delta = K/K_p$ is an integer. However, the sequential version of (3.11) works as long as $\Delta \leq K/L$.

Let us now analyze the complexity of the sequential MMSE algorithm. It follows from (3.40) in step 1 that one needs $4L^2+5L$ real multiplications to compute the gain. Similarly, from (3.39) in step 2, it requires $5L$ real multiplications for the estimator update. Finally, in step 3, $8L^2$ real multiplications are needed for the MMSE matrix update. Therefore, the total sequential MMSE algorithm requires $12L^2 + 10L$ real multiplications for one iteration.

3.2.1 Performance Analysis

Let us turn our attention now to the performance analysis of the adaptive algorithm. Its convergence properties will be evaluated in terms of mean square error. From (3.40) and (3.41),

$$\begin{aligned}\boldsymbol{\kappa}_{m+1}\sigma^2 &= (\mathbf{I}_L - \boldsymbol{\kappa}_{m+1}\mathbf{u}^{\dagger}(m+1))\mathbf{M}_m\,\mathbf{u}(m+1)\\ &= \mathbf{M}_{m+1}\mathbf{u}(m+1)\end{aligned} \tag{3.42}$$

is concluded. Substituting (3.42) in (3.40), following result is found.

$$\left(\mathbf{M}_{m+1} - \frac{\sigma^2}{\mathbf{u}^{\dagger}(m+1)\mathbf{M}_m\mathbf{u}(m+1)+\sigma^2}\mathbf{M}_m\right)\mathbf{u}(m+1) = \mathbf{0}_{Lx1} \tag{3.43}$$

Based on (3.43) the following recursion is obtained,

$$\begin{aligned}\mathbf{M}_{m+1} &= \frac{\sigma^2}{\mathbf{u}^{\dagger}(m+1)\mathbf{M}_m\mathbf{u}(m+1)+\sigma^2}\mathbf{M}_m \\ &= \delta_{m+1|m}\mathbf{M}_m \end{aligned} \tag{3.44}$$

Due to positive definite property of error covariance matrix $\mathbf{M}_m$ it follows that $\mathbf{u}^{\dagger}(m+1)\mathbf{M}_m\mathbf{u}(m+1) > 0$. As a result $0 < \delta_{m+1|m} < 1$. Define average MSE at the *m*th step as $\mathrm{MSE}_m = \frac{1}{L}\mathrm{tr}(\mathbf{M}_m)$, then it follows from (3.44) that

$$\mathrm{MSE}_{m+1} = \delta_{m+1|m}\mathrm{MSE}_m \tag{3.45}$$

Thus, as $m \to \infty$, $\mathrm{MSE}_m \to 0$. That means $\hat{\mathbf{g}}_m$ converges to $\mathbf{g}$ in the mean square.

3.3 Simulation Results

In this chapter, the merits of proposed channel estimators are illustrated through simulations. Let us choose average mean square error (MSE) and symbol-error rate (SER) as the figure of merits.

The fading multipath channel with L paths given by (3.46) with an exponentially decaying power delay profile $\theta(\tau) = Ce^{-\tau/\tau_{rms}}$ with delays τ that are uniformly and independently distributed over the duration L_{CP} is considered. Note that $\mathbf{h}$ is chosen as complex Gaussian leading to a Rayleigh fading channel with root mean square (rms) width τ_{rms} and normalizing constant C. In (2.10) and Edfords *et al*. [3], it is shown that the normalized exponential discrete channel correlation for different subcarriers is

$$c_f(k-k') = \frac{1-e^{-L\left(\frac{1}{\tau_{rms}}+j\frac{2\pi(k-k')}{K}\right)}}{\tau_{rms}\left(1-e^{\frac{-L}{\tau_{rms}}}\right)\left(\frac{1}{\tau_{rms}}+j\frac{2\pi(k-k')}{K}\right)} \tag{3.46}$$

The scenario for the simulation study consists of a wireless QPSK OFDM system employing the pulse shape as a unit-energy Nyquist root raised cosine shape with roll off $\alpha = 0.2$, with a sampling period (T_s) of 0.120 μs, corresponding to an uncoded symbol rate of 8.33 Mbit/s. Transmission bandwidth(5 MHz) is divided into 1024 tones. Let us assume that the fading multipath channel has $L=40$ paths with an exponentially decaying power delay profile (3.46) with a $\tau_{rms} = 5$ sample ($0.6\,\mu s$) long.

3.3.1 Batch MMSE Approach

A QPSK-OFDM sequence passes through channel taps and is corrupted by Additive White Gaussian Noise (AWGN), (0dB, 5dB, 10dB, 15dB, 20dB, 25dB and 30dB respectively). A pilot symbol for every twenty $\Delta = 20$ symbols is used. The MSE at each SNR point is averaged over 1000 realizations. The experimental MSE performance and its theoretical Bayesian MSE of the proposed full-rank MMSE estimator are compared with ML estimator and its corresponding CRLB. Figure 3.3 confirms that MMSE estimator performs better than ML estimator at low SNR. However, the two approaches have comparable performance at high SNRs.

To observe the performance, the MMSE and ML estimated channel SER results together with theoretical SER are also presented in Figure 3.4.

Due to the fact that spaces between the pilot symbols are not chosen as a factor of the number of subcarriers, an error floor is observed in Figure 3.3 and Figure 3.4. In the case of choosing the pilot space as a factor of number of subcarriers, the error floor vanishes because of the fact that the orthogonality condition between the subcarriers

at pilot locations is satisfied. In other words, the curves labeled as simulation results for MMSE estimator and ML estimator fit to the theoretical curve sat high SNRs. It also shows that the MMSE estimated channel SER results are better than ML estimated channel SER especially at low SNR.

3.3.1.1 SNR Design Mismatch

In order to evaluate the performance of the proposed full-rank MMSE estimator to mismatch only in SNR design, the estimator is tested when SNRs of 10 and 30 dB are used in the design. The SER curves for a design SNR of 10, 30dB are shown in Figure 3.5. The performance of the MMSE estimator for high SNR (30 dB) design is better than low SNR (10 dB) design across a range of SNR values (0 - 30 dB). These results confirm that channel estimation error is concealed in noise for low SNR whereas it tends to dominate for high SNR. Thus, the system performance degrades especially for low SNR design.

3.3.1.2 Correlation Mismatch

In order to analyze full-rank MMSE estimator's performance further, sensitivity of the estimator to design errors needs to be studied, i.e., correlation mismatch. Therefore the estimator is designed for a uniform channel correlation which gives the worst MSE performance among all channels Edfords *et al*. [3], Li *et al*. [5] and evaluated for an exponentially decaying power-delay profile. The uniform channel correlation between the attenuations can be obtained by letting $\tau_{rms} \to \infty$ in (3.46), resulting in

$$c_f(k-k') = \frac{1-\exp(j\frac{2\pi L(k-k')}{K})}{j\frac{2\pi L(k-k')}{K}} \tag{3.47}$$

Figure 3.6 and Figure 3.7 demonstrate the estimator's sensitivity to the channel statistics in terms of average MSE and SER performance measures respectively. As it

can be seen from Figure 3.6 and Figure 3.7 only small performance loss is observed for low SNRs when the estimator is designed for mismatched channel statistics. This justifies the result that a design for worst correlation is robust to mismatch.

3.3.1.3 Performance of the Truncated Estimator

The truncated estimator performance is also studied as a function of the number of KL coefficients. Figure 3.8 presents the MSE result of the truncated MMSE estimator for SNR=10, 20 and 30 dB. If only a few expansion coefficients is employed to reduce the complexity of the proposed estimator, then the MSE between channel parameters becomes large. However, if the number of parameters in the expansion is increased, the irreducible error floor still occurs.

3.3.2 Sequential MMSE Approach

The MSE results of the sequential full-rank MMSE algorithm are obtained and presented in shown in Figure 3.9. In order to better evaluate the performance of the proposed sequential MMSE estimation algorithm, it is compared with previously developed least mean square (LMS) and recursive least squares (RLS) recursive algorithms. It can be seen from simulations that recursive MMSE estimator yields better performance than LMS and RLS approaches and achieves Bayesian MSE especially for low SNR.

For the convergence of the proposed adaptive algorithm, MSE versus iteration is plotted for SNR=10, 20, 30 and 40 dB in the Figure 3.10. As expected, the proposed sequential algorithm converges faster for high SNR values.

Finally, the performance of the algorithm will be evaluated for different values of pilot spacing 10, 20, 30, 40, and 50 by plotting the MSEs and SERs with respect to SNR in the Figure 3.11 and Figure 3.12 respectively. For the values pilot spacing Δ larger than $\frac{K}{L}$, the SER and MSE performances decrease as Δ increases.

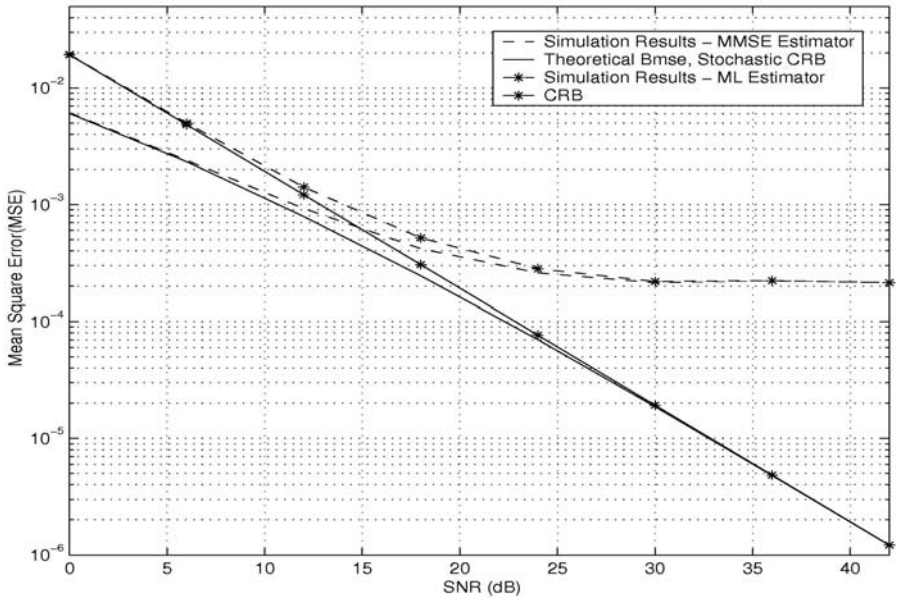

Figure 3.3 Performance of pProposed MMSE and MLE together with B_{MSE} and CRLB

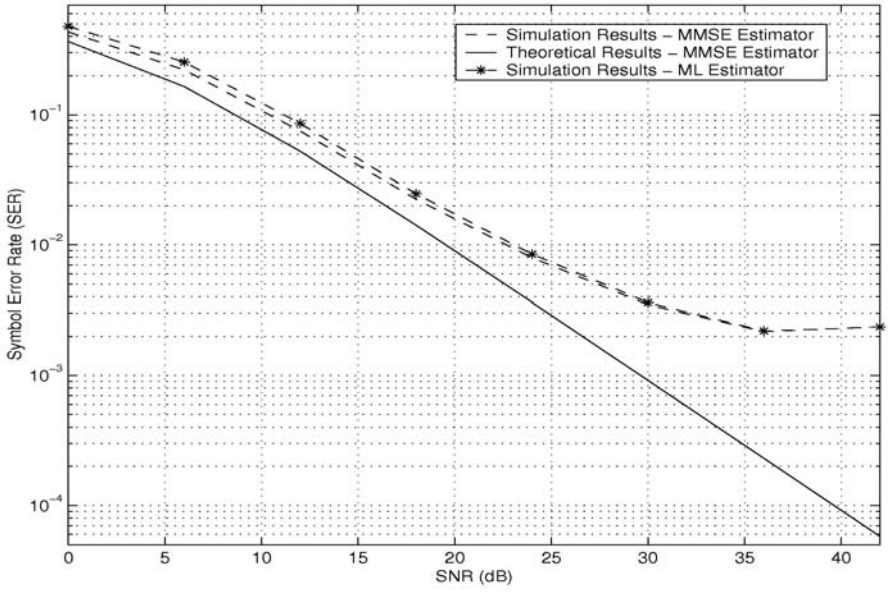

Figure 3.4 Symbol Error Rate results

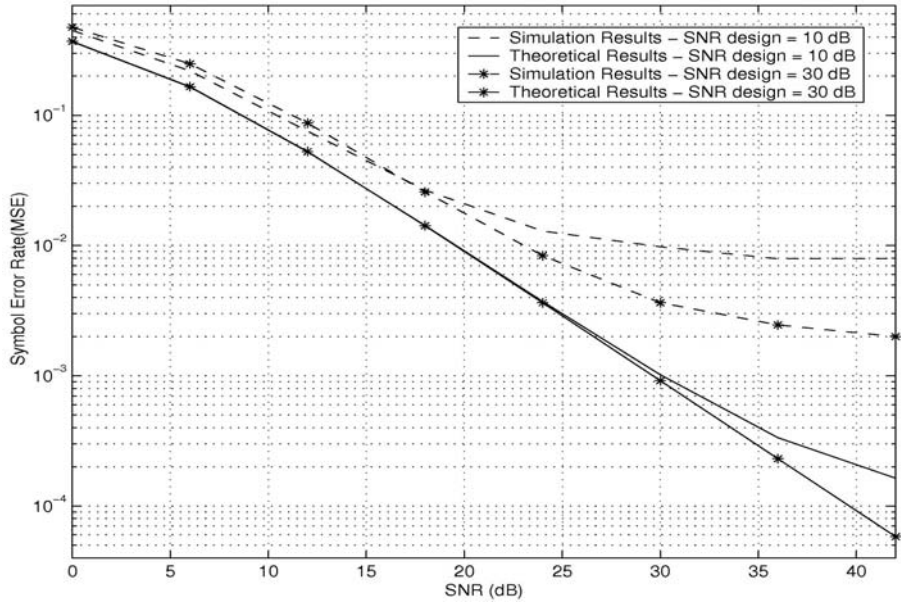

Figure 3.5 Effects of SNR design mismatch on SER

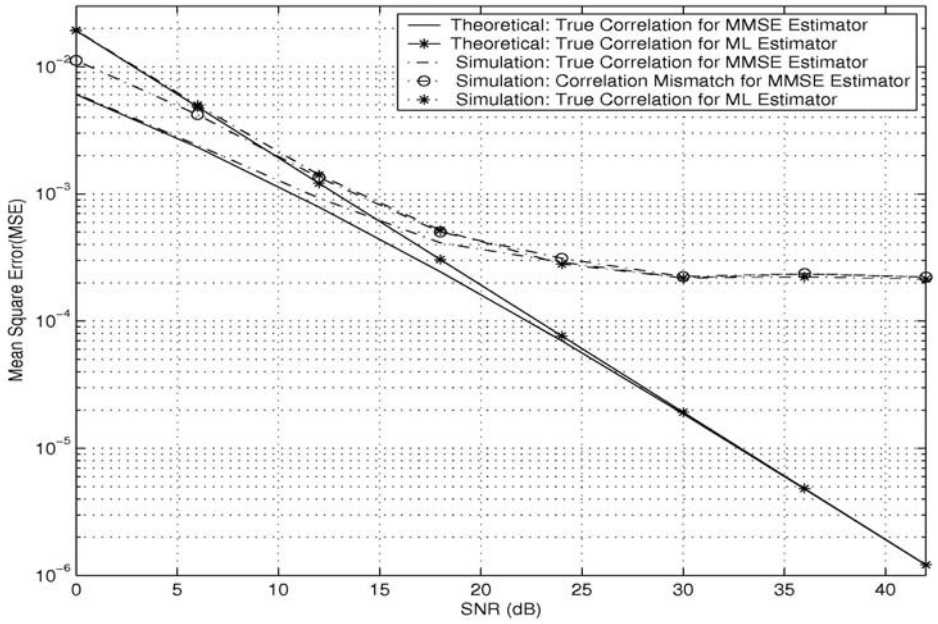

Figure 3.6 Effects of correlation mismatch on MSE

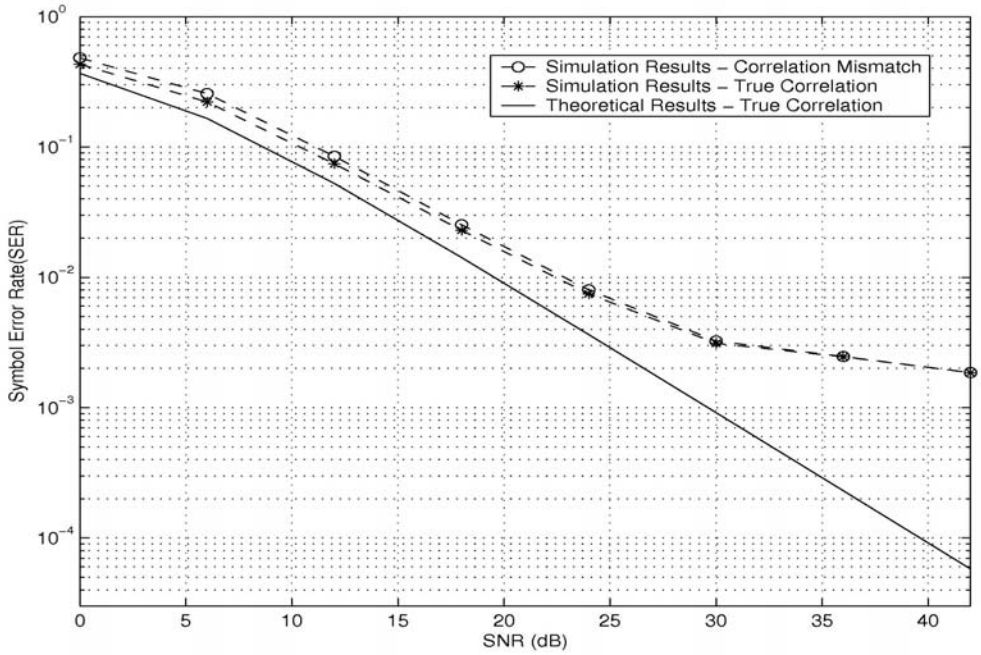

Figure 3.7 Effects of correlation mismatch on SER

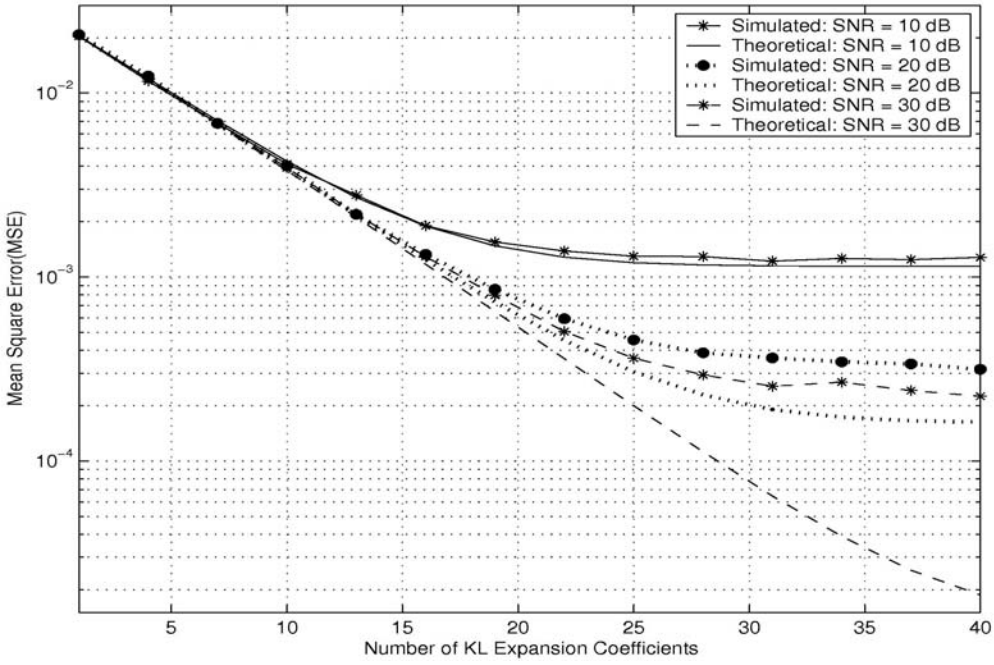

Figure 3.8 MSE as a function of KL expansion coefficients

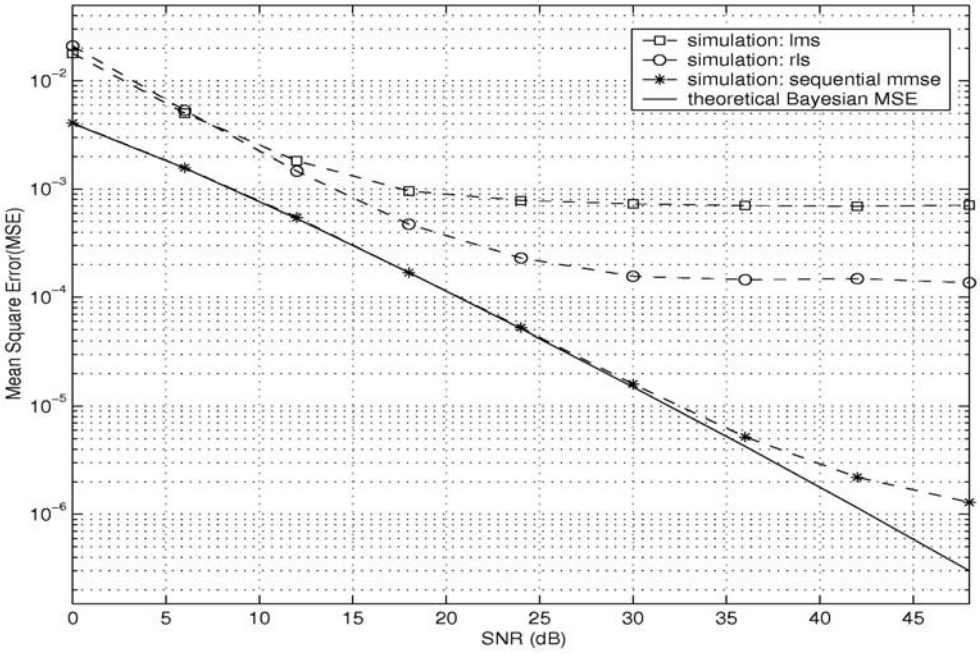

Figure 3.9 MSE sequential MMSE performance

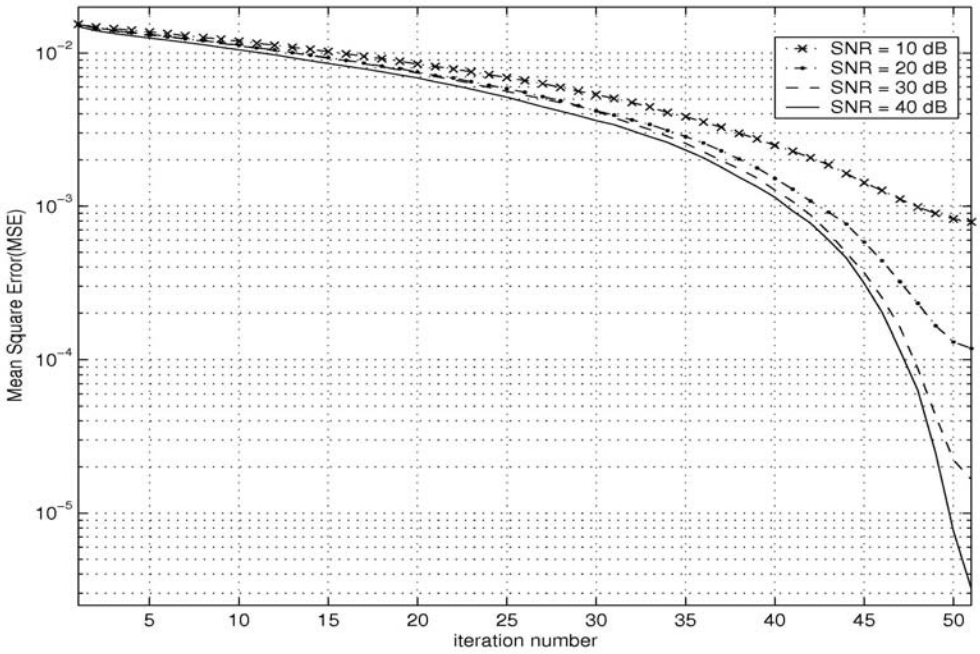

Figure 3.10 Convergence of the sequential MMSE estimator

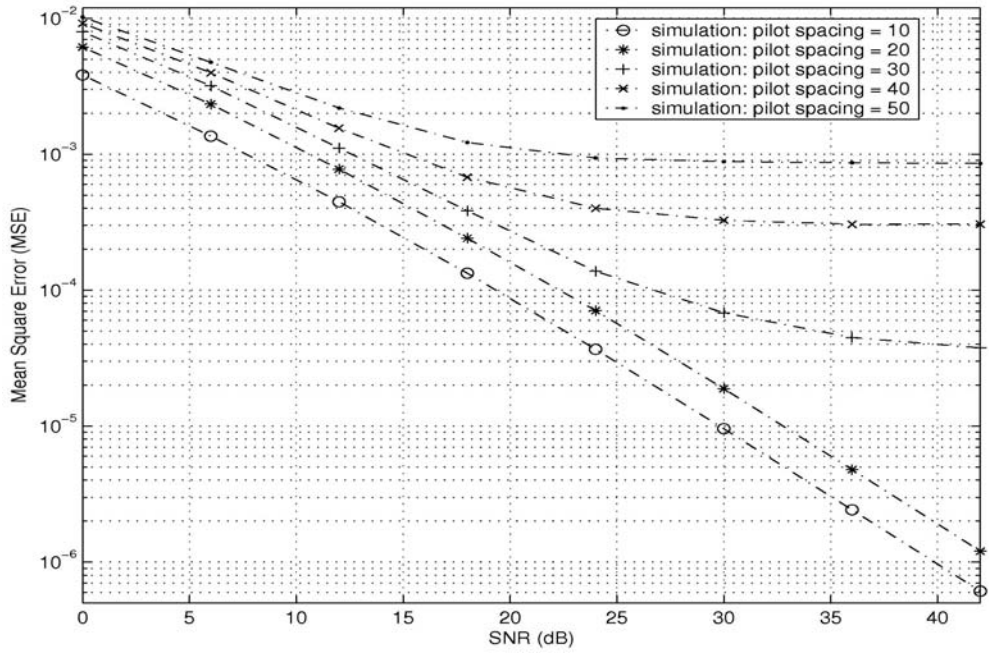

Figure 3.11 Performance of the sequential MMSE for different pilot spacing

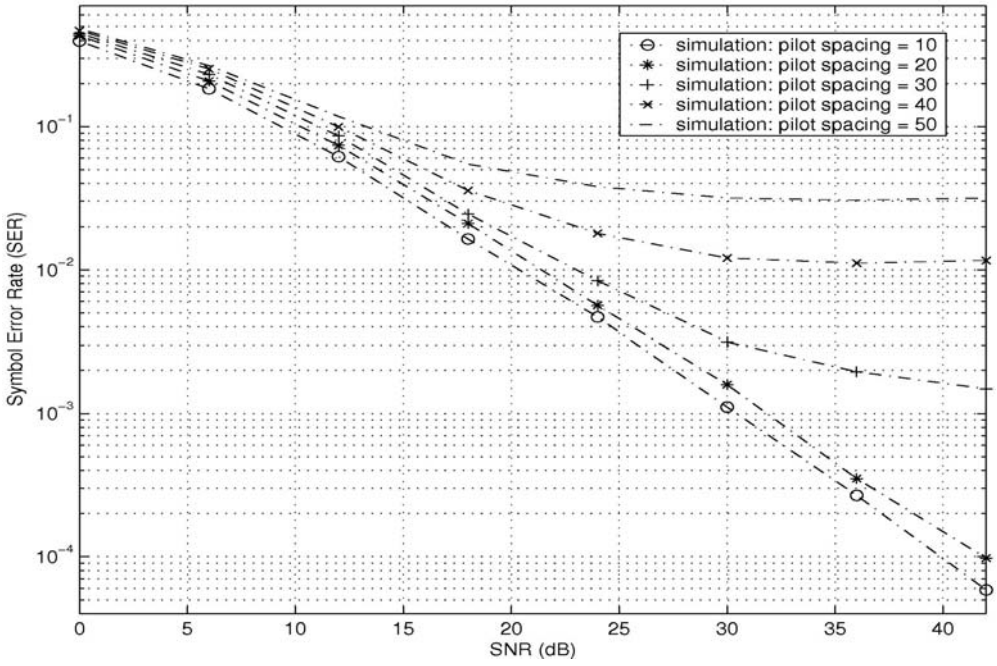

Figure 3.12 Symbol Error Rate of the sequential MMSE for different pilot spacing

Chapter 4

Channel Estimation for OFDM System with Transmit Diversity

In this section, we consider a transmit diversity scheme in conjunction with OFDM signaling. Many transmit diversity schemes have been proposed in the literature offering different complexity vs. performance trade-offs. Alamouti's transmit diversity scheme is chosen in this thesis due to its simple implementation and good performance, Alamouti [15]. The Alamouti's scheme imposes an orthogonal spatio-temporal structure on the transmitted symbols that guarantees full (i.e., order 2) spatial diversity.

We consider the Alamouti transmit diversity coding scheme, employed in an OFDM system utilizing K subcarriers per antenna transmissions. Note that K is chosen as an even integer. The fading channel between the μ*th* transmit antenna and the receive antenna is assumed to be frequency selective and is described by the discrete-time baseband equivalent impulse response $\mathbf{h}_{\mu}(n) = \left[h_{\mu,0}(n), \ldots, h_{\mu,L}(n)\right]^T$ with L standing for the channel order.

Each time index n, the input serial information symbols with symbol duration T_s is converted into a data vector $\mathbf{X}(n) = \left[X(n,0), \ldots, X(n,K-1)\right]^T$ by means of a serial-to-parallel converter. Its block duration is KT_s. Moreover, $\mathbf{X}(n,k)$ denote the kth forward polyphase component of the serial data symbols, i.e, $\mathbf{X}(n,k) = \mathbf{X}(nK+k)$ for $k=0,1,2,\ldots,K-1$ and $n=0,1,2,\ldots,N-1$.

Polyphase component $\mathbf{X}(n,k)$ can also be viewed as the data symbol to be transmitted on the *kth* tone during the block instant *n*. The transmit diversity encoder arranges $\mathbf{X}(n)$ into two vectors $\mathbf{X}_1(n)$ and $\mathbf{X}_2(n)$ according to a appropriate coding scheme described in Alamouti [15], Lee and Williams [20]. The coded vector $\mathbf{X}_1(n)$ is modulated by an IFFT into an OFDM sequence. Then cyclic prefix is added to the OFDM symbol sequence, and the resulting signal is transmitted through the first transmit antenna. Similarly, $\mathbf{X}_2(n)$ is modulated by IFFT, cyclically extended, and transmitted from the second transmit antenna.

At the receiver side, the antenna receives a noisy superposition of the transmissions through the fading channels. We assume ideal carrier synchronization, timing and perfect symbol-rate sampling, and the cyclic prefix is removed at the receiver end.
The generation of coded vectors $\mathbf{X}_1(n)$ and $\mathbf{X}_2(n)$ from the information symbols lead to corresponding transmit diversity OFDM scheme. In our system, the generation of $\mathbf{X}_1(n)$ and $\mathbf{X}_2(n)$ is performed via the space-frequency coding and space-time coding respectively, which were first suggested in Alamouti[15] and later generalized in Liu *et al*. [21], Bolcskei and Paulraj [22].

4.1 Space-Frequency Coding in OFDM Systems

We first consider a strategy, which basically consists of coding across OFDM tones and is therefore called space frequency coding Lee and Williams [20], Liu *et al*. [21], Bolcskei and Paulraj [22]. Resorting to coding across tones, the set of generally correlated OFDM subchannels is first divided into groups of subchannels. This subchannel grouping with appropriate system parameters does preserve diversity gain while simplifying not only the code construction but decoding algorithm significantly as well Lee and Williams [20].

A block diagram of a two-branch space-frequency OFDM transmit diversity system is shown in Figure 8.1. Resorting subchannel grouping, $\mathbf{X}(n)$ is coded into two vectors $\mathbf{X}_1(n)$ and $\mathbf{X}_2(n)$ by the space-frequency encoder as

$$\mathbf{X}_1(n) = \left[X(n,0), -X^*(n,1), \cdots, X(n,K-2), -X^*(n,K-1)\right]^T$$
$$\mathbf{X}_2(n) = \left[X(n,1), -X^*(n,0), \cdots, X(n,K-1), -X^*(n,K-2)\right]^T \quad (4.1)$$

where $(.)^*$ stands for complex conjugation. In space-frequency Alamouti scheme, $\mathbf{X}_1(n)$ and $\mathbf{X}_2(n)$ are transmitted through the first and second antenna element respectively during the OFDM block instant *n*.

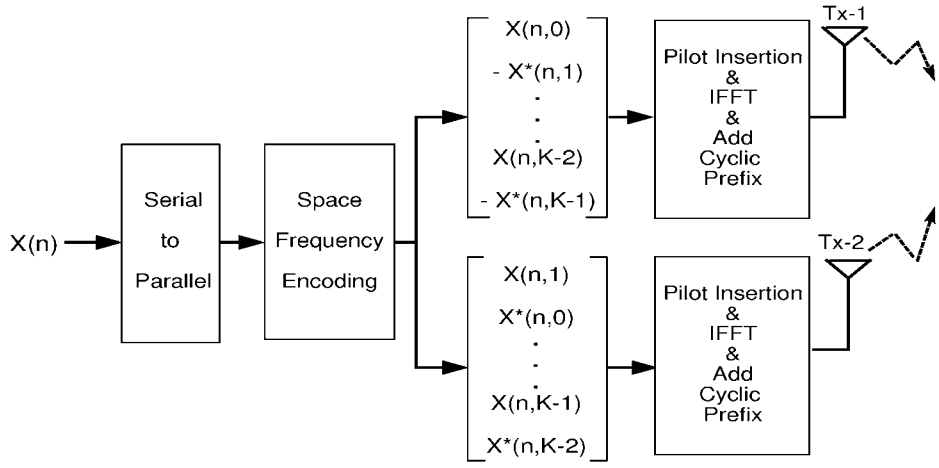

Figure 4.1 Space-frequency coding on two adjacent FFT frequency bins

The operations of the space-frequency block encoder can best be described in terms of even and odd polyphase component vectors. If we denote even and odd component vectors of $\mathbf{X}(n)$ as

$$\mathbf{X}_e(n) = \left[X(n,0), X(n,2), \cdots, X(n,K-4), X(n,K-2)\right]^T$$
$$\mathbf{X}_o(n) = \left[X(n,1), X(n,3), \cdots, X(n,K-3), X(n,K-1)\right]^T \quad (4.2)$$

then the space-frequency block code transmission matrix may be represented by,

$$\begin{array}{c} \\ \text{frequency} \\ \downarrow \end{array} \begin{array}{c} \text{space} \rightarrow \\ \begin{bmatrix} \mathbf{X}_e(n) & \mathbf{X}_o(n) \\ -\mathbf{X}_o^*(n) & \mathbf{X}_e^*(n) \end{bmatrix} \end{array} \quad (4.3)$$

If the received signal sequence is parsed in even and odd blocks of $K/2$ tones, $\mathbf{Y}_e(n) = [Y(n,0), Y(n,2), \cdots, Y(n,K-2)]^T$ and $\mathbf{Y}_o(n) = [Y(n,1), Y(n,3), \cdots, Y(n,K-1)]^T$, the received signal can be expressed in vector form as

$$\mathbf{Y}_e(n) = \mathcal{X}_e(n)\mathbf{H}_{1,e}(n) + \mathcal{X}_o(n)\mathbf{H}_{2,e}(n) + \boldsymbol{\eta}_e(n)$$
$$\mathbf{Y}_o(n) = -\mathcal{X}_o^{\dagger}(n)\mathbf{H}_{1,o}(n) + \mathcal{X}_o^{\dagger}(n)\mathbf{H}_{2,o}(n) + \boldsymbol{\eta}_o(n) \tag{4.4}$$

where $\mathcal{X}_e(n)$ and $\mathcal{X}_o(n)$ are $K/2 \times K/2$ diagonal matrices whose elements are $\mathbf{X}_e(n)$ and $\mathbf{X}_o(n)$ respectively. $K/2$ length even and odd component vectors of the channel attenuations between the μth transmitter and the receiver are

$$\mathbf{H}_{\mu,e}(n) = [H_\mu(n,0), H_\mu(n,2), \cdots, H_\mu(n,K-2)]^T \tag{4.5}$$

and

$$\mathbf{H}_{\mu,o}(n) = [H_\mu(n,1), H_\mu(n,3), \cdots, H_\mu(n,K-1)]^T \tag{4.6}$$

Finally, $\boldsymbol{\eta}_e(n)$ and $\boldsymbol{\eta}_o(n)$ are zero-mean, independent identical distributed Gaussian vectors with covariance matrix $\sigma^2 \mathbf{I}_{K/2}$.

Equation (4.4) shows that the information symbols $\mathcal{X}_e(n)$ and $\mathcal{X}_o(n)$ are transmitted twice in two consecutive adjacent subchannel groups through two different channels. In order to estimate the channels and decode $\mathcal{X}$ with the embedded diversity gain through the repeated transmission, for each *n*, we can write the following from (4.4):

$$\begin{bmatrix} \mathbf{Y}_e(n) \\ \mathbf{Y}_o(n) \end{bmatrix} = \begin{bmatrix} \mathcal{X}_e(n) & \mathcal{X}_o(n) \\ -\mathcal{X}_o^{\dagger}(n) & \mathcal{X}_e^{\dagger}(n) \end{bmatrix} \begin{bmatrix} \mathbf{H}_{1,e}(n) \\ \mathbf{H}_{2,e}(n) \end{bmatrix} + \begin{bmatrix} \boldsymbol{\eta}_e(n) \\ \boldsymbol{\eta}_o(n) \end{bmatrix} \tag{4.7}$$

where the complex channel gains between adjacent subcarriers are assumed to be approximately constant, i.e., $\mathbf{H}_{1,e}(n) \cong \mathbf{H}_{1,o}(n)$ and $\mathbf{H}_{2,e}(n) \cong \mathbf{H}_{2,o}(n)$. The effect of this assumption allows us to omit dependence of $\mathbf{H}_{1,e}(n)$ and $\mathbf{H}_{2,e}(n)$ on even channel components.

4.2 Space-Time Coding in OFDM Systems

In contrast to SF-OFDM coding, ST encoder maps every two consecutive symbol blocks $\mathbf{X}(n)$ and $\mathbf{X}(n+1)$ to the following $2K \times 2$ matrix:

$$\begin{array}{c} \\ \text{time} \\ \downarrow \end{array} \begin{array}{c} \text{space} \rightarrow \\ \begin{bmatrix} \mathbf{X}(n) & \mathbf{X}(n+1) \\ -\mathbf{X}^*(n+1) & \mathbf{X}^*(n) \end{bmatrix} \end{array} \tag{4.8}$$

whose columns are transmitted in successive time intervals with the upper and lower blocks in a given column sent simultaneously through the first and second transmit antenna respectively as shown in Figure 4.2.

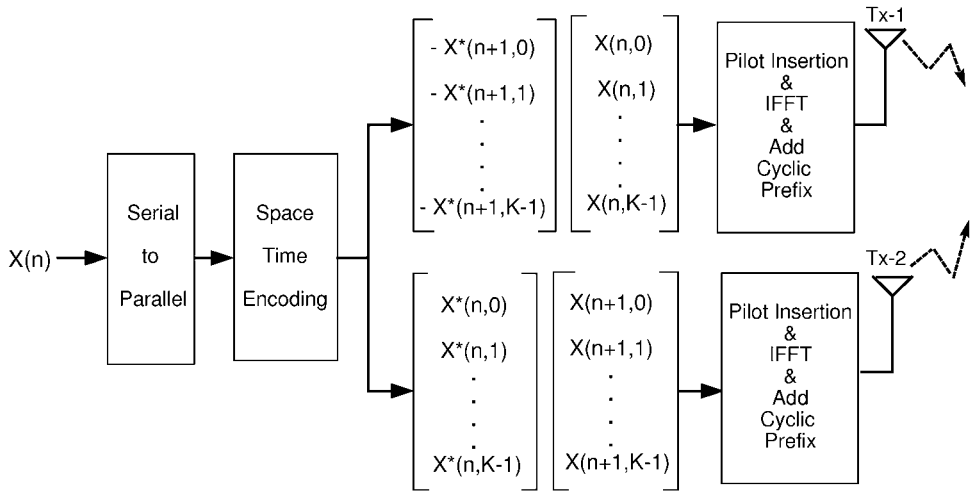

Figure 4.2 Space time coding on two adjacent OFDM blocks

If we focus on each received block separately, each pair of two-consecutive received block $\mathbf{Y}(n) = [Y(n,0), \cdots, Y(n,K-1)]^T$ and $\mathbf{Y}(n+1) = [Y(n+1,0), \cdots, Y(n+1,K-1)]^T$

are given by

$$\mathbf{Y}(n) = \mathcal{X}(n)\mathbf{H}_1(n) + \mathcal{X}(n+1)\mathbf{H}_2(n) + \boldsymbol{\eta}(n)$$
$$\mathbf{Y}(n+1) = -\mathcal{X}^{\dagger}(n+1)\mathbf{H}_1(n+1) + \mathcal{X}^{\dagger}(n)\mathbf{H}_2(n+1) + \boldsymbol{\eta}(n) \tag{4.9}$$

where $\mathcal{X}(n)$ and $\mathcal{X}(n+1)$ are $K \times K$ diagonal matrices whose elements are $\mathbf{X}(n)$ and $\mathbf{X}(n+1)$ respectively. $\mathbf{H}_{\mu}(n)$ is the channel frequency response between the μ th transmitter and the receiver antenna at the *n*th time slot which is obtained from channel impulse response $\mathbf{h}_{\mu}(n)$. Finally, $\boldsymbol{\eta}(n)$ and $\boldsymbol{\eta}(n+1)$ are zero-mean, independent identical distributed Gaussian vectors with covariance matrix $\sigma^2\mathbf{I}_K$ per dimension.

From the above description, it is seen that joint estimation/decoding in an ST-OFDM system involves the received signals over two consecutive OFDM blocks. To simplify the problem, we assume that the complex channel gains remain constant over the duration of one ST-OFDM code word, i.e., $\mathbf{H}_1(n) \cong \mathbf{H}_1(n+1)$ and $\mathbf{H}_2(n) \cong \mathbf{H}_2(n+1)$. As will be seen, such an assumption significantly simplifies the channel estimation algorithm. Similarly, the effect of this assumption allows us to omit dependence of channel attenuations on two different time indexes. Using (4.9) and dropping dependence on *n*, we have

$$\begin{bmatrix} \mathbf{Y}(n) \\ \mathbf{Y}(n+1) \end{bmatrix} = \begin{bmatrix} \mathcal{X}(n) & \mathcal{X}(n+1) \\ -\mathcal{X}^{\dagger}(n+1) & \mathcal{X}^{\dagger}(n) \end{bmatrix} \begin{bmatrix} \mathbf{H}_1(n) \\ \mathbf{H}_2(n) \end{bmatrix} + \begin{bmatrix} \boldsymbol{\eta}(n) \\ \boldsymbol{\eta}(n+1) \end{bmatrix} \tag{4.10}$$

4.3 Unifying Space-Frequency and Space-Time OFDM Signal Models

Comparing (4.7) and (4.10), we unify SF-OFDM and ST-OFDM in the following equivalent model:

$$\begin{bmatrix}\mathbf{Y}_1\\ \mathbf{Y}_2\end{bmatrix}=\begin{bmatrix}\mathcal{X}_1 & \mathcal{X}_2\\ -\mathcal{X}_2^{\dagger} & \mathcal{X}_1^{\dagger}\end{bmatrix}\begin{bmatrix}\mathbf{H}_1\\ \mathbf{H}_2\end{bmatrix}+\begin{bmatrix}\boldsymbol{\eta}_1\\ \boldsymbol{\eta}_2\end{bmatrix} \tag{4.11}$$

For convenience, we list the corresponding vectors and matrix for SF-OFDM as

$$\begin{bmatrix}\mathbf{Y}_1\\ \mathbf{Y}_2\end{bmatrix}=\begin{bmatrix}\mathbf{Y}_e(n)\\ \mathbf{Y}_o(n)\end{bmatrix}\ ,\ \begin{bmatrix}\mathcal{X}_1 & \mathcal{X}_2\\ -\mathcal{X}_2^{\dagger} & \mathcal{X}_1^{\dagger}\end{bmatrix}=\begin{bmatrix}\mathcal{X}_e(n) & \mathcal{X}_o(n)\\ -\mathcal{X}_o^{\dagger}(n) & \mathcal{X}_e^{\dagger}(n)\end{bmatrix}$$

$$\begin{bmatrix}\mathbf{H}_1\\ \mathbf{H}_2\end{bmatrix}=\begin{bmatrix}\mathbf{H}_{1,e}(n)\\ \mathbf{H}_{2,e}(n)\end{bmatrix}\ ,\ \begin{bmatrix}\boldsymbol{\eta}_1\\ \boldsymbol{\eta}_2\end{bmatrix}=\begin{bmatrix}\boldsymbol{\eta}_e(n)\\ \boldsymbol{\eta}_o(n)\end{bmatrix}$$

and for ST-OFDM as

$$\begin{bmatrix}\mathbf{Y}_1\\ \mathbf{Y}_2\end{bmatrix}=\begin{bmatrix}\mathbf{Y}(n)\\ \mathbf{Y}(n+1)\end{bmatrix}\ ,\ \begin{bmatrix}\mathcal{X}_1 & \mathcal{X}_2\\ -\mathcal{X}_2^{\dagger} & \mathcal{X}_1^{\dagger}\end{bmatrix}=\begin{bmatrix}\mathcal{X}(n) & \mathcal{X}(n+1)\\ -\mathcal{X}^{\dagger}(n+1) & \mathcal{X}^{\dagger}(n)\end{bmatrix}$$

$$\begin{bmatrix}\mathbf{H}_1\\ \mathbf{H}_2\end{bmatrix}=\begin{bmatrix}\mathbf{H}_1(n)\\ \mathbf{H}_2(n)\end{bmatrix}\ ,\ \begin{bmatrix}\boldsymbol{\eta}_1\\ \boldsymbol{\eta}_2\end{bmatrix}=\begin{bmatrix}\boldsymbol{\eta}(n)\\ \boldsymbol{\eta}(n+1)\end{bmatrix}$$

Relying on the unifying model (4.11), channel estimation algorithms will be developed according to the MMSE criterion. A different approach is adapted here to explicitly model the channel parameters by the KL series representation since; KL expansion allows one to tackle the estimation of correlated parameters as a parameter estimation problem of the uncorrelated coefficients. Note that KL expansion is well known for its optimal truncation property, Yip and Ng [9]. That is, the KL expansion requires the minimum number of terms among all possible series expansions in representing a random channel for a given mean-squared error. Thus, the optimal truncation property of the KL expansion results in a smaller computational load on the channel estimation algorithm. Therefore, first, the KL representation of the multipath channel will be summarized in the following section.

4.4 MMSE Multipath Channel Estimator for ST/SF-OFDM Systems

Pilot symbol assisted techniques can provide information about an under sampled version of the channel that may be easier to identify. In this paper, we therefore address the problem of estimating multipath channel parameters by exploiting the distributed training symbols.

Since both SF and ST block coded OFDM systems have symmetric structure in frequency and time respectively, the pilot symbols should be uniformly placed in pairs. Specifically, we also assume that even numbers of symbols are placed between pilot pairs for SF-OFDM systems. Based on these pilot structures, Equation (4.11) is modified to represent the signal model corresponding to pilot symbols as follows:

$$\underbrace{\begin{bmatrix}\mathbf{Y}_{1,p}\\ \mathbf{Y}_{2,p}\end{bmatrix}}_{\mathbf{Y}_p}=\underbrace{\begin{bmatrix}X_{1,p} & X_{2,p}\\ -X_{2,p}^{*} & X_{1,p}^{*}\end{bmatrix}}_{\bar{X}_p}\underbrace{\begin{bmatrix}\mathbf{H}_{1,p}\\ \mathbf{H}_{2,p}\end{bmatrix}}_{\mathbf{H}_p}+\underbrace{\begin{bmatrix}\boldsymbol{\eta}_{1,p}\\ \boldsymbol{\eta}_{2,p}\end{bmatrix}}_{\boldsymbol{\eta}_p} \tag{4.12}$$

where $(.)_p$ is introduced to represent the vectors corresponding to pilot locations. Assuming pilot symbols are taken from QPSK modulation, the observation model can be formed by premultiplying both sides of (4.12) by $\bar{X}_p^{\dagger}$

$$\bar{X}_p^{\dagger}\mathbf{Y}_p=\bar{X}_p^{\dagger}\bar{X}_p\mathbf{H}_p+\bar{X}_p^{\dagger}\boldsymbol{\eta}_p \tag{4.13}$$

where $\bar{X}_p^{\dagger}\bar{X}_p=2\mathbf{I}_{2K_p}$ and letting $\tilde{\mathbf{Y}}_p=\bar{X}_p^{\dagger}\mathbf{Y}_p$ and $\tilde{\boldsymbol{\eta}}_p=\bar{X}_p^{\dagger}\boldsymbol{\eta}_p$ we get the following equation:

$$\tilde{\mathbf{Y}}_p=2\mathbf{H}_p+\tilde{\boldsymbol{\eta}}_p \tag{4.14}$$

namely,

$$\begin{bmatrix} \tilde{\mathbf{Y}}_{1,p} \\ \tilde{\mathbf{Y}}_{2,p} \end{bmatrix} = 2\begin{bmatrix} \mathbf{H}_{1,p} \\ \mathbf{H}_{2,p} \end{bmatrix} + \begin{bmatrix} \tilde{\boldsymbol{\eta}}_{1,p} \\ \tilde{\boldsymbol{\eta}}_{2,p} \end{bmatrix} \tag{4.15}$$

where

$$\tilde{\mathbf{Y}}_{1,p} = \mathcal{X}_{1,p}^{\dagger}\mathbf{Y}_{1,p} - \mathcal{X}_{2,p}^{\dagger}\mathbf{Y}_{2,p} \tag{4.16}$$

$$\tilde{\mathbf{Y}}_{2,p} = \mathcal{X}_{2,p}^{\dagger}\mathbf{Y}_{1,p} + \mathcal{X}_{1,p}^{\dagger}\mathbf{Y}_{2,p}$$

$$\tilde{\boldsymbol{\eta}}_{1,p} = \mathcal{X}_{1,p}^{\dagger}\boldsymbol{\eta}_{1,p} - \mathcal{X}_{2,p}^{\dagger}\boldsymbol{\eta}_{2,p}$$

$$\tilde{\boldsymbol{\eta}}_{2,p} = \mathcal{X}_{2,p}^{\dagger}\boldsymbol{\eta}_{1,p} + \mathcal{X}_{1,p}^{\dagger}\boldsymbol{\eta}_{2,p}$$

and note that $\tilde{\boldsymbol{\eta}}_{1,p} \sim \mathcal{N}\left(\mathbf{0}, 2\sigma^2\mathbf{I}_{K_p}\right)$ and $\tilde{\boldsymbol{\eta}}_{2,p} \sim \mathcal{N}\left(\mathbf{0}, 2\sigma^2\mathbf{I}_{K_p}\right)$. By writing each row of the (4.15) separately, we get the following observation equation set to estimate the channels $\mathbf{H}_{1,p}$ and $\mathbf{H}_{2,p}$.

$$\tilde{\mathbf{Y}}_{\mu,p} = 2\mathbf{H}_{\mu,p} + \tilde{\boldsymbol{\eta}}_{\mu,p} \quad , \qquad \mu=1, 2 \tag{4.17}$$

and substituting $\mathbf{H}_{\mu,p} = \mathbf{F}\mathbf{h}_{\mu}$ in (4.17), we get the following observation models for the channel impulse responses $\mathbf{h}_{\mu}$ is obtained

$$\tilde{\mathbf{Y}}_{\mu,p} = 2\mathbf{F}\mathbf{h}_{\mu} + \tilde{\boldsymbol{\eta}}_{\mu,p} \quad , \qquad \mu=1, 2 \tag{4.18}$$

where $\mathbf{F}$ is a $K_p \times L$ FFT matrix generated based on pilot indices and K_p is the number of pilot symbols per one OFDM block. Equation (4.18) offers a Bayesian linear model representation. Based on these representations, the minimum variance estimator for the time-domain channel vectors $\mathbf{h}_1$ and $\mathbf{h}_2$ can be obtained using the

MMSE estimator. We should clearly make the assumptions that impulse responses $\mathbf{h}_1$ and $\mathbf{h}_2$ are independent identical zero-mean complex Gaussian vectors with covariance $\mathbf{C_h}$, and $\mathbf{h}_1$ and $\mathbf{h}_2$ are independent from $\tilde{\boldsymbol{\eta}}_{1,p}$ and $\tilde{\boldsymbol{\eta}}_{2,p}$. Therefore, MMSE estimates of $\mathbf{h}_1$ and $\mathbf{h}_2$ are given by Kay [11]:

$$\hat{\mathbf{h}}_\mu = \left((2\mathbf{F})^\dagger \mathbf{C}^{-1}_{\tilde{\boldsymbol{\eta}}_{\mu,p}} (2\mathbf{F}) + \mathbf{C}^{-1}_{\mathbf{h}} \right)^{-1} (2\mathbf{F})^\dagger \mathbf{C}^{-1}_{\tilde{\boldsymbol{\eta}}_{\mu,p}} \tilde{\mathbf{Y}}_{\mu,p} \ , \qquad \mu = 1, 2 \tag{4.19}$$

Due to PSK pilot symbol assumption together with the result $\tilde{\boldsymbol{\eta}}_{1,p} \sim \mathcal{N}\left(\mathbf{0}, 2\sigma^2 \mathbf{I}_{K_p}\right)$ and $\tilde{\boldsymbol{\eta}}_{2,p} \sim \mathcal{N}\left(\mathbf{0}, 2\sigma^2 \mathbf{I}_{K_p}\right)$ we can therefore express (4.19) by

$$\hat{\mathbf{h}}_\mu = \left(2\mathbf{F}^\dagger \mathbf{F} + \sigma^2 \mathbf{C}^{-1}_{\mathbf{h}} \right)^{-1} \mathbf{F}^\dagger \tilde{\mathbf{Y}}_{\mu,p} \qquad , \qquad \mu = 1, 2 \tag{4.20}$$

Under the assumption that uniformly spaced pilot symbols are inserted with pilot spacing interval Δ and $K = \Delta \times K_P$, correspondingly, $\mathbf{F}^\dagger \mathbf{F}$ reduces to $\mathbf{F}^\dagger \mathbf{F} = K_p \mathbf{I}_L$. Then according to (20), and $\mathbf{F}^\dagger \mathbf{F} = K_p \mathbf{I}_L$, following expression is obtained

$$\hat{\mathbf{h}}_\mu = \left(2K_p \mathbf{I}_L + \sigma^2 \mathbf{C}^{-1}_{\mathbf{h}} \right)^{-1} \mathbf{F}^\dagger \tilde{\mathbf{Y}}_{\mu,p} \qquad , \qquad \mu = 1, 2 \tag{4.21}$$

As it can be seen from (4.21) MMSE estimation of $\mathbf{h}_1$ and $\mathbf{h}_2$ for SF-OFDM and ST-OFDM systems still requires the inversion of $\mathbf{C}^{-1}_{\mathbf{h}}$. Therefore it suffers from a high computational complexity. However, it is possible to reduce complexity of the MMSE algorithm by expanding multipath channel as a linear combination of orthogonal basis vectors. The orthogonality of the basis vectors makes the channel representation efficient and mathematically convenient KL transform which amounts to a generalization of the FFT for random processes can be employed here. This transformation is related to diagonalization of the channel correlation matrix by the unitary eigenvector transformation:

$$\mathbf{C_h} = \mathbf{\Psi \Lambda \Psi}^{\dagger} \tag{4.22}$$

where $\mathbf{\Psi} = [\boldsymbol{\psi}_0, \boldsymbol{\psi}_1, \ldots, \boldsymbol{\psi}_{L-1}]$ $\boldsymbol{\psi}_\ell$'s are the orthonormal basis vectors, and $\mathbf{g}_\mu = [g_{\mu,0}, g_{\mu,1}, \ldots, g_{\mu,L-1}]$ is zero mean Gaussian vector with diagonal covariance matrix $\mathbf{\Lambda_g} = E[\mathbf{g}_\mu \mathbf{g}_\mu^{\dagger}]$.

Thus the vectors $\mathbf{h}_1$ and $\mathbf{h}_2$ can be expressed as a linear combination of the orthonormal basis vectors as $\mathbf{h}_\mu = \mathbf{\Psi g}_\mu$ where μ is the multipath channel index. As a result, the channel estimation problem in this application is equivalent to estimating the independent identical distributed complex Gaussian vector $\mathbf{h}_1$ and $\mathbf{h}_2$ which represent KL expansion coefficients for multipath channels $\mathbf{h}_1$ and $\mathbf{h}_2$.

4.4.1 Estimation of Karhunen Loeve Coefficients

Substituting $\mathbf{h}_\mu = \mathbf{\Psi g}_\mu$ in unified signal model (4.18), it can be rewritten as

$$\tilde{\mathbf{Y}}_{\mu,p} = 2\mathbf{F\Psi g}_\mu + \tilde{\boldsymbol{\eta}}_{\mu,p} \quad , \qquad \mu = 1, 2 \tag{4.23}$$

this is also recognized as a Bayesian linear model, and recalls that $\mathbf{g}_\mu \sim \mathcal{N}(\mathbf{0}, \mathbf{\Lambda_g})$. As a result, the MMSE estimator of $\mathbf{g}_\mu$ for SF-OFDM and ST-OFDM systems is

$$\begin{aligned} \hat{\mathbf{g}}_\mu &= \mathbf{\Lambda_g}(2K_p\mathbf{\Lambda_g} + \sigma^2\mathbf{I}_L)^{-1}\mathbf{\Psi}^{\dagger}\mathbf{F}^{\dagger}\tilde{\mathbf{Y}}_{\mu,p} \\ &= \ddot{\mathbf{\Gamma}}\mathbf{\Psi}^{\dagger}\mathbf{F}^{\dagger}\tilde{\mathbf{Y}}_{\mu,p} \quad , \qquad \mu = 1, 2, \end{aligned} \tag{4.24}$$

where

$$\ddot{\mathbf{\Gamma}} = \mathbf{\Lambda_g}(2K_p\mathbf{\Lambda_g} + \sigma^2\mathbf{I}_L)^{-1}$$

$$= \text{diag}\left\{ \frac{\lambda_0}{2\lambda_0 K_p + \sigma^2}, \ldots, \frac{\lambda_{L-1}}{2\lambda_{L-1} K_p + \sigma^2} \right\} \tag{4.25}$$

and $\lambda_0, \lambda_1, \ldots, \lambda_{L-1}$ are the singular values of $\mathbf{\Lambda_g}$.

From the results presented in Morelli and Mengali [4], ML estimator of $\mathbf{g}_\mu$ for SF-OFDM and ST-OFDM systems can also be obtained as follows:

$$\hat{\mathbf{g}}_\mu = \frac{1}{2K_p} \mathbf{\Psi}^\dagger \mathbf{F}^\dagger \tilde{\mathbf{Y}}_{\mu,p} \qquad , \qquad \mu = 1, 2, \tag{4.26}$$

It is clear that the complexity of the MMSE estimator in (21) is reduced by the application of KL expansion. However, the complexity of the $\hat{\mathbf{g}}_\mu$ can be further reduced by exploiting the optimal truncation property of the KL expansion, Yip and Ng [9]. A truncated expansion *g'r* can be formed by selecting *r* orthonormal basis vectors among all basis vectors that satisfy $\mathbf{C_h \Psi} = \mathbf{\Psi \Lambda_g}$. Thus, a rank-*r* approximation to $\mathbf{\Lambda_{g_r}}$ is defined as $\mathbf{\Lambda_{g_r}} = \text{diag}\{\lambda_0, \lambda_1, \ldots, \lambda_{r-1}, 0, \ldots, 0\}$.

Since the trailing L - *r* variances $\{\lambda_\ell\}_{\ell=r}^{L-1}$ are small compared to the leading *r* variances $\{\lambda_\ell\}_{\ell=0}^{r-1}$, the trailing L - *r* variances are set to zero to produce the approximation. However, typically the pattern of eigen values for $\mathbf{\Lambda_g}$ splits the eigenvectors into dominant and subdominant sets. Then the choice of *r* is more or less obvious. The optimal truncated KL (rank-*r*) estimator of (23) now becomes

$$\hat{\mathbf{g}}_{\mu_r} = \ddot{\mathbf{\Gamma}}_r \, \mathbf{\Psi}^\dagger \mathbf{F}^\dagger \tilde{\mathbf{Y}}_{\mu,p} \tag{4.27}$$

where

$$\ddot{\mathbf{\Gamma}}_r = \mathbf{\Lambda_{g_r}} (2K_p \mathbf{\Lambda_{g_r}} + \sigma^2 \mathbf{I}_L)^{-1}$$

$$= \text{diag}\left\{ \frac{\lambda_0}{2\lambda_0 K_p + \sigma^2}, \cdots, \frac{\lambda_{r-1}}{2\lambda_{r-1} K_p + \sigma^2}, 0, \cdots, 0 \right\} \tag{4.28}$$

Since our ultimate goal is to obtain MMSE estimator for the channel frequency response $\mathbf{H}_\mu$, from the invariance property of the MMSE estimator, it follows that if $\hat{\mathbf{g}}_\mu$ is the estimate of $\mathbf{g}_\mu$, then the corresponding estimate of $\mathbf{H}_\mu$ can be obtained as

$$\hat{\mathbf{H}}_\mu = \mathcal{F} \Psi \hat{\mathbf{g}}_\mu \quad , \qquad \mu = 1, 2, \tag{4.29}$$

where $\mathcal{F}$ is a $K \times K$ FFT matrix.

4.4.2 Performance Analysis

In this section, we turn our attention again to analytical performance results. Derivation details of the subsections will be passed, and follow as chapter 3 since observation models (3.10) and (4.23) are similar.

4.4.2.1 Cramer-Rao Lower Bound for Karhunen Loeve Coefficients

Under the assumption that $\mathbf{g}_\mu$ and $\tilde{\boldsymbol{\eta}}_{\mu,p}$ are independent, the modified FIM as follows

$$\mathbf{J}_M(\mathbf{g}_\mu) = \frac{1}{\sigma^2} \ddot{\boldsymbol{\Gamma}}^{-1}$$

Inverting the matrix $\mathbf{J}_M(\mathbf{g}_\mu)$ yields

$$\begin{aligned} \text{CRLB}(\mathbf{g}_\mu) &= \mathbf{J}_M^{-1}(\mathbf{g}_\mu) \\ &= \sigma^2 \ddot{\boldsymbol{\Gamma}} \end{aligned} \tag{4.30}$$

4.4.2.2 Bayesian MSE

Keeping in mind $\hat{\boldsymbol{\varepsilon}}_{\mu} = \mathbf{g}_{\mu} - \hat{\mathbf{g}}_{\mu}$ and $\mathbf{C}_{\hat{\boldsymbol{\varepsilon}}_{\boldsymbol{\mu}}} = \sigma^2 \ddot{\boldsymbol{\Gamma}}$, the minimum Bayesian MSE of the full rank estimator becomes (see Appendix D and Appendix E)

$$\begin{aligned} B_{MSE}(\hat{\mathbf{g}}_{\mu}) &= \frac{1}{L}\text{trace}(\mathbf{C}_{\hat{\boldsymbol{\varepsilon}}_{\boldsymbol{\mu}}}) \\ &= \frac{1}{L}\text{trace}(\sigma^2 \ddot{\boldsymbol{\Gamma}}) = \frac{1}{L}\sum_{i=0}^{L-1} \frac{\lambda_i}{1 + 2K_p \lambda_i \, SNR} \end{aligned} \tag{4.31}$$

where $SNR = 1/\sigma^2$.

As the details are given in Appendix C and Appendix D, $\mathbf{B}_{MSE}(\hat{\mathbf{g}}_{\mu})$ given in (4.31) can also be computed for the truncated (low-rank) case as follows:

$$\mathbf{B}_{MSE}(\hat{\mathbf{g}}_{\mu_r}) = \frac{1}{L}\sum_{i=0}^{r-1} \frac{\lambda_i}{1 + 2K_p \lambda_i \, SNR} + \frac{1}{L}\sum_{i=r}^{L-1} \lambda_i \tag{4.32}$$

Notice that, the second term in (4.32) is the sum of the powers in the KL transform coefficients not used in the truncated estimator. Thus, truncated $\mathbf{B}_{MSE}(\hat{\mathbf{g}}_{\mu})$ can be lower bounded by $\frac{1}{L}\sum_{i=r}^{L-1} \lambda_i$ which will cause an irreducible error floor in the SER results.

4.4.3 Mismatch Analysis

The proposed estimator will be designed according to the channel statistics and the SNR assumptions but these can be different from the true channel statistics and the SNR values. This causes the performance degradation.

Hence, mismatch analysis is important to explore the performance degradation due to a mismatch of the estimator to the channel statistics as well as the SNR, and to study the choice of the channel correlation, and SNR for this estimator so that it is robust to variations in the channel statistics. As a performance measure, we use uncoded Symbol Error Rate (SER) of Maximum Ratio Receive Combiner (MRRC) for QPSK signaling. The SER expression for this case is given in Appendix F as a function of the SNR as follows:

$$\mathrm{Pr(error)} = \frac{3}{4} - \left(\frac{1}{2} + \frac{1}{\pi}\arctan(\gamma_2)\right)\gamma_2^3\,\gamma_3 - \gamma_2^2\,\gamma_1 \tag{4.33}$$

or approximately we get

$$\mathrm{Pr(error)} = 1 - \gamma_2^3\,\gamma_3 \tag{4.34}$$

where

$$\gamma_1 = \frac{1}{2\pi(\mathrm{SNR}+1)} \quad , \quad \gamma_2 = \sqrt{\frac{\mathrm{SNR}}{\mathrm{SNR}+2}} \quad , \quad \gamma_3 = \frac{\mathrm{SNR}+3}{\mathrm{SNR}}$$

In practice, the true channel correlations and SNR are not known. If the MMSE channel estimator is designed to match the correlation of a multipath channel impulse response $\mathbf{C_h}$ and SNR, but the true channel parameters $\tilde{\mathbf{h}}_\mu$ has the correlation $\mathbf{C}_{\tilde{\mathbf{h}}}$ and the true $\tilde{\mathrm{SNR}}$, then average Bayesian MSE for the designed channel estimator is obtained as (see Appendix D and E)

- SNR mismatch:

$$\mathbf{B}_{\mathrm{MSE}}(\hat{\mathbf{g}}_\mu) = \frac{1}{L}\sum_{i=0}^{L-1}\frac{\lambda_i}{(1+2K_p\lambda_i\mathrm{SNR})^2}\left[1 + 2K_p\lambda_i\frac{\mathrm{SNR}^2}{\tilde{\mathrm{SNR}}}\right] \tag{4.35}$$

- Correlation mismatch:

$$\mathbf{B}_{MSE}(\hat{\mathbf{g}}_\mu) = \frac{1}{L}\sum_{i=0}^{L-1}\frac{\tilde{\lambda}_i + 2K_p SNR\,\lambda_i(\tilde{\lambda}_i + \lambda_i - 2\beta_i)}{1 + 2K_p SNR\,\lambda_i} \tag{4.36}$$

where $\tilde{\lambda}_i$ is the ith diagonal element of $\mathbf{\Lambda}_{\tilde{\mathbf{g}}} = \mathbf{\Psi}^\dagger \mathbf{C}_{\tilde{\mathbf{h}}} \mathbf{\Psi}$, and β_i is ith diagonal element of the real part of the cross correlation matrix between $\tilde{\mathbf{g}}_\mu$ and $\mathbf{g}_\mu$.

4.5 Simulation Results

In this section, we investigate the performance of the pilot aided MMSE channel estimation algorithm proposed for both SF-OFDM and ST-OFDM systems. The diversity scheme with two transmit and one receive antenna is considered. Channel impulse responses $\mathbf{h}_\mu$ are generated according to $\mathbf{C_h} = \frac{1}{K^2}\mathbf{F}^\dagger \mathbf{C_H F}$ where C_H is the covariance matrix of the doubly-selective fading channel model. In this model, $\mathbf{H}_\mu(k)$'s are with an exponentially decaying power delay profile $\theta(\tau) = Ce^{-\tau/\tau_{rms}}$. C is power normalization constant. Note that the normalized discrete channel-correlations for different subcarriers and blocks of this channel model were presented in Li *et al*. [5] as follows,

$$c_f(k-k') = \frac{1 - e^{-L\left(\frac{1}{\tau_{rms}} + j\frac{2\pi(k-k')}{K}\right)}}{\tau_{rms}\left(1 - e^{\frac{-L}{\tau_{rms}}}\right)\left(\frac{1}{\tau_{rms}} + j\frac{2\pi(k-k')}{K}\right)} \tag{4.37}$$

$$c_t(n-n') = J_0\left(2\pi f_m (n-n')T_s\right) \tag{4.38}$$

where J_o is the *zero* th-order Bessel function of the first kind and f_m is the maximum Doppler frequency.

The scenario for SF-OFDM simulation study consists of a wireless QPSK OFDM system. The system has a 2.34 MHz bandwidth (for the pulse roll-off factor 0.2) and is divided into 512 tones with a total period of 136 μs, of which 5.12 μs constitute the cyclic prefix (L=20). The uncoded data rate is 7.8 Mbit/s. $\tau_{rms} = 5$ samples ($1.28\,\mu s$) for the power-delay profile. Keeping the transmission efficiency 3.32 bits/sec/Hz fixed, we also simulate ST-OFDM system.

4.5.1 Mean Square Error Performance of the Channel Estimation

The proposed MMSE channel estimators of (4.24) are implemented for both SF-OFDM and ST-OFDM, and compared in terms of average Bayesian MSE for a wide range of SNR levels. Average B_{MSE} is defined as the norm of the difference between the vectors $\mathbf{g} = \left[\mathbf{g}_1^T, \mathbf{g}_2^T\right]^T$ and $\hat{\mathbf{g}}$, representing the true and the estimated values of channel parameters, respectively. Namely,

$$\mathrm{MSE} = \frac{1}{2L}\left\|\mathbf{g} - \hat{\mathbf{g}}\right\|^2 \tag{4.39}$$

4.5.2 MMSE Approach

A pilot symbol for every ten ($\Delta = 10$) symbols is used in the simulation. The MSE at each SNR point is averaged over 10000 realizations. The experimental MSE performance and its theoretical Bayesian MSE of the proposed full-rank MMSE estimator with ML estimator and its corresponding CRLB for SF and ST OFDM systems are compared. Figure 4.3 and Figure 4.4 confirm that MMSE estimator performs better than ML estimator at low SNR. However, the two approaches have comparable performance at high SNRs. To observe the performance, the MMSE and ML estimated channel SER results together with theoretical SER are also presented in Figure 4.5 and Figure 4.6.

Due to the fact that spaces between the pilot symbols are not chosen as a factor of the number of subcarriers, an error floor is observed in Figure 4.3, Figure 4.4, Figure 4.5, and Figure 4.6. In the case of choosing the pilot space as a factor of number of subcarriers, the error floor vanishes because of the fact that the orthogonality condition between the subcarriers at pilot locations is satisfied. In other words, the curves labeled as simulation results for MMSE estimator and ML estimator fit to the theoretical curves at high SNRs. It also shows that the MMSE estimated channel SER results are better than ML estimated channel SER especially at low SNR.

4.5.2.1 SNR Design Mismatch

In order to evaluate the performance of the proposed full-rank MMSE estimator to mismatch only in SNR design, the estimator is tested when SNRs of 10 and 30 dB are used in the design. The SER curves for a design SNR of 10, 30 dB are shown in Figures 4.7 and 4.8. The performance of the MMSE estimator for high SNR (30 dB) design is better than low SNR (10 dB) design across a range of SNR values (0 - 28 dB). These results confirm that channel estimation error is concealed in noise for low SNR whereas it tends to dominate for high SNR. Thus, the system performance degrades especially for low SNR design.

4.5.2.2 Correlation Mismatch

To analyze full-rank MMSE estimator's performance further, sensitivity of the estimator to design errors, i.e., correlation mismatch needs to be studied. Therefore the estimator is designed for a uniform channel correlation which gives the worst MSE performance among all channels Edfords *et al*. [3], Li *et al*. [5] and evaluated for an exponentially decaying power-delay profile. The uniform channel correlation between the attenuations can be obtained by letting $\tau_{rms} \to \infty$, resulting in

$$c_f(k-k') = \frac{1-e^{j\frac{2\pi(k-k')}{K}}}{j\frac{2\pi(k-k')}{K}} \tag{4.40}$$

Figure 4.9 and Figure 4.10 demonstrate the estimator's sensitivity to the channel statistics in terms of average MSE performance measure. As it can be seen from Figure 4.9 and 4.10 only small performance loss is observed for low SNRs when the estimator is designed for mismatched channel statistics. This justifies the result that a design for worst correlation is robust to mismatch.

4.5.2.3 Performance of the Truncated Estimator

The truncated estimator performance is also studied as a function of the number of KL coefficients. Figure 4.11 and Figure 4.12 are plotted for $L = 40$, $\tau_{rms} = 5$ sample and $L = 40$, $f_m = 100$ Hz respectively. Figure 4.11 and Figure 4.12 present the MSE result of the truncated MMSE estimator for SNR = 10, 20 and 30 dB. If only a few expansion coefficients are employed to reduce the complexity of the proposed estimator, then the MSE between channel parameters becomes large. However, if the number of parameters in the expansion is increased, the irreducible error floor still occurs.

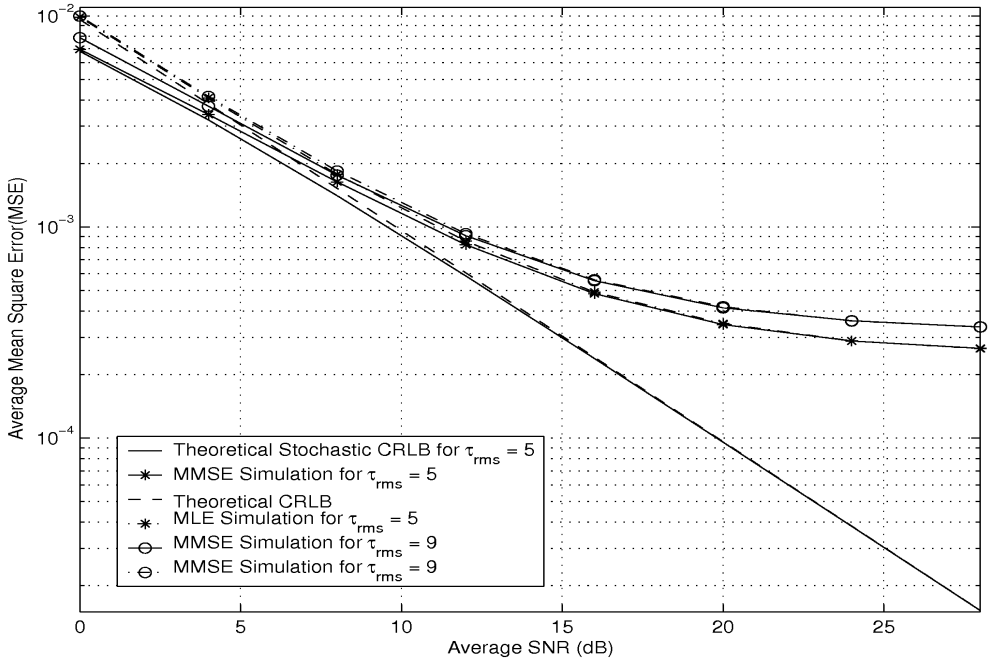

Figure 4.3 Performance of proposed MMSE and MLE together with B_{MSE} and CRLB for SF-OFDM

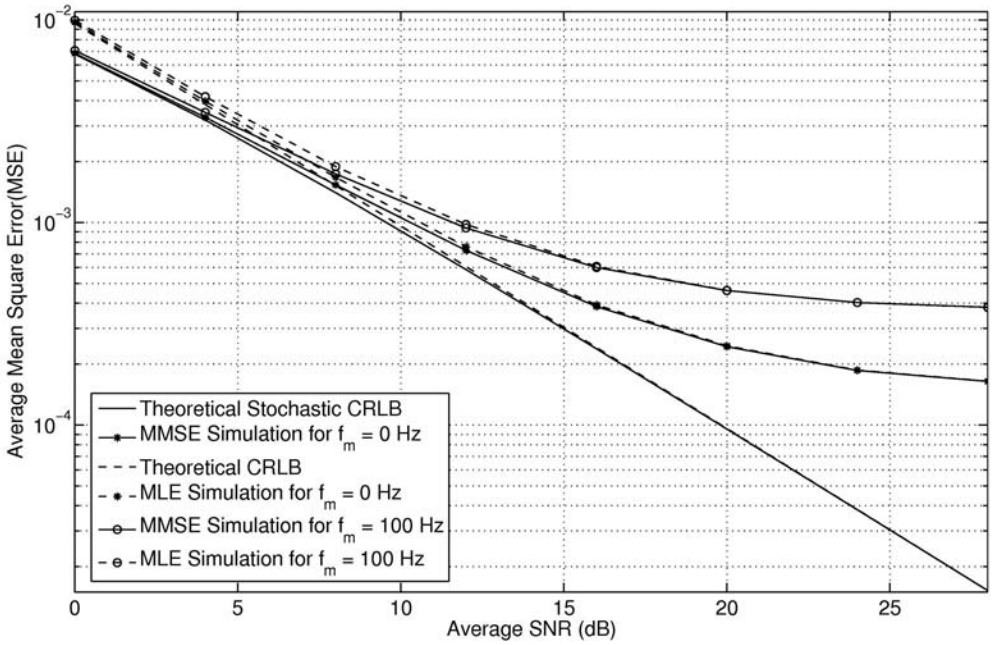

Figure 4.4 Performance of proposed MMSE and MLE together with B_{MSE} and CRLB for ST-OFDM

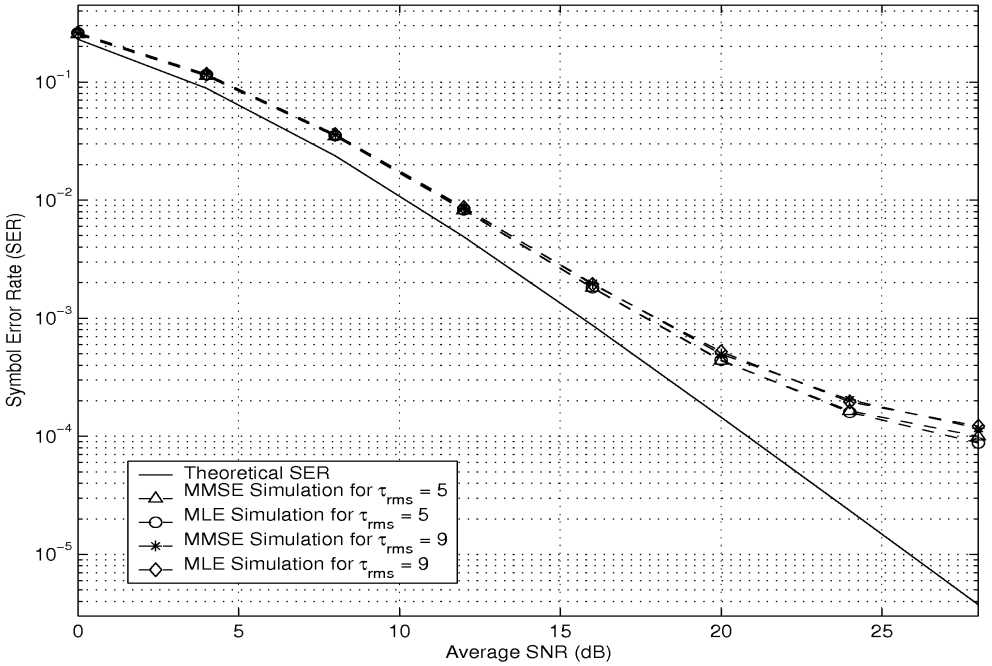

Figure 4.5 Symbol Error Rate results for SF-OFDM

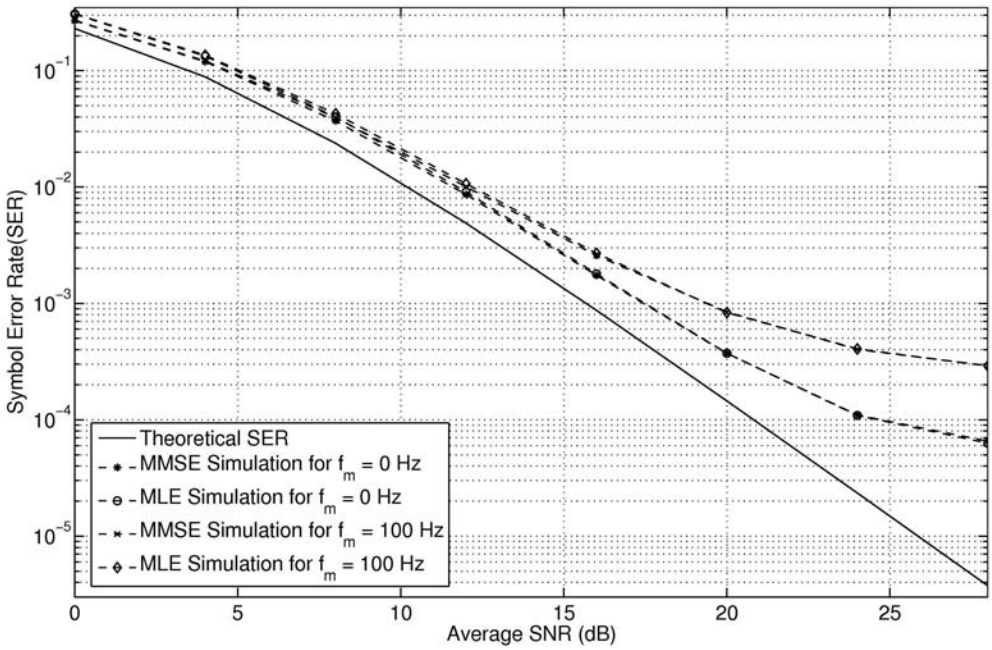

Figure 4.6 Symbol Error Rate results for ST-OFDM

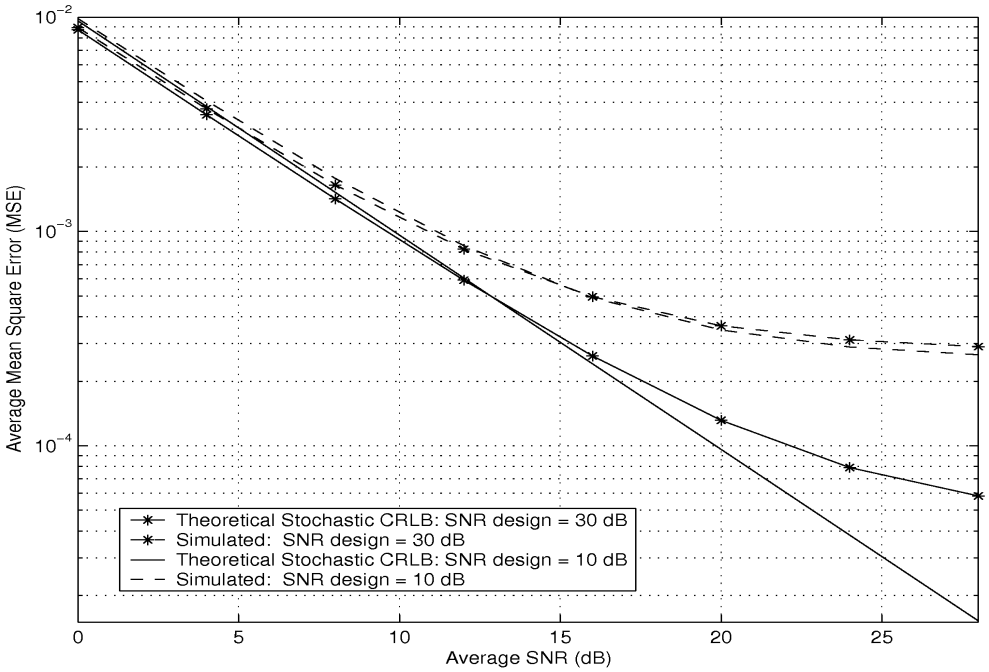

Figure 4.7 Effects of SNR mismatch on MSE for SF-OFDM

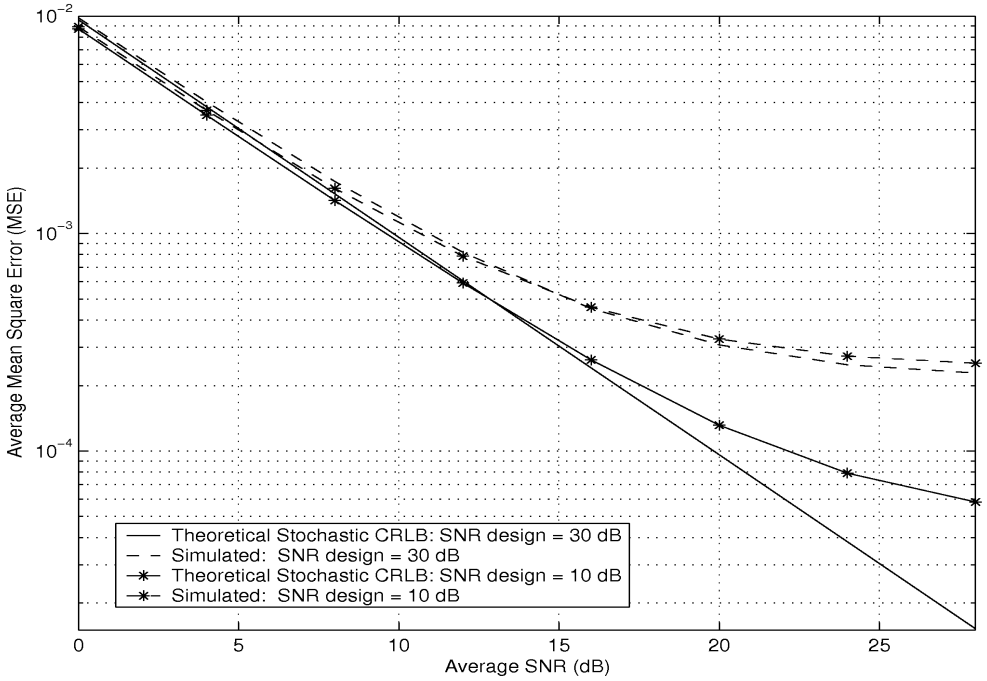

Figure 4.8 Effects of SNR mismatch on MSE for ST-OFDM(f_m=100 Hz)

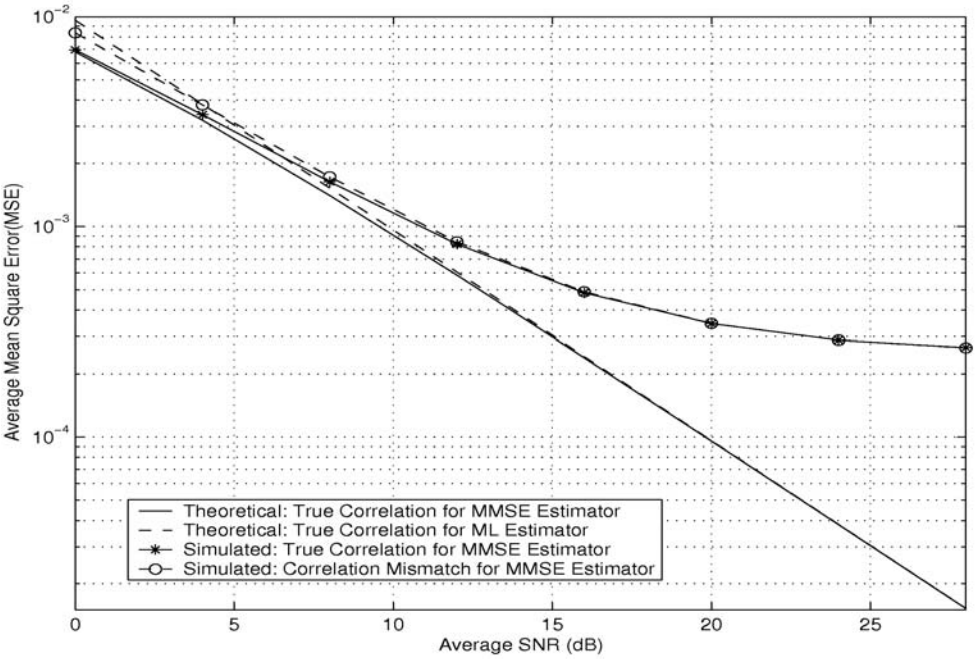

Figure 4.9 Effects of correlation mismatch on MSE for SF-OFDM

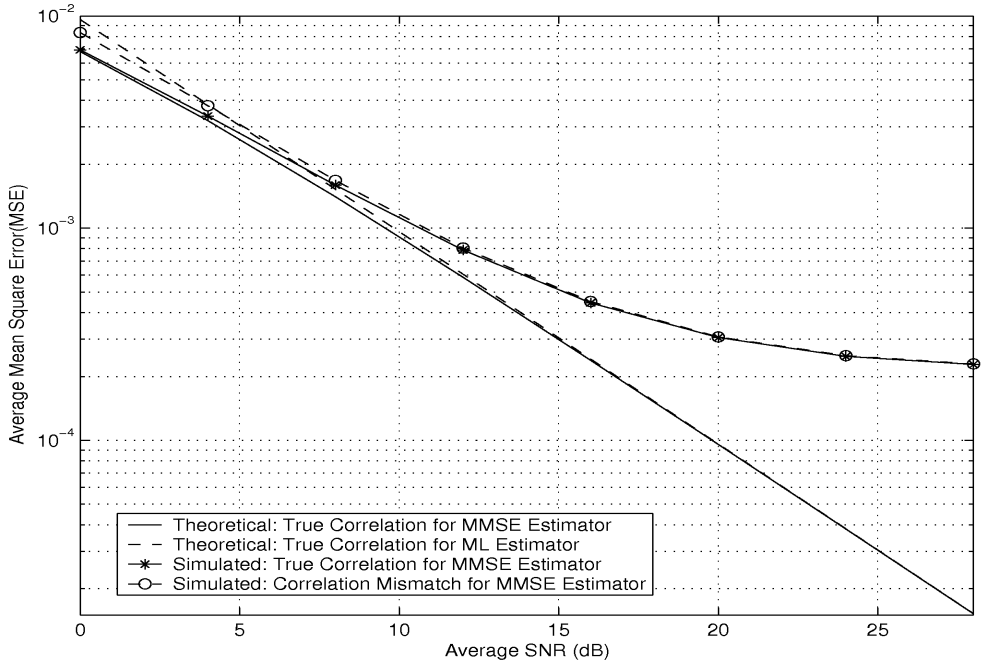

Figure 4.10 Effects of correlation mismatch on MSE for ST-OFDM(f_m=100 Hz)

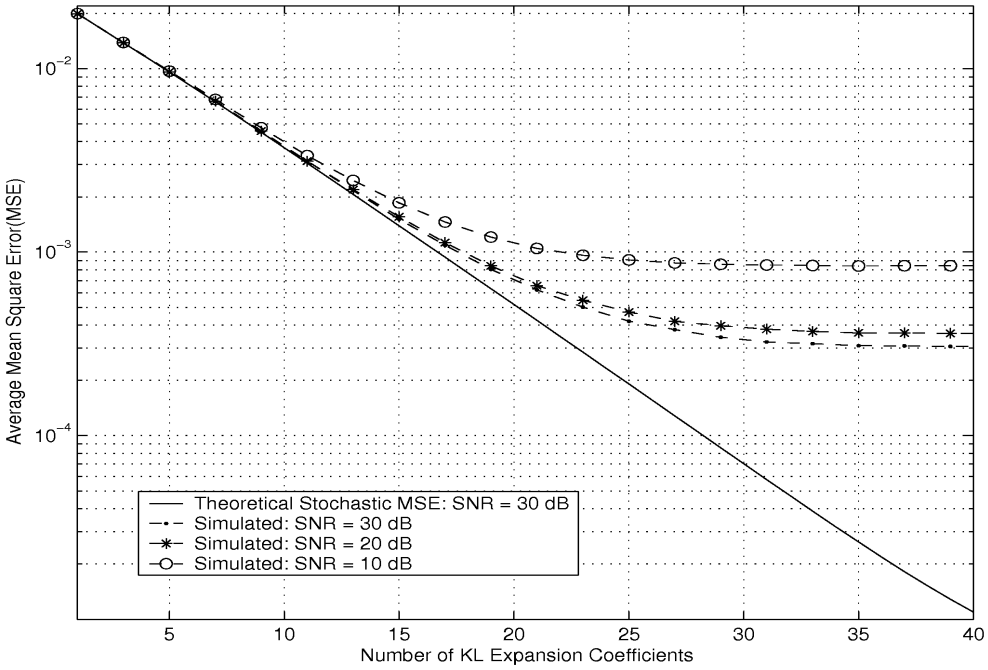

Figure 4.11 MSE as a function of KL expansion coefficients for SF-OFDM

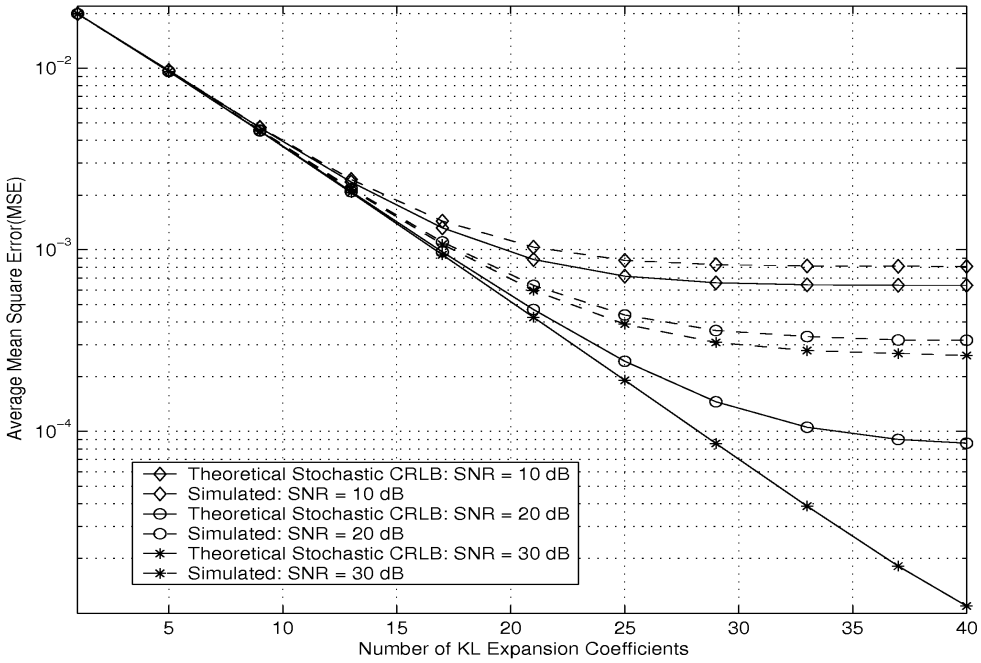

Figure 4.12 MSE as a function of KL expansion coefficients for ST-OFDM (f_m=100 Hz)

Chapter 5

Conclusion and Future Works

In this thesis, the design of low complexity pilot based MMSE channel estimators for OFDM systems with and without transmit diversity in unknown wireless dispersive fading channels was considered. In general, MMSE channel estimators require inversion of channel covariance matrix. According to OFDM structure, channel estimation is mostly performed in frequency domain resulting in higher computational complexity due to large of number channel parameters to be estimated as well as large channel covariance matrix needed in estimation. Since the number channel parameters to be estimated in time domain is much smaller than the frequency domain, time domain approaches therefore present alternative low complexity solutions.

In this thesis, optimum time domain channel estimation approaches based on MMSE criterion are also proposed , and the complexity of the proposed approaches are further reduced by the application of KL expansion. Thus, as a first contribution, a low complexity pilot MMSE channel estimator is proposed in time domain. In other words, the problem is considered as the multipath channel estimation. Due to the invariance property of the MMSE estimator, MMSE estimate of the channel frequency response can be obtained by taking FFT of the multipath channel. Taking FFT of the multipath channel also provides an interpolation between frequency responses at pilot and data locations.

However, in the frequency domain channel estimation approach, a suitable interpolation method for finding channel frequency response at data locations by

making use of frequency response at pilot locations is required. These interpolation methods affect the performance of the frequency domain channel estimator.

Inverse of the channel correlation matrix used in frequency domain MMSE estimation results in higher computational complexity. Especially adaptive and sequential MMSE estimators must take the inverse of the channel correlation matrix in each step of the algorithm. Therefore, computational complexity is a highly important issue for adaptive and sequential MMSE estimators. The channel estimation problem is therefore considered as the MMSE estimation of the stochastic coefficient vector when the stochastic orthogonal expansion representation of the multipath is exploited. In this case, computational complexity of the estimator is significantly reduced since correlation matrix of the coefficient matrix becomes diagonal.

In the case of receiver or transmitter mobility, according to the speed of mobile component, channel may vary within OFDM block duration. This causes fast fading environments. Alamouti diversity scheme proposes a solution for combating fast fading. When Alamouti diversity scheme is applied to OFDM systems, different diversity coding types come out such as space-time OFDM, space-frequency OFDM, e.t.c.

In this thesis, as a second major contribution the batch MMSE estimators were derived based on the stochastic orthogonal expansion representation for ST/SF-OFDM systems. Based on KL representation, the fact that no matrix inversion is needed in the MMSE algorithm is shown. Therefore, the computational costs for implementing the proposed MMSE estimators are low and computations are numerically stable.

As a conclusion the contribution of this thesis is summarized as follows:

- Time domain MMSE channel estimator is developed and analyzed for OFDM.

- Performance of the proposed batch approach is evaluated based on the evaluation of CRLB and Bayesian MSE.
- Performance of the low-rank approximation of the proposed estimator and theoretical SER results are studied both theoretically and analytically.
- Sequential version of the batch estimator is also derived.
- The proposed MMSE estimator approach and performance results are then extended to transmit diversity OFDM systems.

In addition to MMSE based estimation approaches proposed in this thesis, computationally efficient advanced iterative signal processing algorithms such as sequential Monte Carlo (SMC), expectation-maximization (EM), provide MMSE solutions will be applied to solve difficult signal processing problems in wireless communications in future research. To achieve full benefit of efficient algorithms a wide variety of problems, such as synchronization, equalization, and sequence estimation problems can be considered. Another possible future work will be the development of blind channel estimation approaches that provide much more bandwidth efficiency.

Appendix A

Bayesian Estimators

Bayesian estimation depart from the classical approach to statistical estimation in which the parameter Θ of interest is assumed to be a deterministic but unknown constant. Instead, Θ is assumed as a random variable whose particular realization is to be estimated. This is the Bayesian approach, so named because its implementation is based directly on Bayes' theorem. The motivation for doing so is twofold. First, if some prior knowledge about Θ is available, it can be incorporated into estimator design. The mechanism for doing this requires us to assume that Θ is a random variable with a given prior PDF. Classical estimation, on the other hand, finds it difficult to make use of any prior knowledge. Bayesian approach can therefore improve the estimation accuracy. Second, Bayesian estimation is useful in situations where an MVU estimator can not be found. In this case, especially for the classical approach, a strategy can be devised to find that estimator by assigning a PDF to Θ. The resultant estimator can then be said to be optimal "on the average".

In Bayesian estimation, first step is to choose a cost function that is the function of estimation error

$$\varepsilon = \Theta - \hat{\Theta} \tag{A.1}$$

where Θ and $\hat{\Theta}$ are true and estimated values of the parameter Θ, respectively.

Three well known cost functions are;

- Squared Error $Q(\varepsilon) = \varepsilon^2$,

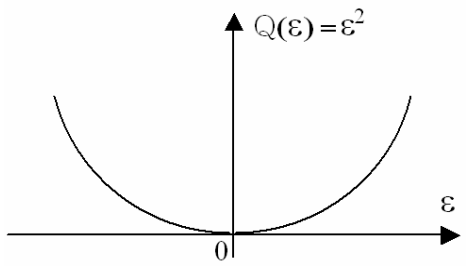

Figure A.1 Squared error cost function

- Absolute Error $Q(\varepsilon) = |\varepsilon|$,

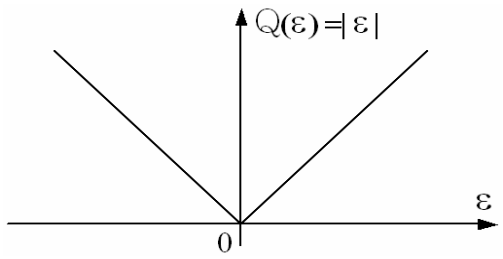

Figure A.2 Absolute error cost function

- Hit-or-miss $Q(\varepsilon) = \begin{cases} 0 & , \quad |\varepsilon| < \delta \\ 1 & , \quad |\varepsilon| > \delta \end{cases}$,

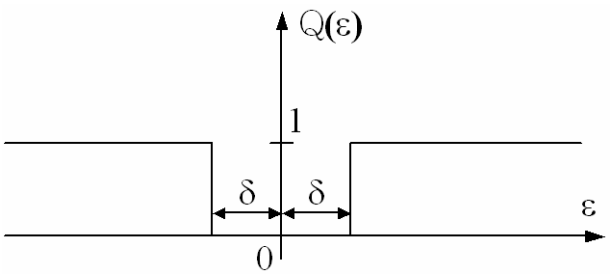

Figure A.3 Hit-or-miss cost function

Cost functions, and δ is very small positive number. Also, the averaged cost function is termed as the *Bayes risk, or*

$$\mathcal{R} = \mathsf{E}\left[Q(\varepsilon)\right] \tag{A.2}$$

For a squared error cost function, the mean of the posterior probability density function (PDF) or the usual MMSE estimator minimizes the risk. An absolute error cost function (A.2) results in an optimal estimator, which is the median of the posterior PDF. For a hit-or-miss cost function (A.3) the mode of maximum location of the posterior PDF is the optimal estimator termed as the maximum a posteriori (MAP) estimator.

We now determine the optimal estimators for these cost functions. Note that ε depends on Θ and observation vector $\mathbf{Z}$, because the estimation value $\hat{\Theta}$ in (A.1) is a function of observation vector $\mathbf{Z}$, such that $\hat{\Theta} = \hat{\Theta}(\mathbf{Z})$. Therefore, the expectation integral of the cost function must be taken over the joint probability density function of the observation vector $\mathbf{Z}$ and the parameter Θ to be estimated.

$$\begin{aligned}
\mathcal{R} &= \mathsf{E}\left[Q(\varepsilon)\right] \\
&= \int Q(\varepsilon)\, p(\varepsilon)\, d\varepsilon \\
&= \int_{-\infty}^{+\infty}\int_{-\infty}^{+\infty} Q(\Theta - \hat{\Theta})\, p(\mathbf{Z}, \Theta)\, d\mathbf{Z}\, d\Theta \\
&= \int_{-\infty}^{+\infty}\left(\int_{-\infty}^{+\infty} Q(\Theta - \hat{\Theta})\, p(\Theta \mid \mathbf{Z})\, d\Theta\right) p(\mathbf{Z})\, d\mathbf{Z}
\end{aligned} \tag{A.3}$$

In order to minimize Bayes risk in (A.4), we have to minimize the inner integral according to $\hat{\Theta}$. First, considering the absolute error cost function and denoting the inner integral by $u(\hat{\Theta})$, we have for the inner integral of (A.4)

$$u(\hat{\Theta}) = \int_{-\infty}^{+\infty} |\Theta - \hat{\Theta}|\, p(\Theta \mid \mathbf{Z})\, d\Theta \tag{A.4}$$

and differentiate with respect to $\hat{\Theta}$

$$\frac{\partial u(\hat{\Theta})}{\partial \hat{\Theta}} = \int_{-\infty}^{+\infty} \frac{\partial |\Theta - \hat{\Theta}|}{\partial \hat{\Theta}} \, p(\Theta \mid \mathbf{Z}) d\Theta$$

$$= \int_{-\infty}^{\hat{\Theta}} p(\Theta \mid \mathbf{Z}) d\Theta - \int_{\hat{\Theta}}^{+\infty} p(\Theta \mid \mathbf{Z}) d\Theta = 0$$

or

$$\int_{-\infty}^{\hat{\Theta}} p(\Theta \mid \mathbf{Z}) d\Theta = \int_{\hat{\Theta}}^{+\infty} p(\Theta \mid \mathbf{Z}) d\Theta \tag{A.5}$$

By definition $\hat{\Theta}$ is the *median* of the posterior PDF or the point for which $\mathbf{Pr}\{(\Theta \mid \mathbf{Z}) \le \hat{\Theta}\} = \mathbf{Pr}\{(\Theta \mid \mathbf{Z}) \ge \hat{\Theta}\} = \frac{1}{2}$. Now, MAP and MMSE estimators will be considered. These two estimator types are most commonly used in channel estimation problems.

A.1 Maximum A Posteriori (MAP) Estimator

For the hit-or-miss cost function, the inner integral in (A.4) is

$$u(\hat{\Theta}) = \int_{|\varepsilon|>\delta} 1 . p(\Theta \mid \mathbf{Z}) d\Theta = \int_{|\Theta - \hat{\Theta}|>\delta} p(\Theta \mid \mathbf{Z}) d\Theta$$

$$= \int_{-\infty}^{\hat{\Theta}-\delta} p(\Theta \mid \mathbf{Z}) d\Theta + \int_{\hat{\Theta}+\delta}^{+\infty} p(\Theta \mid \mathbf{Z}) d\Theta$$

$$= \int_{-\infty}^{+\infty} p(\Theta \mid \mathbf{Z}) d\Theta - \int_{\hat{\Theta}-\delta}^{\hat{\Theta}+\delta} p(\Theta \mid \mathbf{Z}) d\Theta$$

$$= 1 - \int_{\hat{\Theta}-\delta}^{\hat{\Theta}+\delta} p(\Theta \mid \mathbf{Z}) d\Theta \tag{A.6}$$

$u(\hat{\Theta})$ can be minimized by maximizing the following integral

$$\int_{\hat{\Theta}-\delta}^{\hat{\Theta}+\delta} p(\Theta \mid \mathbf{Z})\, d\Theta \tag{A.7}$$

This integral is maximized by choosing $\hat{\Theta}$ corresponding to the location of the *maximum of* $p(\hat{\Theta} \mid \mathbf{Z})$. The estimator that minimizes the Bayes risk for the hit-or-miss cost function is therefore the location of the maximum of the posterior probability density function. It is termed as the *maximum a posteriori* (MAP) estimator.

A.2 Minimum Mean Square Error (MMSE) Estimator

For the MMSE estimator, the cost function is squared error, $Q(\varepsilon) = \varepsilon^2$, and the Bayes risk is the MSE. Therefore, the MMSE estimator minimizes the MSE. The inner integral in (A.4) turns to

$$u(\hat{\Theta}) = \int_{-\infty}^{+\infty} (\Theta - \hat{\Theta})^2\, p(\Theta \mid \mathbf{Z})\, d\Theta \tag{A.8}$$

and is differentiated with respect to $\hat{\Theta}$ as follows

$$\frac{\partial u(\hat{\Theta})}{\partial \hat{\Theta}} = \int_{-\infty}^{+\infty} \frac{\partial\, (\Theta - \hat{\Theta})^2}{\partial\, \hat{\Theta}}\, p(\Theta \mid \mathbf{Z})\, d\Theta = -2 \int_{-\infty}^{+\infty} (\Theta - \hat{\Theta})\, p(\Theta \mid \mathbf{Z})\, d\Theta = 0$$

This yield

$$\hat{\Theta} \underbrace{\int_{-\infty}^{+\infty} p(\Theta \mid \mathbf{Z})\, d\Theta}_{1} = \int_{-\infty}^{+\infty} \Theta\, p(\Theta \mid \mathbf{Z})\, d\Theta = \int_{-\infty}^{+\infty} \Theta\, p(\Theta \mid \mathbf{Z})\, d\Theta$$

Therefore, the MMSE estimator is obtained as

$$\hat{\Theta} = E[\Theta \mid Z] \tag{A.9}$$

the mean of the posterior PDF. For this reason it is also commonly referred as the *conditional mean estimator.* Nevertheless, the prior PDF of Θ, $p(\Theta)$, plays an important role in MMSE estimator, because posterior PDF $p(\Theta \mid Z)$ depends on prior PDF $p(\Theta)$. This can be proved by Bayes rule as follows:

$$\begin{aligned} p(\Theta \mid Z) &= \frac{p(Z,\Theta)}{p(Z)} \\ &= \frac{p(Z \mid \Theta)p(\Theta)}{\int_{-\infty}^{+\infty} p(Z \mid \Theta)p(\Theta)\,d\Theta} \end{aligned} \tag{A.10}$$

For the vector parameter $\Theta = [\Theta_1 \quad \Theta_2 \quad .... \quad \Theta_N]^T$ which has independent identical distributed elements,

$$\begin{aligned} \hat{\Theta} &= [\, E[\Theta_1 \mid Z] \quad E[\Theta_2 \mid Z] \quad .... \quad E[\Theta_N \mid Z]\,]^T \\ &= E[\Theta \mid Z] \end{aligned} \tag{A.11}$$

Note that the vector MMSE estimator $E[\Theta \mid Z]$ minimizes the mean squared error (MSE) for each component of the unknown vector parameter. The minimum Bayesian MSE for a scalar parameter is the posterior PDF variance when averaged over the PDF of Z. This is because

$$\begin{aligned} u(\hat{\Theta}_i) &= \int_{-\infty}^{+\infty} (\Theta_i - E[\Theta_i \mid Z])^2 \, p(\Theta_i \mid Z)\, d\Theta_i \\ &= \sigma^2_{\Theta_i \mid Z} \quad , \quad i=1, 2, \ldots, N \end{aligned} \tag{A.12}$$

and replacing this result by the inner integral in (A.3), we obtain minimized risk function, in other words, minimum Bayesian MSE as follows

$$\mathbf{B}_{\mathrm{MSE}}(\Theta_i) = \int_{-\infty}^{+\infty} \sigma^2_{\Theta_i|\mathbf{Z}}\, p(\mathbf{Z})\, d\mathbf{Z} \tag{A.13}$$

In order to obtain a scalar MSE measure for the vector parameter $\boldsymbol{\Theta} = [\Theta_1 \quad \Theta_2 \quad \ldots \quad \Theta_N]^T$, the minimum Bayesian MSE's of the elements can be averaged as follows

$$\mathbf{B}_{\mathrm{MSE}}(\boldsymbol{\Theta}) = \frac{1}{N}\sum_{i=1}^{N} B_{\mathrm{MSE}}(\Theta_i) \tag{A.14}$$

Bearing in mind $\sigma^2_{\Theta_i|\mathbf{Z}} = \left[\mathbf{C}_{\Theta|\mathbf{Z}}\right]_{i,i}$ and substituting (A.13) in (A.14)

$$\begin{aligned}
\mathbf{B}_{\mathrm{MSE}}(\boldsymbol{\Theta}) &= \frac{1}{N}\sum_{i=1}^{N}\int_{-\infty}^{+\infty} \sigma^2_{\Theta_i|\mathbf{Z}}\, p(\mathbf{Z})\, d\mathbf{Z} \\
&= \frac{1}{N}\int_{-\infty}^{+\infty} \left(\sum_{i=1}^{N} \sigma^2_{\Theta_i|\mathbf{Z}}\right) p(\mathbf{Z})\, d\mathbf{Z} \\
&= \frac{1}{N}\int_{-\infty}^{+\infty} \mathrm{trace}\left\{\mathbf{C}_{\Theta|\mathbf{Z}}\right\} p(\mathbf{Z})\, d\mathbf{Z}
\end{aligned} \tag{A.15}$$

where $\mathbf{C}_{\Theta|\mathbf{Z}}$ is the posterior covariance matrix of the vector parameter $\boldsymbol{\Theta}$, and $\mathrm{trace}\{.\}$ operator represents sum of diagonal entries of a square matrix. If variances $\{\sigma^2_{\Theta_i|\mathbf{Z}}\}_{i=1}^{N}$ does not depend on the observation vector $\mathbf{Z}$, the minimum Bayesian MSE in (A.15) is

$$\mathbf{B}_{\mathrm{MSE}}(\boldsymbol{\Theta}) = \frac{1}{N}\mathrm{trace}\left\{\mathbf{C}_{\Theta|\mathbf{Z}}\right\} \underbrace{\int_{-\infty}^{+\infty} p(\mathbf{Z})\, d\mathbf{Z}}_{1}$$

$$= \frac{1}{N}\text{trace}\left\{\mathbf{C}_{\Theta|\mathbf{Z}}\right\} \tag{A.16}$$

If the observed data $\mathbf{Z}$ can be modeled as

$$\mathbf{Z} = \mathbf{U}\Theta + \mathbf{w} \tag{A.17}$$

where $\mathbf{Z}$ is an $M\times 1$ data vector, $\mathbf{U}$ is a known $M\times N$ matrix, Θ is a $N\times 1$ random vector with prior PDF $\mathcal{N}\left(\mathrm{E}[\Theta], \mathbf{C}_{\Theta}\right)$, and $\mathbf{w}$ is an $M\times 1$ noise vector with PDF $\mathcal{N}\left(\mathbf{0}, \mathbf{C}_{\mathbf{w}}\right)$ and independent of Θ, then the posterior PDF $p(\Theta \mid \mathbf{Z})$ is Gaussian with mean[11, pp.364]

$$\mathrm{E}[\Theta \mid \mathbf{Z}] = \mathrm{E}[\Theta] + \left(\mathbf{U}^{\mathsf{T}}\mathbf{C}_{\mathbf{w}}^{-1}\mathbf{U} + \mathbf{C}_{\Theta}^{-1}\right)^{-1}\mathbf{U}^{\mathsf{T}}\mathbf{C}_{\mathbf{w}}^{-1}\left(\mathbf{Z} - \mathbf{U}\mathrm{E}[\Theta]\right) \tag{A.18}$$

and covariance

$$\mathbf{C}_{\Theta|\mathbf{Z}} = \left(\mathbf{U}^{\mathsf{T}}\mathbf{C}_{\mathbf{w}}^{-1}\mathbf{U} + \mathbf{C}_{\Theta}^{-1}\right)^{-1} \tag{A.19}$$

For the complex Gaussian parameter Θ to be estimated, replace transpose operator $(.)^{\mathsf{T}}$ in (A.18) and (A.19) by Hermitian transpose operator $(.)^{\dagger}$.

Appendix B

Bayesian MSE for Truncated MMSE KL Estimator under SNR Mismatch in OFDM Systems Without Diversity

Substituting (3.11) in (3.16), truncated MMSE KL estimator becomes

$$\hat{\mathbf{g}}_r = K_p \boldsymbol{\Gamma}_r \mathbf{g} + \boldsymbol{\Gamma}_r \boldsymbol{\Psi}^\dagger \mathbf{F}^\dagger \tilde{\boldsymbol{\eta}} \tag{B.1}$$

The estimation error

$$\begin{aligned}\hat{\boldsymbol{\varepsilon}}_r &= \mathbf{g} - \hat{\mathbf{g}}_r \\ &= \mathbf{g} - \left(K_p \boldsymbol{\Gamma}_r \mathbf{g} + \boldsymbol{\Gamma}_r \boldsymbol{\Psi}^\dagger \mathbf{F}^\dagger \tilde{\boldsymbol{\eta}}\right) \\ &= \left(\mathbf{I}_L - K_p \boldsymbol{\Gamma}_r\right)\mathbf{g} - \boldsymbol{\Gamma}_r \boldsymbol{\Psi}^\dagger \mathbf{F}^\dagger \tilde{\boldsymbol{\eta}}\end{aligned} \tag{B.2}$$

and then the average Bayesian MSE is

$$\begin{aligned}\mathbf{B}_{\mathrm{MSE}}(\hat{\mathbf{g}}_r) &= \frac{1}{L}\mathrm{tr}(\mathbf{C}_{\hat{\boldsymbol{\varepsilon}}_r}) \\ &= \frac{1}{L}\mathrm{trace}\left(\boldsymbol{\Lambda}_{\mathbf{g}}(\mathbf{I}_L - K_p\boldsymbol{\Gamma}_r)^2 + K_p\tilde{\sigma}^2\boldsymbol{\Gamma}_r^2\right) \\ &= \frac{1}{L}\sum_{i=0}^{r-1}\left[\lambda_i\left(1 - K_p\frac{\lambda_i}{\lambda_i K_p + \sigma^2}\right)^2 + K_p\tilde{\sigma}^2\left(\frac{\lambda_i}{\lambda_i K_p + \sigma^2}\right)^2\right] + \frac{1}{L}\sum_{i=r}^{L-1}\lambda_i \\ &= \frac{1}{L}\sum_{i=0}^{r-1}\lambda_i\frac{\tilde{\sigma}^2 K_p\lambda_i + \sigma^4}{(\lambda_i K_p + \sigma^2)^2} + \frac{1}{L}\sum_{i=r}^{L-1}\lambda_i \quad \text{where } \sigma^2 = \frac{1}{\mathrm{SNR}},\ \tilde{\sigma}^2 = \frac{1}{\mathrm{SNR}}\end{aligned}$$

$$= \frac{1}{L}\sum_{i=0}^{r-1}\frac{\lambda_i}{(1+K_p\lambda_i SNR)^2}\left[1+K_p\lambda_i\frac{SNR^2}{\tilde{SNR}}\right]+\frac{1}{L}\sum_{i=r}^{L-1}\lambda_i \tag{B.3}$$

Based on the result obtained in (B.3), Bayesian estimator performance can be further elaborated for the following scenarios:

- By taking $SNR = \tilde{SNR}$, the performance result for the case of no SNR mismatch is

$$\mathbf{B}_{MSE}(\hat{\mathbf{g}}_r) = \frac{1}{L}\sum_{i=0}^{r-1}\frac{\lambda_i}{1+K_p\lambda_i SNR}+\frac{1}{L}\sum_{i=r}^{L-1}\lambda_i \tag{B.4}$$

- As $r \to L$ in (B.3), $\mathbf{B}_{MSE}(\hat{\mathbf{g}})$ under SNR mismatch results in the following Bayesian MSE:

$$\mathbf{B}_{MSE}(\hat{\mathbf{g}}) = \frac{1}{L}\sum_{i=0}^{L-1}\frac{\lambda_i}{(1+K_p\lambda_i SNR)^2}\left[1+K_p\lambda_i\frac{SNR^2}{\tilde{SNR}}\right] \tag{B.5}$$

- Finally, the Bayesian MSE in the case of no SNR mismatch is also be obtained as,

$$\mathbf{B}_{MSE}(\hat{\mathbf{g}}) = \frac{1}{L}\sum_{i=0}^{L-1}\frac{\lambda_i}{1+K_p\lambda_i SNR} \tag{B.6}$$

Appendix C

Bayesian MSE for Truncated MMSE KL Estimator under Correlation Mismatch in OFDM Systems Without Diversity

In this appendix, the Bayesian MSE of the truncated MMSE KL estimator under correlation mismatch will be derived. Although the real multipath channel $\tilde{\mathbf{h}}$ has the expansion correlation $\mathbf{C}_{\tilde{\mathbf{h}}}$, the estimator is designed for the multipath channel $\mathbf{h} = \mathbf{\Psi g}$ with correlation $\mathbf{C}_{\mathbf{h}}$. To evaluate the estimation error $\tilde{\mathbf{g}} - \tilde{\mathbf{g}}_r$ in the same space, the real channel $\tilde{\mathbf{h}}$ is expanded onto the eigen space of $\tilde{\mathbf{h}} = \mathbf{\Psi}\tilde{\mathbf{g}}$ resulting in correlated expansion coefficients. For the real channel, data model in (3.10) can be rewritten as

$$\tilde{\mathbf{Y}} = \mathbf{F\Psi}\tilde{\mathbf{g}} + \tilde{\boldsymbol{\eta}} \tag{C.1}$$

and substituting in (3.16), truncated MMSE KL estimator now becomes

$$\hat{\mathbf{g}}_r = \mathsf{K}_p \mathbf{\Gamma}_r \mathbf{g} + \mathbf{\Gamma}_r \mathbf{\Psi}^\dagger \mathbf{F}^\dagger \tilde{\boldsymbol{\eta}} \tag{C.2}$$

For the truncated MMSE estimator, the error is

$$\begin{aligned} \hat{\boldsymbol{\varepsilon}}_r &= \tilde{\mathbf{g}} - \hat{\mathbf{g}}_r \\ &= \tilde{\mathbf{g}} - \mathsf{K}_p \mathbf{\Gamma}_r \mathbf{g} - \mathbf{\Gamma}_r \mathbf{\Psi}^\dagger \mathbf{F}^\dagger \tilde{\boldsymbol{\eta}} \end{aligned} \tag{C.3}$$

As a result, the average Bayesian MSE is

$$\mathbf{B}_{\mathrm{MSE}}(\hat{\mathbf{g}}_r) = \frac{1}{L}\mathrm{trace}(\mathbf{C}_{\hat{\boldsymbol{\varepsilon}}_r})$$

$$= \frac{1}{L}\mathrm{trace}(\boldsymbol{\Lambda}_{\tilde{\mathbf{g}}} + K_p^2\boldsymbol{\Gamma}_r^2\boldsymbol{\Lambda}_{\mathbf{g}} + \sigma^2 K_p\boldsymbol{\Gamma}_r^2 - 2K_p\boldsymbol{\Gamma}_r\boldsymbol{\beta})$$

$$= \frac{1}{L}\sum_{i=0}^{r-1}\left[\tilde{\lambda}_i + \frac{K_p\lambda_i(\lambda_i - 2\beta_i)}{\lambda_i K_p + \sigma^2}\right] + \frac{1}{L}\sum_{i=r}^{L-1}\tilde{\lambda}_i \quad \text{and } \sigma^2 = \frac{1}{\mathrm{SNR}}$$

$$= \frac{1}{L}\sum_{i=0}^{r-1}\left[\tilde{\lambda}_i + \frac{K_p\,\mathrm{SNR}\,\lambda_i(\lambda_i - 2\beta_i)}{1 + K_p\,\mathrm{SNR}\,\lambda_i}\right] + \frac{1}{L}\sum_{i=r}^{L-1}\tilde{\lambda}_i$$

$$= \frac{1}{L}\sum_{i=0}^{r-1}\frac{\tilde{\lambda}_i + K_p\mathrm{SNR}\,\lambda_i(\tilde{\lambda}_i + \lambda_i - 2\beta_i)}{1 + K_p\,\mathrm{SNR}\,\lambda_i} + \frac{1}{L}\sum_{i=r}^{L-1}\tilde{\lambda}_i \qquad \text{(C.4)}$$

where β is the real part of $\mathrm{E}[\tilde{\mathbf{g}}\mathbf{g}^{\dagger}]$ and β_i's are the diagonal elements of β. With this result, some special cases can be highlighted as:

- Letting $\beta_i = \lambda_i = \tilde{\lambda}_i$ in (B.4) for the case of no mismatch in the correlation of KL expansion coefficients, truncated Bayesian MSE is identical to that obtained in (B.4).
- As $r \to L$ in (B.4), Bayesian MSE under correlation mismatch is obtained to yield:

$$\mathbf{B}_{\mathrm{MSE}}(\hat{\mathbf{g}}) = \frac{1}{L}\sum_{i=0}^{L-1}\frac{\tilde{\lambda}_i + K_p\,\mathrm{SNR}\,\lambda_i(\tilde{\lambda}_i + \lambda_i - 2\beta_i)}{1 + K_p\,\mathrm{SNR}\,\lambda_i} \qquad \text{(C.5)}$$

- Under no correlation mismatch in (C.4) where $\beta_i = \lambda_i = \tilde{\lambda}_i$, Bayesian MSE obtained from (C.4) is identical to that in (B.6).
- Also note that as $\mathrm{SNR} \to \infty$ reduces to $\mathrm{MSE}(\tilde{\mathbf{g}} - \hat{\mathbf{g}}_r)$.

Appendix D

Bayesian MSE for Truncated MMSE KL Estimator under SNR Mismatch in ST/SF – OFDM Systems

Some derivation steps will be passed in appendices D and E since these steps will be taken as in appendices B and C. The estimation error is

$$\hat{\boldsymbol{\varepsilon}}_{\mu_r} = \mathbf{g}_{\mu} - \hat{\mathbf{g}}_{\mu_r} \quad , \qquad \mu = 1, 2 \tag{D.1}$$

and then the average Bayesian MSE is

$$\begin{aligned} \mathbf{B}_{\mathrm{MSE}}(\hat{\mathbf{g}}_{\mu_r}) &= \frac{1}{L}\mathrm{trace}(\mathbf{C}_{\hat{\boldsymbol{\varepsilon}}_{\mu_r}}) \\ &= \frac{1}{L}\mathrm{trace}\left(\boldsymbol{\Lambda}_{\mathbf{g}}(\mathbf{I}_L - 2K_p\ddot{\Gamma}_r)^2 + 2K_p\tilde{\sigma}^2\ddot{\Gamma}_r^2\right) \\ &= \frac{1}{L}\sum_{i=0}^{r-1}\frac{\lambda_i}{(1+2K_p\lambda_i\mathrm{SNR})^2}\left[1 + 2K_p\lambda_i\frac{\mathrm{SNR}^2}{\tilde{\mathrm{SNR}}}\right] + \frac{1}{L}\sum_{i=r}^{L-1}\lambda_i \end{aligned} \tag{D.2}$$

Based on the result obtained in (D.2), Bayesian estimator performance can be further elaborated for the following scenarios:

- By taking $\mathrm{SNR} = \tilde{\mathrm{SNR}}$, the performance result for the case of no SNR mismatch is

$$\mathbf{B}_{\mathrm{MSE}}(\hat{\mathbf{g}}_{\mu_r}) = \frac{1}{L}\sum_{i=0}^{r-1}\frac{\lambda_i}{1+2K_p\lambda_i\mathrm{SNR}} + \frac{1}{L}\sum_{i=r}^{L-1}\lambda_i \tag{D.3}$$

- As $r \rightarrow L$ in (D.2), $\mathbf{B}_{MSE}(\hat{\mathbf{g}}_{\mu_r})$ under SNR mismatch results in the following Bayesian MSE:

$$\mathbf{B}_{MSE}(\hat{\mathbf{g}}_{\mu_r}) = \frac{1}{L}\sum_{i=0}^{L-1}\frac{\lambda_i}{(1+2K_p\lambda_i SNR)^2}\left[1+2K_p\lambda_i\frac{SNR^2}{\widetilde{SNR}}\right] \tag{D.4}$$

- Finally, the Bayesian MSE in the case of no SNR mismatch is also be obtained as

$$\mathbf{B}_{MSE}(\hat{\mathbf{g}}_{\mu_r}) = \frac{1}{L}\sum_{i=0}^{L-1}\frac{\lambda_i}{1+2K_p\lambda_i SNR} \tag{D.5}$$

Appendix E

Bayesian MSE for Truncated MMSE KL Estimator under Correlation Mismatch in ST/SF – OFDM Systems

The truncated estimation error is

$$\hat{\boldsymbol{\varepsilon}}_{\mu_r} = \tilde{\mathbf{g}}_{\mu} - \hat{\mathbf{g}}_{\mu_r} \tag{E.1}$$

where $\tilde{\mathbf{g}}_{\mu}$ is the KL coefficient vector of the true μ^{th} multipath channel. As a result, the average Bayesian MSE is

$$\begin{aligned} B_{MSE}(\hat{\mathbf{g}}_{\mu_r}) &= \frac{1}{L}\operatorname{trace}(\mathbf{C}_{\hat{\boldsymbol{\varepsilon}}_{\mu_r}}) \\ &= \frac{1}{L}\operatorname{trace}(\boldsymbol{\Lambda}_{\tilde{\mathbf{g}}} + 4K_p^2\ddot{\boldsymbol{\Gamma}}_r^2\boldsymbol{\Lambda}_{\mathbf{g}} + 2\sigma^2 K_p\ddot{\boldsymbol{\Gamma}}_r^2 - 4K_p\ddot{\boldsymbol{\Gamma}}_r\boldsymbol{\beta}) \\ &= \frac{1}{L}\sum_{i=0}^{r-1}\left[\tilde{\lambda}_i + \frac{2K_p\lambda_i(\lambda_i - 2\beta_i)}{2\lambda_i K_p + \sigma^2}\right] + \frac{1}{L}\sum_{i=r}^{L-1}\tilde{\lambda}_i \quad \text{and} \quad \sigma^2 = \frac{1}{SNR} \\ &= \frac{1}{L}\sum_{i=0}^{r-1}\frac{\tilde{\lambda}_i + 2K_p SNR\,\lambda_i(\tilde{\lambda}_i + \lambda_i - 2\beta_i)}{1 + 2K_p\,SNR\,\lambda_i} + \frac{1}{L}\sum_{i=r}^{L-1}\tilde{\lambda}_i \end{aligned} \tag{E.2}$$

where β is the real part of $E[\tilde{\mathbf{g}}_{\mu}\mathbf{g}_{\mu}^{\dagger}]$ and β_i's are the diagonal elements of β. With this result, we will now highlight some special cases:

- Letting $\beta_i = \lambda_i = \tilde{\lambda}_i$ in (E.2) for the case of no mismatch in the correlation of KL expansion coefficients, truncated Bayesian MSE is identical to that obtained in

(D.3).

- As $r \to L$ in (E.2), Bayesian MSE under correlation mismatch is obtained to yield:

$$\mathbf{B}_{\mathrm{MSE}}(\hat{\mathbf{g}}_{\mu_r}) = \frac{1}{L}\sum_{i=0}^{L-1}\frac{\tilde{\lambda}_i + 2K_p \mathrm{SNR}\,\lambda_i(\tilde{\lambda}_i + \lambda_i - 2\beta_i)}{1 + 2K_p\,\mathrm{SNR}\,\lambda_i} \tag{E.3}$$

- Under no correlation mismatch in (E.3) where $\beta_i = \lambda_i = \tilde{\lambda}_i$, Bayesian MSE obtained from (E.3) is identical to that in (D.5).
- Also note that as $\mathrm{SNR} \to \infty$, (E.2) reduces to $\mathrm{MSE}(\tilde{\mathbf{g}}_{\mu} - \hat{\mathbf{g}}_{\mu_r})$.

Appendix F

Theororetical SER for SF/ST-OFDM Systems

Define $\overline{\mathbf{Y}} = \left[\mathbf{Y}_1 \ \mathbf{Y}_2^*\right]^{\mathsf{T}}$, and cast (4.11) in a matrix/vector form:

$$\underbrace{\begin{bmatrix}\mathbf{Y}_1 \\ \mathbf{Y}_2^*\end{bmatrix}}_{\overline{\mathbf{Y}}} = \underbrace{\begin{bmatrix}\mathcal{H}_1 & \mathcal{H}_2 \\ \mathcal{H}_2^{\dagger} & -\mathcal{H}_1^{\dagger}\end{bmatrix}}_{\overline{\mathcal{H}}} \underbrace{\begin{bmatrix}\mathbf{X}_1 \\ \mathbf{X}_2\end{bmatrix}}_{\mathbf{X}} + \underbrace{\begin{bmatrix}\boldsymbol{\eta}_1 \\ \boldsymbol{\eta}_2^*\end{bmatrix}}_{\overline{\boldsymbol{\eta}}} \tag{F.1}$$

where $\mathcal{H}_{\mu} = \mathrm{diag}(\mathbf{H}_{\mu})$. By premultiplying (F.1) by $\overline{\mathcal{H}}^{\dagger}$ the signal model for Maximal Ratio Receive Combiner (MRRC) can be obtained as

$$\begin{bmatrix}\breve{\mathbf{Y}}_1 \\ \breve{\mathbf{Y}}_2\end{bmatrix} = \begin{bmatrix}\|\mathcal{H}_1\|^2 + \|\mathcal{H}_2\|^2 & \mathbf{0} \\ \mathbf{0} & \|\mathcal{H}_1\|^2 + \|\mathcal{H}_2\|^2\end{bmatrix} \begin{bmatrix}\mathbf{X}_1 \\ \mathbf{X}_2\end{bmatrix} + \begin{bmatrix}\breve{\boldsymbol{\eta}}_1 \\ \breve{\boldsymbol{\eta}}_2\end{bmatrix} \tag{F.2}$$

where

$$\breve{\mathbf{Y}}_1 = \mathcal{H}_1^{\dagger}\mathbf{Y}_1 + \mathcal{H}_2\mathbf{Y}_2^* \tag{F.3}$$

$$\breve{\mathbf{Y}}_2 = \mathcal{H}_2^{\dagger}\mathbf{Y}_1 - \mathcal{H}_1\mathbf{Y}_2^* \tag{F.4}$$

$$\breve{\boldsymbol{\eta}}_1 = \mathcal{H}_1^{\dagger}\boldsymbol{\eta}_1 + \mathcal{H}_2\boldsymbol{\eta}_2^* \tag{F.5}$$

$$\breve{\eta}_2 = \mathcal{H}_2\,\eta_1 - \mathcal{H}_1\,\eta_2^* \tag{F.6}$$

Thus, at the output of MRRC the signal for k[th] subchannel is

$$\breve{Y}_\mu(k) = \left(|H_1(k)|^2 + |H_2(k)|^2\right)X_\mu(k) + \breve{\eta}_\mu(k) \tag{F.7}$$

Assuming $H_\mu(k) = \rho_\mu e^{-j\phi_\mu}$ and $(\breve{\eta}_\mu(k) \mid \rho_1,\rho_2,\phi_1,\phi_2) \sim \mathcal{N}(0,\breve{\sigma}^2)$, where $\breve{\sigma}^2 = (\rho_1^2+\rho_2^2)\sigma^2$, and the faded signal energy at MRRC $\breve{E}_s = (\rho_1^2+\rho_2^2)^2 E_s$. Thus, the symbol error probability of QPSK for given $\rho_1,\rho_2,\phi_1,\phi_2$ is

$$\Pr(\text{error} \mid \rho_1,\rho_2,\phi_1,\phi_2) = 2Q\left(\sqrt{\breve{E}_s/\breve{\sigma}^2}\right) - Q^2\left(\sqrt{\breve{E}_s/\breve{\sigma}^2}\right)$$

$$= 2Q\left(\sqrt{(\rho_1^2+\rho_2^2)^2 E_s/\sigma^2}\right) - Q^2\left(\sqrt{(\rho_1^2+\rho_2^2)^2 E_s/\sigma^2}\right)$$

$$= 2Q\left(\sqrt{(\rho_1^2+\rho_2^2)^2 SNR}\right) - Q^2\left(\sqrt{(\rho_1^2+\rho_2^2)^2 SNR}\right) \tag{F.8}$$

Bearing in mind $\Pr(\text{error} \mid \rho_1,\rho_2,\phi_1,\phi_2)$ does not depend on ϕ_1 and ϕ_2, note that

$$\Pr(\text{error} \mid \rho_1,\rho_2) = \int_{-\pi}^{\pi}\int_{-\pi}^{\pi} \Pr(\text{error},\phi_1,\phi_2 \mid \rho_1,\rho_2)\,d\phi_2\,d\phi_1$$

$$= \int_{-\pi}^{\pi}\int_{-\pi}^{\pi} \Pr(\text{error} \mid \rho_1,\rho_2,\phi_1,\phi_2)\,p(\phi_1)p(\phi_2)\,d\phi_2\,d\phi_1$$

$$= \Pr(\text{error} \mid \rho_1,\rho_2,\phi_1,\phi_2)\int_{-\pi}^{\pi}\int_{-\pi}^{\pi} p(\phi_1)p(\phi_2)\,d\phi_2\,d\phi_1$$

$$= \Pr(\text{error} \mid \rho_1,\rho_2,\phi_1,\phi_2) \tag{F.9}$$

substituting (F.9) in the following equation:

$$\Pr(\text{error}) = \int_0^{\infty}\int_0^{\infty}\int_{-\pi}^{\pi}\int_{-\pi}^{\pi} p(\rho_1,\rho_2,\phi_1,\phi_2)\Pr(\text{error}\mid \rho_1,\rho_2,\phi_1,\phi_2)\,d\phi_2\,d\phi_1\,d\rho_2\,d\rho_1$$

$$= \int_0^{\infty}\int_0^{\infty}\int_{-\pi}^{\pi}\int_{-\pi}^{\pi} p(\rho_1,\rho_2,\phi_1,\phi_2)\Pr(\text{error}\mid \rho_1,\rho_2)\,d\phi_2\,d\phi_1\,d\rho_2\,d\rho_1$$

$$= \int_0^{\infty}\int_0^{\infty} p(\rho_1,\rho_2)\Pr(\text{error}\mid \rho_1,\rho_2)\,d\rho_2\,d\rho_1 \qquad \text{(F.10)}$$

Since channels $\mathbf{H}_1$ and $\mathbf{H}_2$ are independent ρ_1 and ρ_2 are also independent $p(\rho_1,\rho_2) = p(\rho_1)p(\rho_2)$. Thus (F.10) takes the following form:

$$\Pr(\text{error}) = \int_0^{\infty}\int_0^{\infty} p(\rho_1)p(\rho_2)\Pr(\text{error}\mid \rho_1,\rho_2)\,d\rho_2\,d\rho_1$$

$$= \int_0^{\infty}\int_0^{\infty} 4\rho_1\rho_2 e^{-(\rho_1^2+\rho_2^2)} \left(2Q\left(\sqrt{(\rho_1^2+\rho_2^2)^2\,\text{SNR}}\right) - Q^2\left(\sqrt{(\rho_1^2+\rho_2^2)^2\,\text{SNR}}\right)\right)d\rho_2\,d\rho_1 \qquad \text{(F.11)}$$

If we now apply $\rho_1 = \varsigma\cos(\alpha)$ and $\rho_2 = \varsigma\sin(\alpha)$ transformations we arrive the following SER expression for ST-OFDM and SF-OFDM systems,

$$\Pr(\text{error}) = \int_0^{\infty}\int_0^{\pi/2} 2\varsigma^3\sin(2\alpha)e^{-\varsigma^2}\left(2Q\left(\sqrt{\varsigma^2\text{SNR}}\right) - Q^2\left(\sqrt{\varsigma^2\text{SNR}}\right)\right)d\alpha\,d\varsigma$$

$$= \int_0^{\infty} 2\varsigma^3 e^{-\varsigma^2}\left(2Q\left(\sqrt{\varsigma^2\,\text{SNR}}\right) - Q^2\left(\sqrt{\varsigma^2\,\text{SNR}}\right)\right)d\varsigma$$

$$= \frac{3}{4} - \left(\frac{1}{2} + \frac{1}{\pi}\arctan(\gamma_2)\right)\gamma_2^3\gamma_3 - \gamma_2^2\gamma_1 \qquad \text{(F.12)}$$

or by neglecting the $Q^2(.)$ term in (F.12), simplified form can be obtained as

$$\Pr(\text{error}) = 1 - \gamma_2^3\gamma_3 \qquad \text{(F.13)}$$

where

$$\gamma_1 = \frac{1}{2\pi(\mathrm{SNR}+1)} \quad , \qquad \gamma_2 = \sqrt{\frac{\mathrm{SNR}}{\mathrm{SNR}+2}} \quad , \qquad \gamma_3 = \frac{\mathrm{SNR}+3}{\mathrm{SNR}}$$

Curriculum Vitae

Publications:

[1] Şenol, H., Çırpan, H. A., Panayırcı, E., and Çevik, M., "A Low Complexity Time-Domain MMSE Channel Estimator for Space-Time/Frequency Block Coded OFDM Systems", *EURASIP Journal on Applied Signal Processing* (accepted for publication).

[2] Şenol, H., Çırpan, H. A., Panayırcı, E., "Linear Expansions for Frequnecy Selective Channels in OFDM Systems," *AEÜ International Journal of Electronics and Communications*, **60**, 224-234, 2006

[3] Şenol, H., Çırpan, H. A., Panayırcı, E., "A Low Complexity KL-Expansion Based Channel Estimator for OFDM Systems," *EURASIP Journal on Wireless Communications and Networking,* **2005**, 163-174, 2005.

[4] Şenol, H., Çırpan, H. A., Panayırcı, E., and Çevik**, M.,** "Low-Complexity MMSE Channel Estimator for Space Time Coded OFDM Systems with Transmit Diversity", *ELECO'05 4th International Conference on Electrical and Electronics Engineering,* December 7-11 2005, Bursa, Turkey.

[5] Şenol, H., Çırpan, H. A., Panayırcı, E., "Frequency Selective Fading Channel Estimation in OFDM Systems using KL Expansion," *13th European Signal Processsing Conference,* EUSIPCO 2005, September 4-8 2005, Antalya, Turkey.

[6] Şenol, H., Çırpan, H. A., Panayırcı, E. and Çevik, M., "KL-Expansion Based MMSE Channel Estimator for Space-Time/Frequency Block Coded OFDM Systems," *2nd COST 289 Workshop, Special Topics on 4G Systems,* July 6-7 2005, Antalya, Turkey.

[7] Şenol, H., Çırpan, H. A., Panayırcı, E., "Pilot Aided Bayesian MMSE Channel Estimation for OFDM Systems: Algorithm and Performance Analysis," GLOBECOM'04*, IEEE Global Telecommunications Conference, 29 November - 3 December*, Dallas, Texas, USA.

[8] Şenol, H., Çırpan, H. A., Panayırcı, E., "Adaptive MMSE channel estimation in OFDM systems," *ELECO'03 Third International Conference on Electrical and Electronics Engineering*, Bursa, Turkey, December 3-7 2003.

[9] Şenol, H., Çırpan, H. A., Panayırcı, E., "MMSE Estimation Approach for Karhunen-Loeve Expansion Coefficients of Multipath Channel in OFDM," *Sixth Baiona Workshop on Signal Processing in Communications*, September 8-10 2003, Baiona, Spain.

[10] Şenol, H., Çırpan, H. A., Panayırcı, E., "OFDM Sistemleri için En Küçük Ortalama Karesel Hata Kanal Kestirimcisi," *SIU'03 11. Sinyal İşleme & Uygulamaları Kurultayı, sayfa 269-272,* Sarıyer, İstanbul, 18-20 Haziran 2003.

References

[1] Van Nee, R. and Prasad, R., *OFDM for Wireless Multimedia Communications*, in Artech House Publishers, 2000.

[2] Sari, H., Karam, G., and Jeanclaude, I., "Transmission techniques for digital terrestrial TV broadcasting", *IEEE Communication Magazine*, **33**, 100-109, February, 1995.

[3] Edfords, O., Sandell, M., Van de Beek, J. J., Wilson, S. K., and Borjesson, P. O., "OFDM Channel estimation by singular value decomposition", *IEEE Transactions on Communication* **46**, 931-938, July, 1998.

[4] Morelli, M., and Mengali, U., "A Comparison of Pilot-Aided Channel Estimation for OFDM Systems", *IEEE Transactions on Signal Processing,* **49**, 3065-3073, December, 2001.

[5] Li, Y., (G.), Cimini, L. J., and Sollenberger, N. R., "Robust channel estimation for OFDM systems with rapid dispersive fading channels", *IEEE Transactiosn on Communication*, 46, 902-914, July, 1998.

[6] Schniter, P., "Low-Complexity Estimation of Doubly-Selective Channels", *IEEE workshop on Signal Processing Advances in Wireless Communications,* SPAWC-2003, Rome, Italy, 15-18 June, 2003.

[7] Biglieri, E., Proakis, J. and Shamai, S., "Fading Channels: Information-Theoretic and Communications Aspects", *IEEE Transactions on Information Theory,* **44**, 2619-2692, Oct., 1998.

[8] Jakes, W. C., "*Microwave Mobile Communications*", New York Plenum, 1974.

[9] Yip, K. and Ng, T., "Karhunen-Loeve Expansion of the WSSUS Channel Output and its Application to Efficient Simulation", *IEEE Journal on Selected Areas in Communications,* **15**, 640-646, May, 1997.

[10] Senol, H., Cirpan, H. A., Panayirci, E., "A Low-Complexity KL Expansion-Based Channel Estimator for OFDM Systems", *EURASIP JWCN* 2005:2 163-174., 2005.

[11] Siala, M. and Dupontiel, D., "Maximum A Posteriori Multipath Fading Channel Estimation for CDMA Systems", *In Proceedings Vehicular Technology Conference (VTC'99),* 1999.

[12] Li, Y.G., Cimini, L.J., Seshadri, N., Ariyavistakul, S., "Channel Estimation for OFDM Systems with Transmitter Diversity in Mobile Wireless Channels", *IEEE Journal Selected Areas on Communication*, **17**, 461-471, 1999.

[13] Alamouti, S. M., "A Simple Trasmitter Diversity Scheme for Wireless Communications", *IEEE Journal Selected Areas on Communication,* **16**, 1451-1458, 1998.

[14] Cirpan, H. A., Panayirci. E., "Blind Channel Estimation for Space-Time Coding Systems with Baum-Welch Algorithm", *IEEE ICC 2002,* New York, ABD, April 28 – May 2, 2002.

[15] Tarokh, V., Seshadri, N., Calderbank, A. R., "Space-Time Codes for High Data Rate Wireless Communications: Performance Analysis and Code Construction", *IEEE Transaction Information Theory,* **44,** 744-765, 1998.

[16] Tarokh V, Jafarkhani H, Calderbank A. R., "Space-Time Block Codes from Orthogonal Designs", *IEEE Transaction Information Theory* **45,** 1456-1467, 1999.

[17] Lee K. F., Williams D. B., "A Space-Frequency Transmitter Diversity Technique for OFDM Systems", *In proceedings of IEEE Globecom,* San Francisco, CA, 1473-1477, November 2000.

[18] Liu Z, Xin Y, Giannakis G. B., "Space-Time-Frequency Coded OFDM for Frequency Selective Fading Channels", *IEEE Transaction on Signal Processing*, **50,** 2465-2476, 2002.

[19] Bolcskei, H., Paulraj, A., "Space-Frequency Coded Broadband OFDM systems", *IEEE Transactions on Wireless Communications and Networking Conference (WCNC),* **1,** 1-6, 2000.

[20] Kay, S.M., "*Fundamentals of Statistical Signal Processing: Estimation Theory*", Prentice Hall, 1993.

[21] Van Trees, H. L., *Detection, Estimation and Modulation Theory, Part I*, Wiley Interscience, 1993.

[22] Proakis, J. G., *Digital Communications,* New York, Mc Graw-Hill, 1983